Synthesis, Characterization, and Application of Nanothermites for Joining

by

Golnaz Bohlouli Zanjani

A thesis
presented to the University of Waterloo
in fulfillment of the
thesis requirement for the degree of
Master of Applied Science
in
Mechanical Engineering - Nanotechnology

Waterloo, Ontario, Canada, 2013

Author's Declaration

I hereby declare that I am the sole author of this thesis. This is a true copy of the thesis, including any required final revisions, as accepted by my examiners.

I understand that my thesis may be made electronically available to public.

Abstract

Thermite reactions were well studied in the past few decades; however, implementation of these reactions with nanoscale components is a new interest for today's researchers both for military and civil industries. Nanothermites are mixtures of a metal fuel and a metal oxide, undergoing a redox reaction while heated, and generating a large amount of energy (heat/thrust) which can reach combustion temperatures above 3000K. Aluminum is commonly used as the fuel because of its abundance, easy handling, high reactivity and benign products. By using nano-sized components, the surface energy, contact area, and mixing homogeneity increase. These properties result in greatly improved reactivity and propagation rate as well as easier ignition compared to traditional thermites, which make them attractive as advanced propellants, pyrotechnics, and heat and thrust generators. They also find civil applications such as joining. Here, the application of nanothermites for joining metal to ceramic/glass is investigated. To approach this goal, composites of nanothermite modified by Copper powder were developed for the first time and their related properties were studied to find the best composition for joining. These energetic composites can be applied where a localized heat source is required. The advantage of using nanothermite for joining is its fast reaction, high energy density and liquid products that can wet surfaces. In this research, the reaction products were studied by X-Ray Diffraction spectroscopy, Scanning Electron Microscopy and Energy Dispersive X-ray spectroscopy. The overall thermite reaction corresponding to the Al-NiO nanothermite was found producing the AlNi phase in a fuel-rich mixture. The microstructures of these reaction products showed the formation of a composite made from copper, AlNi and AlNi/Al_2O_3 spheres in an Al_2O_3 matrix. On the other hand, the influences of the fuel (Al) to oxidizer (NiO or CuO) mass ratio and the amount of Cu additive, on the ignition temperature and energy release were

characterized using Differential Scanning Calorimetry. It was found that both parameters do not affect the ignition temperature significantly but change the energy release dramatically. Furthermore, according to these results, (Al-33%NiO)-50%Cu was selected and applied to join dissimilar materials such as copper, alumina-silica and glass. As a proof of concept, joint cross-sections were studied by SEM-EDAX revealing that the alumina phase produced by this reaction was joined to the glass/ceramic, while the metal phase wetted the metallic surfaces. Therefore, this composite was introduced as a good interlayer for dissimilar metal/ceramic surfaces.

Acknowledgements

I would like to thank my supervisors, Dr. John Z. Wen and Dr. Norman Y. Zhou for all their help, guidance and support. Their patience and valuable teachings helped me overcome difficulties and become a stronger person. I would also like to thank Dr. Anming Hu, for all his help and insightful discussions in our Nano group. My thanks are extended to Mr. John Persic, founder and vice president of Microbonds Inc., for providing materials and support. I would like to express my gratitude to the examining committee members Dr. Mary Wells and Dr. Ehsan Toyserkani whose comments and suggestions were extremely helpful in improving my manuscript. Financial contributions to this research project from both the NSERC and Microbonds Inc. are acknowledged. My thanks are also extended to my colleagues and friends, Dr. Ehsan Marzbanrad, Peng Peng, Jeff Wang and all members of the Center for Advanced Materials Joining (CAMJ) and Laboratory for Emerging Energy Research (LEER), for all their technical help, encouragement, and support.

During the past years I was blessed with enormous love and encouragement from my friends and family members which I will carry in my heart forever. They brought to me such peace and inspiration that was the highest driving force for me to overcome challenges. My very special thanks go to, my sister, Parisa Bohlouli-Zanjani and her family who were a great inspiration for me in these years and made me feel home away from my home country; my sisters Sanaz and Nazila, and my brother Hamidreza for their love and continuous encouragement from miles away; My parents, Mehri and Shokrollah, who have always believed in me and filled me with love and inspiration to discover the unknown and to excel in life. And Finally thanks to my loving husband, Hadi Hosseinzadeh-Khaligh, whose support, guidance and encouragements were endless. Thanks for putting up with all the frustration and hard times.

Dedication

In the name of GOD, the most gracious, the most merciful,

I wholeheartedly dedicate this thesis to my beloved parents, *Mehri & Shokrollah;*

My sister, *Nazila,*

and my *Hadi*...

There is no word to describe the love and care they gifted me …

Table of Contents

List of Figures

List of Tables

List of Equations

List of Reactions

CHAPTER 1

Introduction

1.1. Thermite

Thermite is an energetic mixture of a metal fuel and an oxide undergoing a redox reaction to produce a more stable oxide[1,2]. While ignited, the reaction between the fuel and oxidizer produces a large amount of heat and thrust depending on the type of reactants. The mixture was discovered and named "thermite" by German chemist, Hans Goldschmidt[3], in 1895 while trying to produce very pure metals. The metal (fuel) can be aluminum, magnesium, titanium, zinc, silicon or boron. Aluminum, because of its high affinity for oxygen, is the most commonly used fuel in thermites[4]. The abundance, easy handling, high reactivity, benign products and high boiling temperature (2792 K) of aluminum are its other advantages as a fuel over other metals. It is the third abundant element (after oxygen and silicon) and the most abundant metal in the earth's crust. Being exposed to oxygen, an oxide layer is formed around the core aluminum protecting it from further oxidation and makes its storage and handling easier and safer. The common metal oxides used in thermite reactions include Fe_2O_3[5–7], CuO[8–19], MoO_3[12,20,21], WO_3[12,22,23] Bi_2O_3[12,24,25] NiO[26,27], etc. Thermite reactions are highly exothermic and can rise temperatures above 3000 K[1,28,29]. Appendix A presents a list of thermite reactions with their thermodynamic properties, such as adiabatic flame temperature (AFT), amount of gas production, and heat of reaction. A typical thermite reaction is as follows:

Metal oxide + Aluminum → Metal + Auminum oxide + Heat (R1-1)

1.2. Thermite welding

Thermite welding, also called as aluminothermic welding, is a low-cost type of fusion welding process according to German institute of standardization (DIN 1910[30]). In this process, the parts to be welded are put together in an enclosed sand mould with a defined gap between the faces and are preheated to a suitable temperature. The thermite mixture of aluminum and metal oxide is placed in a highly refractory magnesite funnel above the mould and is ignited with a special igniter[31]. The reaction is exothermic generating a large amount of heat, which increases the temperature up to 2450°C. The aluminum reduces the metal oxide, producing pure metal and aluminum oxide. At the high temperature of about 2450°C, the metal is liquid and the oxide is extremely hot and they separate due to their different densities ($T_{boiling}$ of Al=2519°C, and $T_{boiling}$ of Fe=2862°C). The liquid metal flows through the bottom of the funnel while the oxide accumulates on the top[31]. The preheated base metal parts are then welded together by pouring the molten metal into the mould[30]. Figures 1-1 and 1-2 show a schematic and a real picture of the thermite welding process respectively.

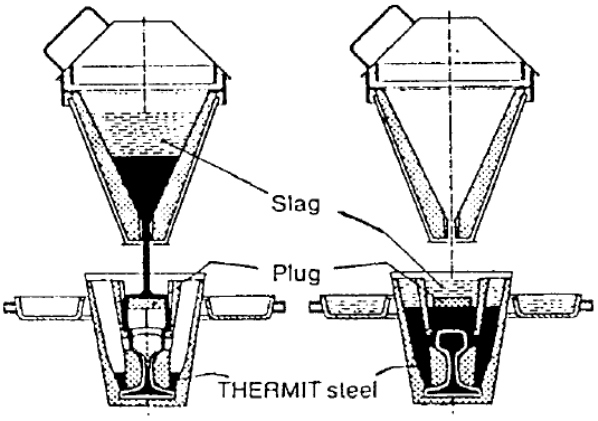

Figure 1-1 Schematic thermite welding apparatus- From the reference [31]

Figure 1-2 Thermite welding of railways- From the reference [32]

The most historical and well known thermite material, composed of aluminum and Fe_2O_3 powder, has been used to weld railway tracks as shown in Figure 1-2. This reaction is as follows:

$$Al+\frac{1}{2}Fe_2O_3 \rightarrow \frac{1}{2}Al_2O_3+Fe+Heat \qquad \text{(R1-2)}$$

1.3. Motivation

A cost-effective, well known process, thermite welding has been used in the railway industry for several decades. However, the conventional thermite welding process requires large activation energy and a huge setup, making it inconvenient for use in small areas. Therefore, it sparks the idea of using an improved version of thermite material to join small parts in micro and nano-scale systems. Therefore, the nanothermites are considered as the improved version of the conventional thermites. They have a great potential for material and component joining purposes when there is a need to achieve localized energy generation and molten metal in space-limited situations. For example, in packaging micro-electronics interconnections and joining silicon and metal components in solar cells, a localized energy source is desired near the joint in order to avoid exposure of the entire component to high temperatures.

In this regard, after studying various thermite compositions in the relevant literature, Al-NiO was chosen for further study due to its low gas generation and high heat of reaction.

1.4. Objective

The objective of this thesis is to investigate synthesis and characterization of Al-NiO and Al-CuO nanothermite composites in order to find a nanothermite composition which can be successfully used in nano and micro-joining applications. According to this goal, thermo-chemical analysis of the aforementioned composites, along with detailed analysis of reactants and products composition and microstructures, were focused in this thesis. This thesis also presents preliminary results of joining dissimilar materials by the use of the selected composite.

1.5. Thesis organization

The outline of this thesis is as following. Chapter 2 briefly reviews the relevant literature on synthesis, characterization, and application of thermite reactions. In this chapter I reviewed the ignition and combustion of thermites as well as their thermal behaviour and phase analysis. The application of thermites for joining is more emphasized amongst their other applications. Chapter 3 explains the experimental procedures and configurations used during the course of this project. Chapter 4 involves characterization of the Al + NiO nanothermite during synthesis and after completion of the reaction, while Chapter 5 focuses on results of synthesis and characterization of copper added nanothermites, including the thermal and microstructural analysis. Chapter 6 introduces a novel joining method being applied to join metal to glass/ceramic and includes the relevant results and discussion. Finally, Chapter 7 summarizes the results and conclusions and suggests the future work on this topic.

CHAPTER 2

Literature Review

This chapter reviews the background information and the relevant literature in the area of nanothermite synthesis and characterization methods, and applications. The thermite reaction was introduced in Chapter 1. In this chapter, first the differences between the nanoscale and bulk-scale thermite are highlighted. Afterwards, the literature on nanothermite synthesis of various compositions is reviewed, which outlines the preparation methods, chemical compositions, and geometric structures of nanothermites. The characterization literature includes a review of the debate on ignition mechanism along with the review of the role of important factors in determining combustion rate. Afterwards, the literature on identification of reaction products, thermodynamic and kinetic analysis of the nanothermite reactions is reviewed. At the end, the traditional thermite joining is explained and the relevant works on the use of nanothermites for joining are reviewed.

2.1. Nanothermites versus conventional thermites

Compared to monomolecular energetic materials such as TNT (trinitrotoluene), RDX (research department explosive) and HMX (high melting explosive), thermites have higher combustion energy density as shown in Figure 2-1[33] . However, conventional thermites have lower energy release rates since the mass transport rate depends on the granulometry of the precursors and therefore limits the energy release rate[2]. To increase the energy release rate of thermite materials to the level of monomolecular materials, one should decrease the mass transfer path as much as possible. This is how the use of thermite material in nano-scale began to overcome the limitations of conventional thermites.

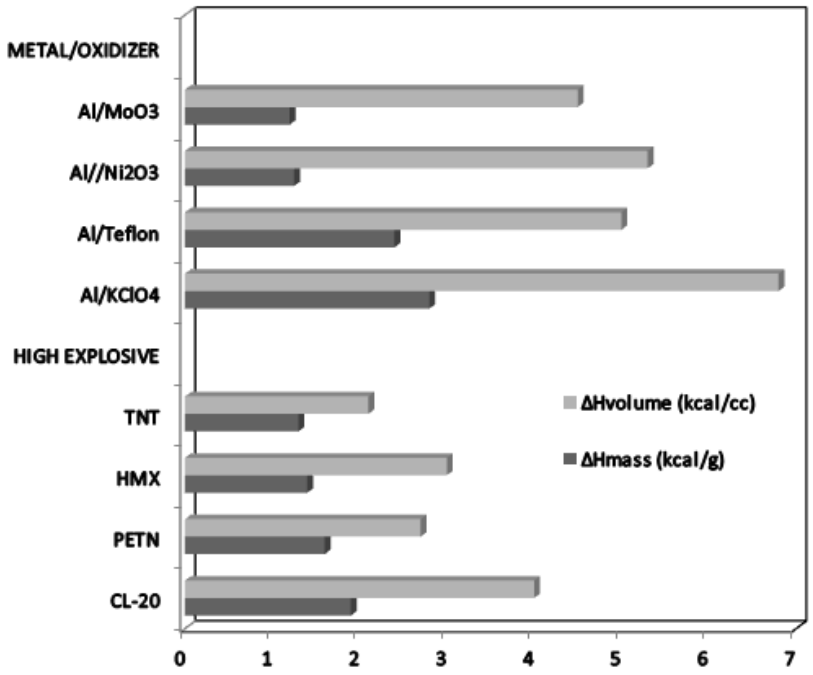

Figure 2-1 Mass and volumetric energy density of example thermites compared to common explosives; From Fischer and Grubelich [33]

Thermites with reactant particle dimensions less than 100 nm are considered nanothermites. Compared to conventional thermites, nanothermites possess higher energy release rates, enhanced reactivity[34], and lower ignition temperature[24,26,28]. Nanoparticles have much higher surface area compared to micron sized thermites. By decreasing the particle size, the ratio of surface/volume increases. Consequently, the surface energy increases. Smaller particle size also improves the contact area and mixing homogeneity. These properties result in greatly improved reactivity and propagation rate as well as easier thermal ignition than traditional thermites, making them attractive as advanced propellants, pyrotechnics, and heat and thrust generators. On the other hand, nanothermites are of interest in civil applications such as micro/nano-joining and energy generation devices for MEMs due to their small size, high energy

density, and tunable reaction parameters, for example, ignition temperature and reaction rate. Following is a review on the preparation approaches of nanothermites.

2.2. Preparation of nanothermite composites

2.2.1. Mixing methods

This section reviews and classifies different approaches to prepare nanothermite composites.

Powder mixing

The most common method to prepare reactive nanomaterials is mixing the reactant nanostructures using an ultrasound bath. In this method, Al nanoparticles are mixed with oxide nanopowders in a bath of isopropanol[12,24], hexane[7,12,24,35], or another liquid using high intensity ultrasound actuators. The liquid is then evaporated and a dried powder is achieved. The major challenge with this method is assessment of mixing quality. In a review by[36] it is shown that most assessment techniques for mechanically mixed nano-powders are based on imaging a small area of the mixed powder. This imaging should be repeated for many parts of the sample powder in order to achieve a reliable assessment. The mixing quality becomes more critical when the morphology of the nanopowders to be mixed is different. In most cases, oxide nanopowders are not spherical or uniaxial. They are usually in the shape of nanorods or flakes. Therefore, taking an image which is a good representative of the mixture is often challenging since larger particles such as flakes might shield the smaller particles. Furthermore, while the mechanical mixing method works very well in laboratory scale, it is challenging to scale it up since the mixing quality decreases by increasing the batch size[2].

Sol-gel

Sol-gel method was proposed as an alternative to mechanical mixing by several papers[7,37–40]. This process makes a matrix of oxide material with metal nanoparticles filling in

the pores of the matrix. Hydrated metal salts are used as precursors and propylene oxide is used as gelation agent. In the process of making reactive nanomaterials, the metal nanopowder is added to the solution just before the gelation happens. Then the fluid in the pores is removed either by slow evaporation or by supercritical extraction with CO_2. Using various silane additives helped to further functionalize the oxide matrix[41]. A very intimate mixing is achieved using this process however, it has some disadvantages including: high porosity of the final product which is not desirable for some applications, the type of materials which can be gelled is limited, it is difficult to scale it up since the metal nanopowder needs to be introduced to the solution at a very specific stage.

Self-assembly

Another approach introduced in the recent years, is self-assembly of aluminum nanoparticles on functionalized nanosized oxide particles[8,42]. This method will produce ordered structures with better properties and higher combustion rate compared to conventionally mixed powders. In this method, Al nanoparticles arrange around the outer surface of a functionalized oxide nanorod or fill the pores of a mesoporous oxide material. As an example, Al-CuO nano composite was achieved by functionalizing CuO nanorods by applying a polymer, poly(4)-vinyl pyridine (P4VP). The Al nanoparticles then self-assembled on the functionalized nanorods and the decorated nanorods became ordered[8]. In a similar approach, Al-Fe_2O_3 nanothermites were prepared. A porous Fe_2O_3 was synthesized using micelles sol-gel synthesis by addition of surfactants. Using surfactants in the synthesis process caused in an ordered structure of pores. In this study a reference sample was also synthesized without the use of surfactants and the pores were not as ordered as the surfactant assisted Fe_2O_3 synthesis. Both oxide samples were mixed with Al nanoparticles and their combustion rates were compared. The ordered sample showed higher combustion rate. The ordered structures offer better control of reaction properties and

combustion rates. Cheng et al.[5] compared the reaction kinetics of self-assembled and solvent-based nanothermite mixtures of Al-Fe_2O_3 and concluded that self-assembled nanothermites enhanced the reaction kinetics more strongly than simple physical solvent mixed samples. Self-assembled nanothermites had a much higher contact area between the fuel and oxidizer and, therefore, a higher propagation rate, etc. since the increased intimacy between the fuel and the oxidizer significantly enhanced the solid-state diffusion between the reactants. The drawbacks of this method are the high cost of oxide preparation the high porosity of the material. Additionally, the functionalizing agents remain in the structure, reducing the energy density of the nanothermite composite.

Layered vapor deposition

Another interesting method of nanothermite synthesis is preparing them in layers of nanosized films. Nanosized films of reactive materials are coated on top of each other by vacuum deposition. Ma et al.[43] introduced Al-Ni multilayer films with each layer to be 60-300 nm thick. The Al and Ni nano layers were deposited by alternate electron beam evaporation of Al and Ni on a glass substrate coated by photo resist at pressure of 10^{-7} torr. In order to achieve a free-standing film, the photo resist was dissolved after deposition of Al and Ni layers. The authors reported rapid Self-propagating High temperature Synthesis (SHS) reaction which resulted in production of Al_3Ni_2, Al_3Ni, and Al. Barbie and Weihs registered a patent[44] with systematic development of this method. Extensive research was done following it[45–50]. The multilayer foils were originally developed for joining applications[45–47], however they later attracted interest as energetic components and their reaction details were further studied[48–50]. Al-CuO multilayer foils were also developed and characterized[49,50].

Arrested reactive milling

Arrested reactive milling[51–55] is the only top to bottom method of preparing thermite nanocomposites. In this method, coarse reactant particles are mixed and ball-milled. During such process, the self-sustaining exothermic reaction occurs inside the milling vessel by mechanical ignition. In order to obtain reactive nanocomposites, the milling process is interrupted just before the self-sustaining reaction initiates. This specific time is identified by preliminary experiments for small batches and numerical modeling for large samples[56]. This method results in fully-dense micron-sized composite particles with nanoscale mixed components. In this approach, the reaction initiation time is a limiting factor for mixing reactants. This time depends on milling parameters such as temperature, batch size, and mass ratio of sample to the milling media[2].

2.2.2. Composition and structure

Various nanothermite compositions are widely used based on different applications. The difference is basically in the type and structure of the oxidizer and the mixing geometry. Following are most commonly used nanothermite compositions listed and relative characteristics are reviewed.

Al-CuO

Umbrajkar et al.[15], Al/CuO nanothermite composite was integrated by mixing Al and CuO micron sized particles in a shaker mill. After 1 hour of milling in the presence of 8 ml hexane, a well-mixed nanothermite composite was achieved with a low ignition temperature of about 400K. The activation energy and reaction enthalpy were calculated and 4 steps were elucidated in the reaction kinetics[15]. In another study, by Ohkura et al.[9] a uniform structure of Al/CuO core-shell nanowires was synthesized. The CuO nanowires were grown uniformly by annealing Cu foils and were used as templates for Al nanoparticles deposition. The Al nanoparticles were subsequently sputtered on the CuO nanowires to form Al shells on the CuO core nanowires. The uniformity of this structure was higher than np/np mixtures and had lower

activation energy accordingly[9]. In a different method, Chowdhury et al.[57] used a mixture of oxide-passivated Al np and CuO nps with average diameter of 50 nm to study the effect of oxide shell thickness on the ignition behavior of the nanothermite. Increasing the thickness of the oxide shell led to an increase in the ignition delay time, suggesting that the reaction is governed by diffusion of Al and oxygen atoms through the oxide shell[57]. Wang et al.[16] studied the mixture of nitrocellulose passivated Al nanoparticles and 12 nm diameter CuO nanoparticles to determine the effect of the fuel/oxidizer mass ratio on the reaction products. The study showed that a fuel rich composition results in the formation of Al_2O_3 and pure Cu[16].

Al-Fe_2O_3

Menon et al.[58] studied the effects of structural parameters on reaction characteristics of an Al-Fe_2O_3 thin film nanothermite. This structure was achieved by processing Fe nanowires formed in a nano-porous alumina template. The alumina template was etched to achieve a composite of Fe_2O_3 nanowires embedded in a thin Al film shown in Figure 2-4.

This method can also be used to produce fuel nanowires embedded in thin oxide films. It enables nano-scale control over the structural parameters such as nanowire diameter and packing density, which will affect reaction parameters such as flame temperature and burn rate. Menon et al. have shown that the dimensions and spacing of the nanowire/thin film nanothermite composite strongly affect the ignition properties.[58]

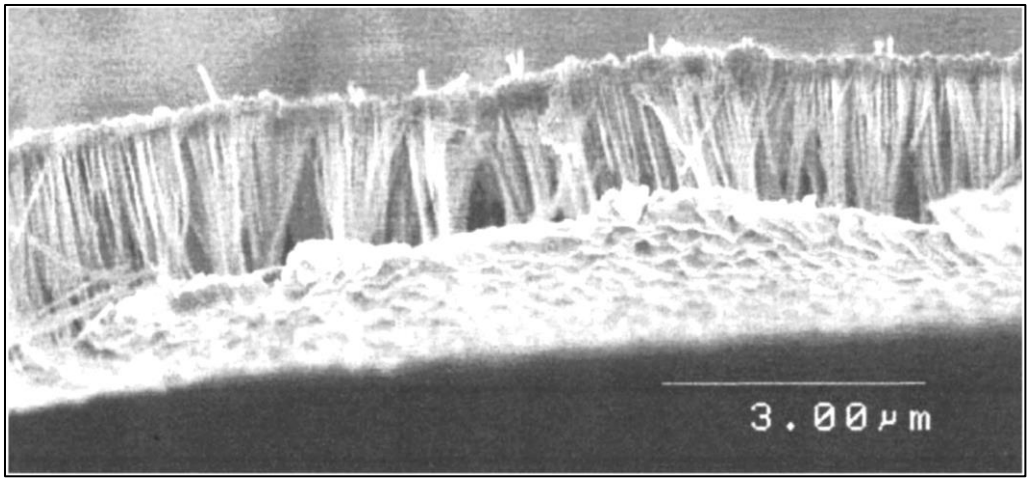

Figure 2-2 Array of Fe_2O_3/Al nanowire-thin film- From Menon et al.[58]

In 2009, Shimojo et al.[59] used a molecular dynamics simulation to investigate the fast diffusion mechanism for ignition of Al/Fe_2O_3 in the interface of Al and Fe_2O_3(diffusion of metal and oxygen atoms).

Al- $AgIO_3$

Sullivan et al.[60] studied the reaction of Al-$AgIO_3$ thermite, which has potential biocidal applications. They determined that the oxidizer first decomposed to AgI, O_2 and O ions. This composition resulted in enhanced pressurization compared to Al-CuO and Al-Fe2O3 because of Iodine gas release in addition to Oxygen.[60]

Al-MoO_3

Son and Pantoya et al.[57,61] studied the effects of particle size and composition (mixture ratio) on the ignition and reaction of nanoscale Al-MoO_3 composites using SEM, SANS and SAXS. They found SANS to be most useful for this characterization. According to their results, sample with smaller Al nanoparticle size exhibited a lower ignition temperature (~40°C) than the sample with larger Al nanoparticle size. On the other hand, their study showed that even small changes in the stoichiometry of the mixture, influenced the propagation rate and pressurization

rate. When the reaction propagation rate increased, the pressurization rate increased as a consequence [61].

Al-WO_3 [12,22,23] Al-Bi_2O_3 [12,24,25], and Al-NiO [26,27] are other compositions of interest. The compositions discussed above are the most common of those used for nanothermites. They have been integrated to different structures such as nano-laminar[62,63], foil geometry [45,47,49,64], nano-honeycomb [27], core-shell nanowires[9], and nanoparticle-nanoparticle as well as nanoparticle-nanowire[16] mixtures.

2.3. Reaction characteristics

2.3.1. Ignition mechanism

The ignition of thermite reactions can be initiated by various methods. These methods include ignition by electrical power, laser radiation, impact[65] or combustion wave from a chemical reaction[66–69]. The ignitability of thermite reactions is primarily influenced by physical and chemical stability of the reactants[70]. In this case, oxide reactants are categorized by Chernenko et al.[70] into two groups based on their stability: chemically stable oxides and chemically unstable oxides. The first group is further divided to two groups: (1) physically stable oxides (while heated don't evaporate, sublime, or fuse); (2) physically unstable oxides. Chemically unstable oxides are also divided to two groups: (3) oxides which decompose and release oxygen upon heating; (4) oxides which further oxidize into higher oxides upon heating in air atmosphere. For class (1) oxides such as NiO, TiO_2, Cr_2O_3, Al_2O_3, Ta_2O_5, and Nb_2O_5, the oxide remains inert until the moment of ignition. In this case, the oxidation of Al with atmospheric oxygen initiates the combustion. Oxides in class (2), i.e. B_2O_3, MoO_3, and WO_3 which either melt or sublime at temperatures below ignition temperature, may enhance the reaction rate upon heating by creating liquid or vapor oxide phases. If the oxide is volatile, the

reaction between Al and the vapor oxide can initiate the reaction. In the case of class (3) oxides, (i.e. V_2O_3, CrO_3, Li_2O_2, and BaO_2), the oxygen released from decomposition of oxides can initiate the combustion. As an example, CrO_3 decomposes at 170°C and releases oxygen which causes the ignition of reaction at this temperature. Class (4) oxides such as FeO and CuO, further oxidize in the air and the heat released from this oxidation process may help initiate the combustion reaction by rising the temperature to the ignition temperature[1,70].

When it comes to Al stability, the Al phase and condition of the oxide layer become important. The stability of the Al nanoparticles strongly depends on the interaction between the core aluminum and the passivating oxide shell. This interaction becomes much more important, with the knowledge of their fairly different properties, such as melting temperature and thermal expansion coefficient. The melting temperature of Aluminum is around 660°C, which is well below the melting temperature of Al oxide (2072°C), making it complicated to determine what exactly happens while heating the nanoparticles. Unlike conventional thermites with ignition temperatures much higher than the melting temperature of Al, nanothermites are ignited at temperatures very close to the Al melting point. This causes a debate on the ignition mechanism of nano aluminum while rapidly heated. This reaction mechanism was previously investigated by many researchers[23,57,71–79] but yet not fully elucidated. There are two main mechanisms proposed for the reaction of Al nanoparticles with oxides while rapidly heated.

The first one is referred to as “melt dispersion”[71–74] mechanism which suggests that the core aluminum melts rapidly and its volumetric expansion induces a large stress on the alumina shell which at a critical point causes the shell to shatter suddenly and the core alumina releases out in the form of small droplets of molten alumina with high velocity. The other proposed mechanism is called “diffusion”[57,75–77] mechanism and argues that during the rapid heating of Al

nanoparticles, the Al core melts [71,80] and induces some stress on the oxide shell and diffuses through the shell. However, the exact diffusion mechanism is still unknown.

Recently, Firmansyah et al.[78] conducted a more detailed investigation on the microstructural behavior of the oxide shell during the ignition of Al nanoparticles in support of the diffusion mechanism. Based on their results from High-temperature X-ray diffraction analysis, it was observed that the nanoaluminum lattice expands under tension at room temperature, and after being heated to about 300°C it passes through a zero-strain state. After passing the melting temperature of bulk aluminum, the aluminum lattice expands without any constraint. The authors attributed this contrary observation to be a result of the inhomogeneous phase transformation of amorphous alumina to the crystalline phase. The new inhomogeneous alumina phase is more ductile due to the presence of weak points of amorphous-crystalline interfaces, which results in no constraint expansion of core aluminum and the shell thickening as a result of diffusion processes of Al cations and O anions. This ductile shell absorbs the pressure built in the Al core.

In an earlier publication, Rai et al.[80] suggested that the Al oxide phase changes with temperature are the key factor in the ignition of Al nanoparticles. The stability of the oxide shell was tested using a hot-stage transmission electron microscope (TEM). The results show that around the melting temperature of bulk aluminum, the oxide shell ruptures and liquid aluminum flows out of the particle. This was explained by the increased tension in the oxide shell due to the high mismatch in the thermal expansion constants (CTE) of aluminum core and aluminum oxide shell. From their observations, the oxide shell on the Al nanoparticle ruptures by increasing temperature and releases the liquid aluminum which instantly ignites and reacts with oxygen.

2.3.2. Combustion of thermite composites

Experimental studies have proven that combustion rate of thermite reactions depends on several factors such as reactant particle size[81,82], inert diluent additives[69,82], powder compact density[81], centrifugal force[83,84], and ambient gas pressure[85,86]. Here, we review the role of these factors on combustion rate of thermite composites.

Particle size: In general, increasing the reactant's particle size reduces the reaction rate. This was shown in a work by Balakir et al[82] reporting that Al particles larger than 100 μm are difficult to ignite. Furthermore, as it was discussed in 2.1 decreasing the particle size to nanoscale has significant effects on the reaction properties including the reaction rate. When it comes to nanoscale, the particle size distribution and the morphology become important factors as well. In nanoscale powders, agglomeration is a common problem making it difficult to measure the particle size distribution precisely. However, various methods were utilized in the recent years to introduce one-factor to demonstrate the particle size and morphology distribution. As a good example of these methods is BET (Branuauer-Emmett-Teller) measurement of surface gas absorption[87–89] by the powder which can be interpreted to the active surface area of the sample powder and eventually be translated to a one-number particle size. All related studies conclude that in identical conditions, the higher the surface area, gives the higher reaction rate.

Aluminum nanoparticles are the key components of a nanothermite composition. In most cases, the Al nanoparticles are coated with a thin oxide shell which prevents them from further oxidation. Figure 2-2 shows a TEM image of an Al nanoparticle. The Al core and the thin Al_2O_3 shell can be distinguished in this image. The oxide shell is usually about 2-5 nm thick[2]. By decreasing Al particle size, particle temperature equilibrates to the ambient temperature and becomes uniform all over the particle more quickly. Therefore, for nanoparticles, the particle

temperature is very sensitive to the ambient temperature changes. Figure 2-3 shows the burning times of Al nanoparticles compared to micron-sized Al particles[90]. Burning time of micron-sized particles is less dependent of the surrounding gas temperature[91]. In case of nanoparticles, we see that the results of Park et al. show much higher burning time compared to Parr et al. These discrepancies are due to the high effect of surrounding gas temperature on the burning rate of nanoparticles.

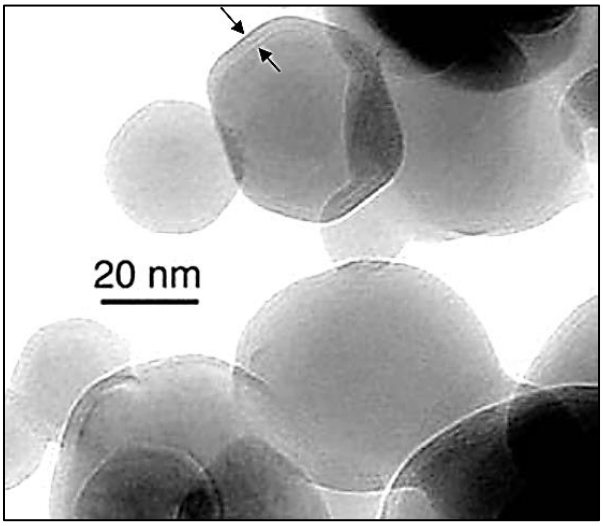

Figure 2-3 TEM image of an oxide passivated Al nanoparticle; From Puszynski et al.[92]

The results for Parr et al. were obtained by injection of Al nanoparticles into a gas burner with a very high temperature. Park et al.[93] and Rai et al.[80] studied the burning rate in a flow reactor on a high-temperature particle laden air flow. After a defined reaction time, the composition of particles was determined by a particle mass spectrometer. Then, the percent conversion and reaction rate were measured accordingly. From these studies, the authors concluded that the oxidation process occurred in condensed phase and was a diffusion limited process where the reactants passed through the oxide shell. Below the melting point of Aluminum, the oxidation process is based on diffusion of oxygen through the oxide layer;

however, in temperatures higher than melting point of Al, both Al and O diffuse through the oxide shell resulting in a faster oxidation. Since Parr et al. injected the nanoparticles into high temperature gases both the Al and O ions diffuse through the oxide shell and result in lower burning time compared to the results from Park et al.

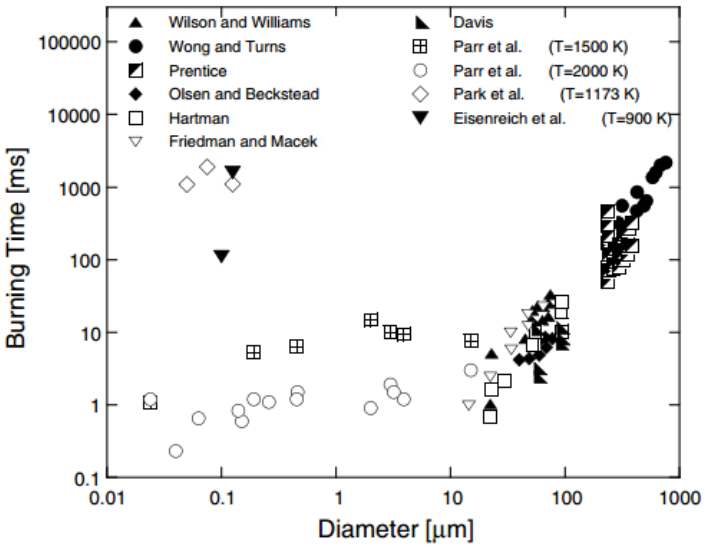

Figure 2-4 Al particle burning times as a function of particle diameter[90,94]

Inert diluent additives: Adding inert diluents to the powder mixture, results in lower combustion rate due to less heat generation and longer diffusion path for the reactants[82,95]. Additionally, different diluents decrease the reaction rate differently. This is due to the different properties of the diluents such as heat capacity and thermal conductivity[69,82].

Powder compact density: The effect of compact density on the combustion rate was investigated by Dubrovin et al.[81], by studying composites of Cr_2O_3, iron ore and Al for various iron ore particle sizes. The authors presented these results in Figure 2-5. For low densities of the mixture (roughly <2 (g/cm^{-3})), the combustion rate decreases by increasing the density.

Dubrovin et al.[81] attributed this to the effective thermal conductivity of the compact which was also found to be a function of compact density with similar dependence[96].

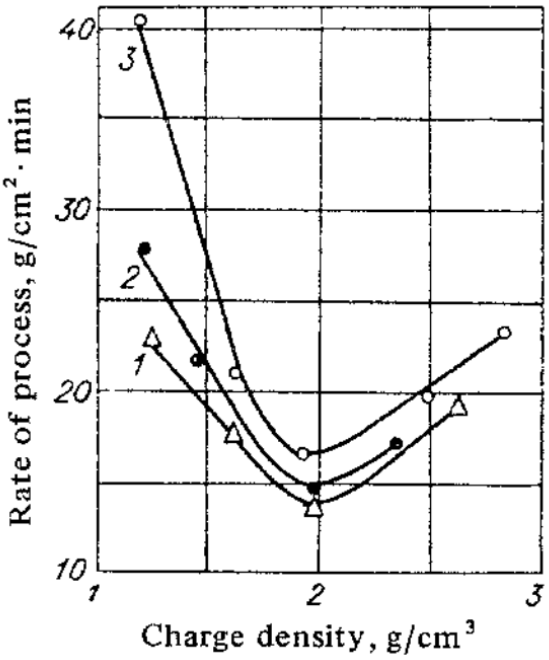

Figure 2-5 Combustion rate as a function of density for energetic composites of Cr_2O_3, iron ore and Al with iron ore particle sizes of (1) 57, (2) 50, (3) 40 μm[81]

For densities higher than the minimum point on the graph, the combustion rate increases by increasing the compact density[81].

Centrifugal force: In studies by Serkov et al.[83] and Karataskov et al.[84], centrifugal force was suggested to enhance the combustion rate of thermites. Centrifugal force is defined as the ratio of centrifugal acceleration (a) to gravitational acceleration (g). Serkov et al.[83] studied a composite which all of its components were in molten state at combustion temperature. They showed that by increasing the acceleration force from 0 to 895 (a/g), reaction rate increases from 5 (mm/s) to 28 (mm/s) which is about 6 times higher than the initial rate. The authors suggested

that the centrifugal force helped the molten Al to penetrate the pores of the unreacted mixture ahead of the combustion wave[83].

Inert ambient pressure: Dependance of combustion rate on ambient pressure is different for different thermite compositions. It is mostly associated with the presence of gaseous phase in the reaction[1]. When the combustion temperature is higher than the boiling temperature of the reactants or products gaseous phases will be generated. This gas generation is influenced by the ambient pressure. If the ambient pressure is low, the vaporized phase leaves the reaction and results in lower combustion temperature, thus lowers the combustion rate as a consequence. Some thermites such as Al-Fe_2O_3-Al_2O_3 were proven to act independent of pressure changes at pressures above 1 atm[1]. However, in vacuum range, boiling temperature of some reactants (such as Al) decrease and becomes lower than the combustion temperature, resulting in evaporation and decrease in combustion rate. In such cases, by increasing the ambient pressure, the reaction rate increases as shown in Figure 2-6[1]. Similarly, nanoscale Al has a lower boiling temperature than bulk Al making it more sensitive to ambient pressure changes.

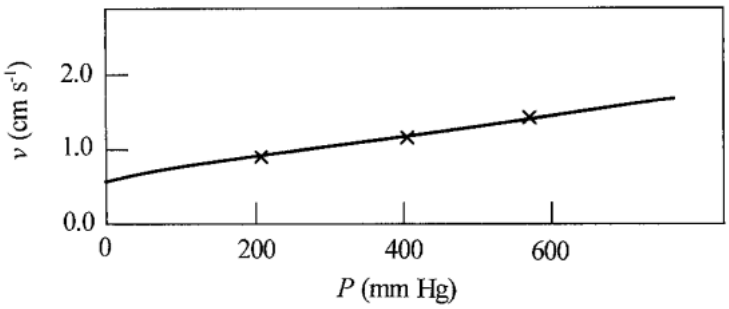

Figure 2-6 Effect of pressure on combustion rate of Al-Fe_2O_3-Al_2O_3 thermite under vacuum; From the reference [1]

In another study by Wang[97] Mg-B_2O_3-C was tested in Argon atmosphere. The results showed that in pressures of 1-13 atm, the combustion rate increased with increasing the pressure.

At 30-150 atm, the combustion change remained constant, but at high pressure atmosphere (200-1020 atm), combustion rate decreased by increasing the pressure. The author explained that in low pressure range, pressure increase reduces the reactant evaporation and loss. For pressures higher than 200 atm, the amount of heat loss to surrounding gas increases due to the increased density and thermal conductivity of the Argon gas. This heat loss results in lower combustion temperature and therefore, lower combustion rate[97].

2.3.3. Thermal analysis

Nanothermites have been studied to measure their thermal behavior such as ignition temperature, reaction enthalpy, and activation energy[24] and product compositions. The latter can be predicted by the theory of minimization of free energy. Thermal analysis has also led to prediction of adiabatic flame temperatures (AFT) and amount of gas generation. Table 2-1 shows some of the important thermodynamic properties of select thermite reactions. The full table is presented in appendix A.

Table 2-1 Thermodynamic properties of selected thermite reactions-reproduced from Puszynski et al. [24]

Thermite reaction	Q, cal/g	Q, cal/cm^3	Gas generation 1 atm, g gas/g mixture	T_{ad}, K
$2Al + Fe_2O_3 \rightarrow 2Fe + Al_2O_3$	945.4	3947	0.0784	3135
$2Al + Bi_2O_3 \rightarrow 2Bi + Al_2O_3$	505.1	3638	0.894	3319
$2Al + MoO_3 \rightarrow Mo + Al_2O_3$	1124	4279	0.2473	3688
$2Al + WO_3 \rightarrow W + Al_2O_3$	696.4	3801	0.1463	3253
$2Al + 3CuO \rightarrow 3Cu + Al_2O_3$	974.1	4976	0.3431	2843

One of the most common ways to measure reaction enthalpies is Differential Scanning Calorimetry (DSC). A schematic picture of a DSC machine is shown in figure 2-7. This machine has a sample holder and a reference material. The chamber is heated by a pre-set heating rate and the heat flow required to keep the sample and reference in the same temperature is recorded.

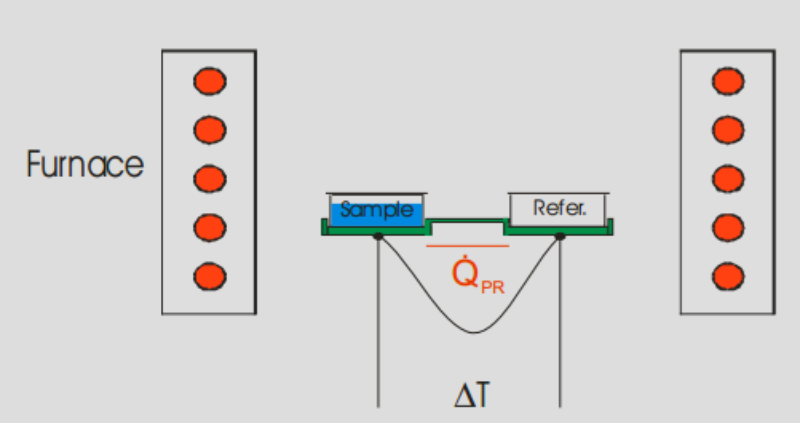

Figure 2-7 Schematic figure of DSC chamber; From the reference [98]

The resulted graph shows the heat flow versus temperature or time. During heating, the sample may undergo endothermic or exothermic transitions. Enthalpy of reaction can be calculated by integrating the area under the heat flow-temperature graph. A sample DSC graph is shown in Figure 2-8. The direction of exothermic reaction is usually shown in the corner of the diagram and the opposite direction peaks indicate endothermic reactions. In Figure 2-8, an exothermic reaction is shown. The onset temperature for this reaction is 435°C which is called ignition temperature. The reaction reaches its peak at 527°C and is completed at 575°C. The area under the peak indicates the absolute value of the heat of the reaction as shown in the figure. The adiabatic flame temperature (AFT) is the maximum flame temperature resulting from an adiabatic combustion process, and is measured theoretically. A list of AFT values for thermite reactions can be found in Appendix A.[29]

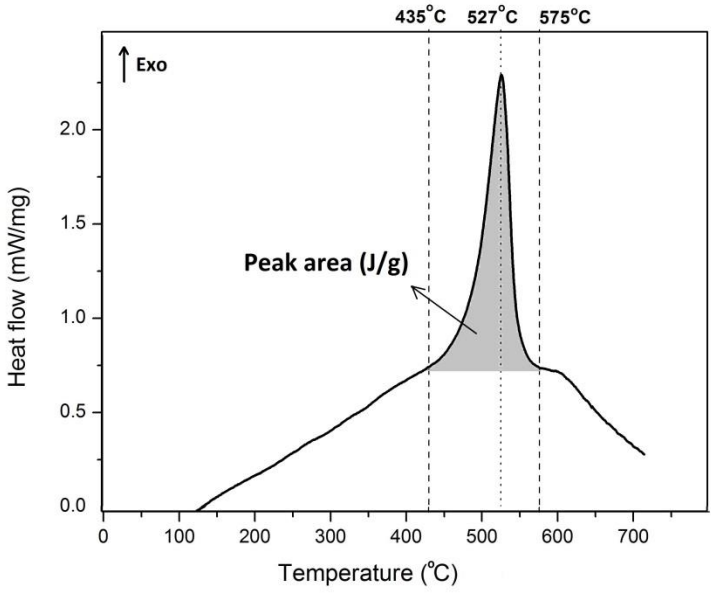

Figure 2-8 Example DSC diagram; the exothermic peak shows an exothermic reaction. Heat of reaction is calculated from the area under the peak.

2.3.4. Microstructure and phase analysis

The reaction kinetics of nanothermite reactions is of interest, when it comes to predicting the products and detailed steps of the reactions. Phase analysis methods such as XRD, are usually combined with thermal analysis results to study the reaction kinetics of thermite reactions. DSC/TGA results show the endothermic and exothermic reactions indicating phase changes at certain temperature. While combined with XRD or EDAX, the reaction pathways are predictable.

As an example, Wang et al.[16] studied the mixture of nitrocellulose passivated Al nanoparticles and 12 nm diameter CuO nanoparticles to determine the effect of the fuel/oxidizer mass ratio on the reaction products. The study showed that a fuel rich composition results in the

formation of Al_2O_3 and pure Cu[16]. The authors have suggested 2 steps for the Al/CuO reaction. First,

At 570°C:

$$Al + 3CuO \rightarrow \frac{1}{2}Al_2O_3 + \frac{3}{2}Cu_2O \qquad \text{(R2-1)}$$

Then at 800-900°C:

$$Al_2O_3 + Cu_2O \rightarrow 2CuAlO_2 \qquad \text{(R2-2)}$$

And finally at 900-1000°C:

$$CuAlO_2 \rightarrow \frac{1}{2}Al_2O_3 + Cu + O_2 \qquad \text{(R2-3)}$$

Umbrajkar et al. [15] and Schoenitz et al. [99] studied Al/CuO and Al/MoO_3 reactions respectively using the similar technique. In general, the products of nanothermite reactions were found to be mainly aluminum oxide (Al_2O_3) and a metal or metal alloy[1,2]. Formation of the metal alloy depends on the flame temperature and duration as well as the size of precursors. Based on these parameters, a wide range of alloys and intermetallic compounds can be achieved as products. Accordingly, specific thermite reactions can be designed in order to produce specific compounds. This process is called reactive sintering which is one of the interesting applications of thermites. As an example, AlNi, which is an attractive structural material, was synthesized by heating Al/Ni thermite under high pressure condition[100]. There is also an amount of gas generated depending on the reactant type. Gas generation from the thermite reactions is mainly attributed to the formation of vapors of metals (such as Cu, Fe and Ni), the elemental oxygen (formed from the decomposition of the oxidizer), the gas of metal oxides if the combustion temperature is high enough, and other gaseous reaction products. While the metal vapor forms at a temperature which is above the boiling temperature of the metal, the release of elemental oxygen from the decomposition of the oxidizer component of MICs can be significant as well.

2.4. Applications

From the time that Goldschmidt[3] discovered thermite reactions, bulk thermite composites were being used in various applications. These applications included: preparation of metals and alloys[101–104], centrifugal coating[105], material synthesis[97,104,106], welding[107,108], and etc. By development of thermites in nanoscale, their applications were brought to another stage ranging from developing and designing nano-initiators[18], micro-thrusters[109–111], micro-propellants[112,113], and rocket fuel[109,112,114] to their application in cancer therapy[115]. This thesis mostly focuses on the potential application of nanothermites in joining and welding where high amount of energy release and presence of molten state are preferred[116].

2.4.1. Joining

There is an extensive work done on the use of micron-sized thermites for joining application but there is little literature on the use of nanothermites. However, the lower activation energy for ignition of nanothermites and therefore, easier ignition, is the advantage of using nanothermite over bulk thermite. In chapter 1, the traditional thermite welding process was described to better understand and suggest the effectiveness of thermite reactions for advanced joining applications. In this section, we review the available literature on the use of thermite reactions for joining of both similar and dissimilar materials. In 1986 Miyamoto et al.[117] used a pressurized combustion reaction to produce ceramic-to-metal welds of Mo-TiB_2-Mo and Mo-TiC-Mo. Ti powder was mixed with B or C and the mixture was pressed between two Mo surfaces. The mixture was then electrically ignited and the exothermic reaction resulted in formation of TiB_2 and TiC welded to Mo at the interfaces. Weld strengths were measured to be 20-40 MPa and ~10 MPa for Mo-TiB_2-Mo and Mo-TiC-Mo couples respectively. In a research by Pascal et al.[118] Al and Ni mixture was used to weld superalloy substrates. The process is referred to as self-propagating high-

temperature synthesis (SHS) joining. By heating the Al+Ni mixture to 920 K, an exothermic reaction starts and forms AlNi. The released heat of the reaction rises the temperature to above melting temperature of NiAl (1950K). This heat also causes surface melting of the substrate, which wetted the contact surfaces. As a result, an Al-rich Ni-base superalloy was formed at the interfaces. Bahrami et al.[119] used a mixture of micron-sized particles of Al-CuO-Ni, with a fuel-rich composition, to join Al 1100 sheets. The process was done under a uniaxial pressure of 9 MPa. A good weld was achieved with mean shear strength of 27 MPa which was much higher than that of diffusion welded samples (8.05 MPa) and by 30% close to that of the base metal (Al 1100). The authors measured the heat affected zone to be 750 µm thick in each side of the weld. SEM and XRD results confirmed the joint to be composed of an Al-matrix composite reinforced by Al_3Ni_2, Al_7Cu_4Ni and Al_2O_3 phases. Due to the high-strength joint achieved, this process was found to be a good potential for welding of non-refractory materials. Swiston et al.[64] used Al/Ni in multilayer foil geometry to join bulk metallic glass through a self-propagating exothermic reaction. They suggest that both the foil thickness and the applied pressure, affect the weld strength. The authors reported shear strengths as high as 480MPa. The reaction was activated by applying electrical potential of 30 V to the foils.

Al-Ni [45–47,119–121] was commonly used as an energetic material for joining, however, its price is much higher than Al-metal oxide composites. Accordingly, I focused on the use of Al/NiO as a good candidate for joining application during the course of this thesis.

CHAPTER 3

Synthesis, Preparation and Characterization Methods

This chapter explains the experimental procedures and methods for synthesis, preparation and characterization of Al-NiO and Al-CuO nanothermite samples.

3.1. Reactants

The nanothermite samples were prepared by mixing reactants of various types and nanostructures. The detailed information for each reactant used in preparation of the above nanothermites is provided in this section.

3.1.1. Al nanoparticles

Aluminum nanoparticles with diameter of 50-120 nm were purchased from Sigma-Aldritch. The nanoparticles had a 5 nm thick oxide shell. By assuming the averaged nanoparticle diameter of 80 nm, this shell thickness indicates the content of Al of about 60%. The oxide shell would protect the Al nanoparticles from further oxidation however it is essential to keep the Al nanoparticles away from the moisture to minimize further oxidation and reduction in active content of Al, so the Al nanoparticles were safely stored in an air-tight bottle in an argon (Ar) filled glovebox.

3.1.2. CuO nanowires

Copper oxide nanowires were made hydrothermally based on a template free solution route introduced by Lu et al.[122]. First, solutions of 1 M KOH and 7 M NH_3 were prepared separately in deionized (DI) water. Then, a solution of 0.1 M $CuSO_4$ was prepared by dissolving 798 mg of anhydrous copper sulfate ($CuSO_4$) in 50 ml of DI water. The solution was put on a hotplate-stirrer and was stirred rigorously using a magnetic stir bar. 20 mL of the 1 M KOH

solution was added to the beaker using an Eppendorf digital pipette. It was stirred for an additional 3 minutes, then, 7.5 mL of the 7 M NH_3 was added to the beaker using the digital pipette slowly and stirred rigorously for another 3 min. The color of the solution turned to turquoise blue at this stage and $Cu(OH)_2$ nanostructure started to form. The beaker was then sealed by parafilm and aged for 12 hours. Then the precipitates were filtered by a filter paper with 0.2 µm pore size and washed 2 times by DI water slowly to allow the $Cu(OH)_2$ to form a thin layer on the paper. The paper was then opened and dried in a convection oven at 50° C for 1 hour. Then the filtrate was peeled off the paper carefully and put in an alumina cup. It was then heated in a furnace at 375°C for 4 hours and the blue $Cu(OH)_2$ nanowires turned into black CuO nanowires. Finally the black product was ground in an alumina mortar to form a fine powder of CuO nanowires. The produced nanowires were stocked in a sealed glass bottle for later use. Figure 3-1 shows an SEM image of the as-produced CuO nanowires. Their diameter is 12-15 nm and their length is in the range of few microns.

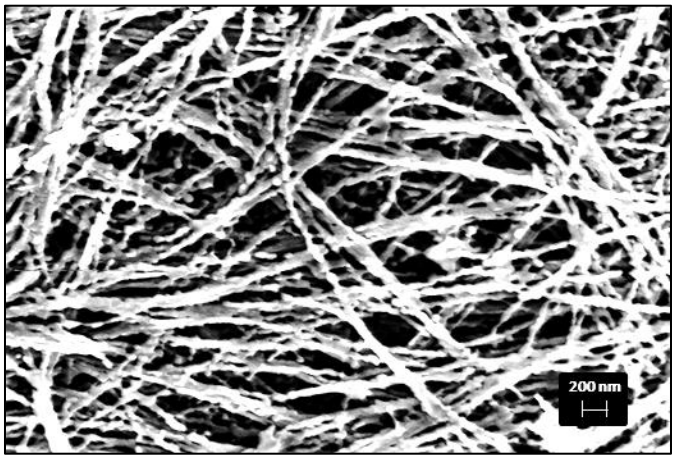

Figure 3-1 SEM image of as produced CuO nanowires; From the reference [123]

3.1.3. NiO nanowires

The NiO nanowires were synthesized in a conceptually similar way to CuO nanowires. First, NiOH nanostructures were formed at 120°C in a weak alkaline solution when $Ni(NO_3)$ reacted with a Ni source. NiO nanowires were then grown by annealing NiOH nanostructures at 500°C for 1 hour in air. Figure 3-2 shows an SEM image of the as-produced NiO nanowires. Their diameter is about 12-15 nm and their length is in the range of few microns.

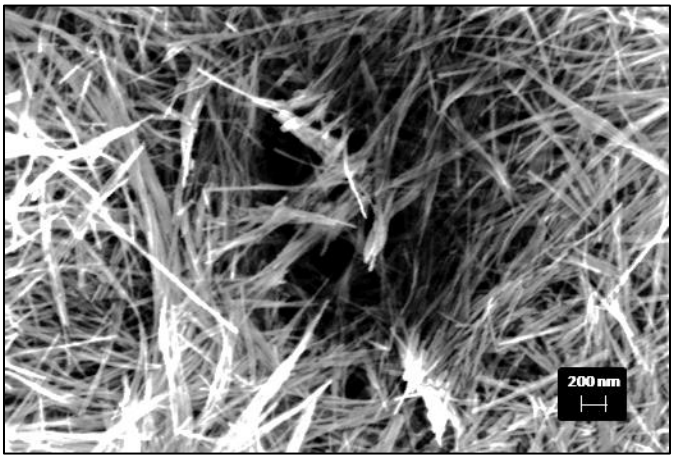

Figure 3-2 SEM image of the as produced NiO nanowires; From the reference [124]

3.2. Nanothermite preparation

To prepare nanothermite mixtures, different amounts of Al nanoparticle, metal oxide and in some cases, other additives such as copper micron powder (Cu, spherical, d=8-10 µm) were used. The copper micron powder was purchased from Sigma Aldritch. In order to choose these amounts, first the equivalence ratio (ϕ) was varied and tested on hot-plate as explained in section 2-3-1. After finding the ratio associated with the most energetic mixture, various amounts of Cu micron powder were added to the most energetic mixture of Al and oxidizer.

The weight ratios of the oxidizer (NiO/CuO) in these composites were used to calculate the fuel to oxidizer equivalence ratio ϕ, defined in this study by

$$\Phi = \frac{\left(\frac{F}{O}\right)_{act}}{\left(\frac{F}{O}\right)_{stoi}} \quad (3\text{-}1)$$

where $(F/O)_{act}$ is the measured mass ratio of the fuel to oxidizer and $(F/O)_{stoi}$ is the stoichiometric ratio calculated from the following thermite reaction between Al and NiO:

$$2Al + 3NiO \rightarrow Al_2O_3 + 3Ni \qquad \Delta H_r = 3.4 \text{ kJ/g} \qquad (R3\text{-}1)$$

And the following reaction between Al and CuO

$$2Al + 3CuO \rightarrow Al_2O_3 + 3Cu \qquad (R3\text{-}2)$$

In this study, the equivalence ratios were calculated from the mass ratio of Al nanoparticles to oxidizer nanowires by taking into account the mass of the alumina shell. For this purpose the content of Al in Al nanoparticles was assumed as 60%. This treatment is rather rough due to the assumption of the averaged particle diameter and the uniform shell thickness.

Table 3-1 shows the compositions of samples prepared. After accurately weighing the precursors, they were poured in a 50 ml beaker and 10 mL of isopropanol was added to the beaker. The mixture was stirred carefully with a spatula in order to break the granulated clusters and was then put in a bigger beaker (200 mL) with 20 ml water in it. The larger beaker was then put in an ultrasonic bath for about 3 hours until complete evaporation of the solvent. The remaining powder was in the form of granulates and some paste stuck to the wall of the beaker. This mixture was then scraped carefully from the beaker's wall using a small spatula and let dry completely at room temperature for 5-6 hours. Then, granulates were broken down with a spatula very carefully to reach the consistency of a loose powder. This powder was pressed in a stainless steel die with diameter of 3 mm and height of 5 mm to make nanothermite pellets with diameter of 3 mm and height of 0.7 mm.

The prepared samples were characterized by several methods to determine their structural properties before and after reaction as well as their thermal and physical behaviors during reaction.

Table 3-1 The compositions of nanothermite mixtures studied in this thesis

Sample #	Composition	Al/oxidizer (mass)	Equivalence ratio (ϕ)	Cu (% mass)
1	Al-NiO	1.62	4	0
2	Al-NiO-Cu	0.24	0.6	50
3	Al-NiO-Cu	0.60	1.5	50
4	Al-NiO-Cu	1.62	4	50
5	Al-NiO-Cu	1.62	4	60
6	Al-NiO-Cu	1.62	4	80
7	Al-CuO-Cu	1.53	4	75
8	Al-CuO-Cu	1.53	4	77.5
9	Al-CuO-Cu	1.53	4	80

3.3. Characterization

3.3.1. Feasibility test on hot-plate

The as-produced pellets were initially tested on a hotplate at 500°C to observe the optical emission and reaction rate. This preliminary characterization was only a qualitative test by observing the light emission from the sample by bare eye and the ratios mentioned in Table 3-1, were selected from a wide range of compositions after the initial test on hot plate. These compositions were found to be the most effective in terms of light emission and controllability.

3.3.2. Thermal analysis (DSC)

For further quantitative characterization of nanothermite samples, thermal analysis was conducted using a STA machine combining a differential scanning calorimeter (DSC) and thermo-gravimetric analysis (TGA). For these DSC tests, samples were weighed (with about 10-25 mg) before placing into the chamber. These tests were performed in a NETZSCH STA 409 PG/PC simultaneous thermal analysis (STA) machine shown in Figure 3-3. In order to eliminate reactions with oxygen and nitrogen from the air, a sapphire reference and argon atmosphere were used. The heating rate was set to 10 K/min. The experimental data was analyzed by the NETZSCH Proteus Analysis software and used to determine the energy release and the onset temperature of ignition.

Figure 3-3 Netzsch STA machine used for thermal analysis-From the reference [125]

In DSC diagrams, exothermic peaks are an indication of the thermite reaction. The ignition temperature was achieved by finding the onset temperature of the reaction peak. The reaction enthalpy was calculated by integrating the area under the reaction peak by the software. Appendix B shows an example of a DSC test result analyzed by the Proteus analysis software. A typical graph was also explained in Chapter 2.

3.3.3. X-Ray Diffraction (XRD)

To determine the compositions of reaction products and their microstructures, DSC processed samples were examined by XRD, SEM and EDAX to determine the final products of the thermite reaction. The XRD patterns were captured using a Rigaku SA-HF3 (1.54 Å Cu Kα) x-ray source equipped with an 800 µm collimator, operating at an excitation voltage of 50 kV, 40 mA current and 2 kW power, shown in Figure 3-4.

Figure 3-4 X-Ray Diffraction equipment for phase analysis of samples-From CAMJ lab[126]

3.3.4. Secondary Electron Microscope (SEM)

In order to characterize the reactants and reaction products, both unreacted and DSC processed pellets were studied by Scanning Electron Microscope (SEM), and Energy Dispersive X-ray Spectroscopy (EDAX). Prior to SEM imaging, the samples were 10 nm gold coated.

CHAPTER 4

Characterization of Al Nanoparticle/NiO Nanowire Composites

This chapter is a preliminary investigation of Al-NiO nanothermite composite. The samples are studied by SEM during the preparation process. After completion of the exothermic reaction, the products are studied by SEM, EDAX and XRD to identify the produced phases. These results, combined with thermo-chemical characterization and MD modeling of the nanothermite reaction, were published as a journal paper titled "Characterization of thermochemical properties of Al nanoparticle and NiO nanowire composites"[127] in collaboration with other researchers.

4.1. Introduction

Metastable intermolecular composites (or MICs) have drawn much attention recently in developing reliable and high performance power generation systems due to their nano-sized components which allow for tuning of the ignition temperature, reaction propagation rate and volumetric energy density[2,19,20,128–130]. Applications include gas generators, micro-heaters, micro-thrusters, micro-detonators, micro-initiators[26], and combustion joining. Gasless thermite reactions are desired for the later application since the thrust generated from the gas production disturbs the joining process and results in cracks and defects. Gas generation from the thermite reactions is mainly attributed to the formation of vapors of metals (such as Cu, Fe and Ni), the elemental oxygen (formed from the decomposition of the oxidizer), the gas of metal oxides if the combustion temperature is high enough, and other gaseous reaction products. While the metal vapor forms at a temperature which is above the boiling temperature of the metal, the release of

elemental oxygen from the decomposition of the oxidizer component of MICs can be significant as well. Recently Sullivan and Zachariah characterized the reaction mechanism of a variety of MICs[131] and they found that, while most oxidizers such as CuO and SnO_2 decompose before the thermite reactions occur, which possibly indicates solid-state reactions, the decomposition of Fe_2O_3 becomes rate-limiting for igniting its thermite reaction. More investigations are needed in order to understand the cause of these different ignition mechanisms. Among the bulk scale thermite reactions, the Al-NiO system was reported to produce less gas [132]. Theoretically, the gas (vapor and oxygen) generation from the Al/NiO thermite is about 2% of the gas produced from the Al/CuO thermite and is much lower than other comparable thermite systems. It is therefore worthwhile to investigate the properties of the corresponding MIC made of the Al and NiO nanostructures. The research objectives of this work were to synthesize and characterize the microstructures of the powder type Al nanoparticle and NiO nanowire MIC and to investigate its products.

In literature there are few research papers on characterizing the Al/NiO based composites. Recently an Al/NiO MIC was developed on a silicon substrate [27] for fabricating a two-dimensional geometry. The process started from the thermal oxidation of a Ni film to form a NiO honeycomb. Then an Al layer was coated onto this honeycomb using the thermal evaporation. The produced Al/NiO MIC exhibited a low ignition temperature and improved interfacial contact area between Al and NiO. The energy release per mass data was reported but the method for determining that data was not reported. In that same study the fabrication method was developed with the presence of a silicon substrate and may not be suitable for other previously mentioned applications. A more detailed investigation on thermo-chemical behaviors and product microstructures of the powder type Al/NiO MIC is highly desired. Thermal behavior

of the nanothermite and its heat production is of extreme importance for its candidacy for joining applications, as a promising thermite reaction for combustion joining, should have enough energy density to melt the adjacent surfaces upon ignition.

The reaction properties of a powder MIC depend on the particle size, shape, morphology and microstructure of its fuel and oxidizer components. A variety of metal-oxide nanostructures have been fabricated and implemented in developing high energy density MICs, which take the forms of nanospheres [133], nanowires [9,134], nanofibers [135], and nanorods [10,136]. Usually the fineness (or particle sizes) and bulk density of these oxidizers and the degree of their intermixing and interfacial contacting with the Al nanoparticles are among the critical factors which influence the ignition mechanism [134,137]. A recent study showed that the use of CuO nanowires resulted in better mixing between the fuel and oxidizer components of MIC and subsequently facilitated a low-temperature ignition [134]. Their measurements demonstrated the pressurization rate from a composite of Al nanoparticles and porous CuO nanowires was about ten times of that from the Al nanoparticle and CuO nanoparticle MIC. Other means such as the fabrication of the core-shell nanostructures [9,138–140] and intermetallic multilayers [129,141–143] were recently developed to enhance the energetic properties of MICs. And the core/shell nanowire based thermites indeed exhibited an improved mixing homogeneity and low activation energy [9]. In this study, an effective preparation method to improve intermixing between two components was first developed. And then the reaction products were examined by the electron microscopy and x-ray diffraction in order to identify their chemical compositions and microstructures.

4.2. Experimental

The Al-NiO samples were prepared as mentioned in Chapter 2. Due to safety requirements, the pure Al-NiO samples were sent to a collaborating group in Ottawa to conduct

the thermal analysis tests. To determine the compositions of reaction products and their microstructures, three Al/NiO pellets with Φ = 4 were heated in argon to 150°C, 450°C and 800°C on a hotplate. These experiments were performed in a glove box and the processed pellets were then examined by SEM, EDAX and XRD. For SEM imaging, the samples were 10 nm gold coated. The XRD patterns were captured using a Rigaku SA-HF3 (1.54 Å Cu Kα) x-ray source equipped with an 800 μm collimator, operating at an excitation voltage of 50 kV, 40 mA current and 2 kW power as explained in Chapter 2.

4.3. Results and discussion

Figure 4-1 shows three SEM images of the mixed Al nanoparticles and NiO nanowires composite before (a) and after (b and c) mixing in ultrasound bath. Figure 4-1(a) demonstrates the sizes of Al nanoparticles (about 80 nm) and the diameter (about 20 nm) and length (about 1.5 μm) of NiO nanowires after mixing two components. These distinct images of two components show a poor dispersion of nanoparticles in the network of nanowires. After the solution was sonicated and dried, Al nanoparticles were able to decorate on NiO nanowires, as shown in Figure 4-1(b). A higher resolution SEM image shown in Figure 4-1(c) demonstrates the nanowire branches beneath the Al nanoparticles. This process was expected to significantly increase the contact area between two components improving thermite performance.

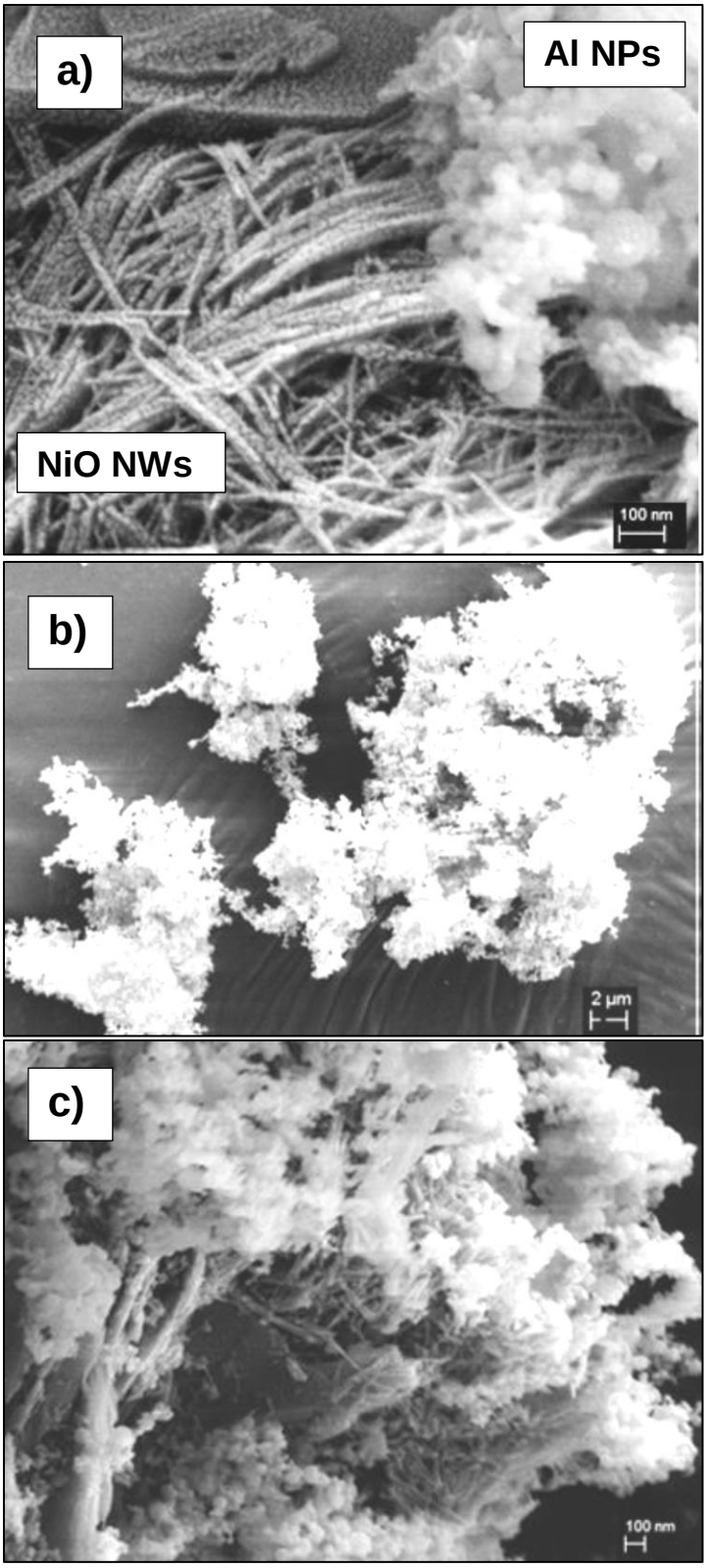

Figure 4-1 SEM images of the Al nanoparticle and NiO nanowire composites before (a) and after (b and c) sonication. Scale bar: 100 nm in (a), 2 µm in (b) and 100 nm in (c).

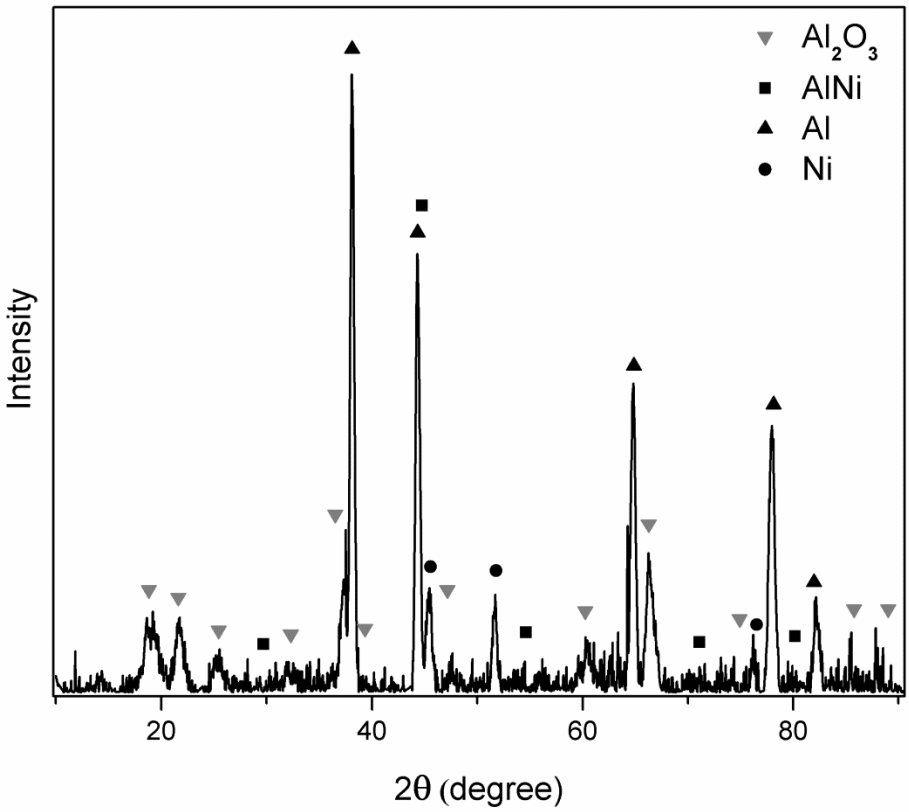

Figure 4-2 XRD patterns measured from the reaction product of Sample 1, Al-NiO (ϕ=4)

The XRD analysis was performed on the reaction products of an Al-NiO sample after DSC test. The sample was a fuel rich MIC with ϕ = 4. As shown in Figure 4-2, the chemical compositions were identified as Ni, Al, AlNi and Al_2O_3. Note that the identification of Al_2O_3 using XRD is evidential from the previous study[144]. In addition to those solid products, gaseous species such as O_2 possibly was formed as well. It is interesting to reveal the production of AlNi from the Al/NiO MIC. As a comparison, the formation of Ni was shown with lower and fewer XRD peaks, while Al still existed as a relatively large amount. Based on these observations, the following reaction was responsible

$$5Al + 3NiO \rightarrow 3AlNi + Al_2O_3 \qquad \Delta H_r = 3.2\ kJ/g \qquad (R4\text{-}1)$$

Note that in this study, the Φ = 4 MIC contained abundant Al nanoparticles and thus made the reaction (R4-1) feasible. Note that the propagation of (R4-1) does not necessarily require the completeness of (R3-1), since the decomposition of NiO may occur first and be followed by the reaction between Al and Ni. A further study on elementary reactions related to (R3-1) and (R4-1) is needed in order to gain more insights on this issue. To further characterize these microstructures of the products, the SEM and EDAX analyses were performed on the same product examined by XRD. Figure 4-3 shows two typical structures observed from the Φ = 4 MIC: (a) a sphere which was rich in Ni and Al; and (b) a bunch of Al_2O_3 crystalline structures. The co-existence of Ni and Al in the sphere is possibly in the form of AlNi.

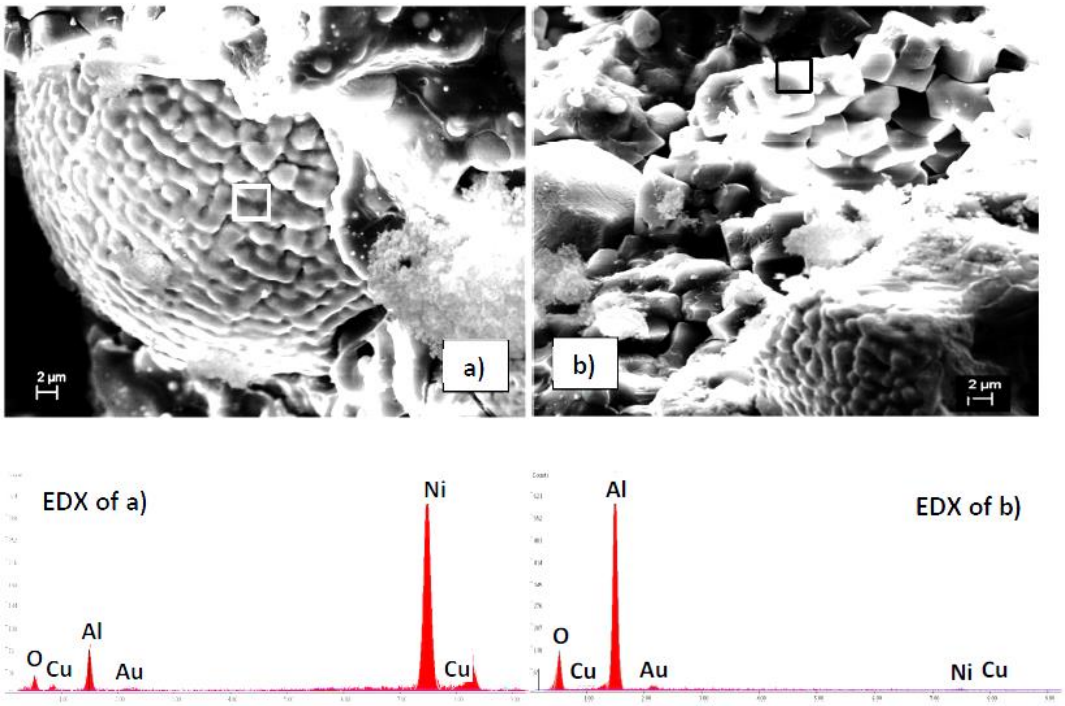

Figure 4-3 SEM images and respective EDX patterns obtained from the reaction products of Sample 1, Al-NiO (ϕ=4).

4.4. Conclusions

In summary, the Al/NiO MIC was prepared using the NiO nanowires synthesized hydrothermally with an average diameter of about 20 nm and a length of a few microns. A fuel rich sample with equivalence ratio of $\Phi = 4$ was studied. The sonication process of 20 minutes helped produce the well dispersed Al nanoparticles which were decorated on the NiO nanowires. The chemical compositions and microstructures of these MICs were examined using XRD, SEM and EDAX, which showed the evidence of the AlNi phase, together with the Al, Ni and Al_2O_3, from the fuel rich Al/NiO MICs.

CHAPTER 5

Thermo-Chemical Characterization of an Al Nanoparticle and NiO Nanowire Composite Modified by Cu Powder

In this chapter, thermo-chemical properties of the Al nanoparticle and NiO nanowire composites modified by the micro-sized copper additive were investigated experimentally. Their onset temperatures of ignition and energy release data per mass were characterized using differential thermal analysis measurements. These microstructures and chemical compositions of reaction products were analyzed using scanning electron microscopy, energy dispersive X-ray spectroscopy and X-ray diffraction. The fuel-rich Al/NiO/Cu composites produced two types of metallic spheres. Copper spheres were formed from melting and solidification of the copper additive, while AlNi composite spheres were identified by the energy dispersive X-ray spectroscopy and X-ray diffraction analyses. It was found that the amount of the copper additive did not significantly influence the onset temperature of thermite peaks, but caused a dramatic change in energy release. The aforementioned ignition and energetic properties were compared with those from the Al nanoparticle and CuO nanowire composites. The content of this chapter was presented in a paper submitted in March 2013 titled "Thermo-Chemical characterization of an Al nanoparticle and NiO nanowire composite modified by Cu powder".

5.1. Introduction

In a vast range of Al/metal-oxide nanocomposites which have been investigated with their potential applications in advanced manufacturing [26,27], the Al/NiO composite shows its

advantage due to its low gas generation, confirmed by the data shown in Table 5-1, which is preferable for achieving a localized heat management [145]. For some applications an inert metal can be added into the MIC, which provides an extra heat absorber for adjusting the heat transfer rate. The objectives of this study were to fabricate and characterize a powder type MIC composed of Al nanoparticles and NiO nanowires and to investigate the role of the copper additive in tuning the onset temperature of ignition and energy release of the produced MIC.

Table 5-1 The adiabatic flame temperature (AFT), amount of gas/vapor production, melting point ($T_{melting}$) and boiling ($T_{boiling}$) temperature of the produced metal from a variety of thermite systems [29]

Composition	AFT (°C)	Gas production (moles gas/100 g)	$T_{melting}$ (°C)	$T_{boiling}$ (°C)
Al + CuO	**2570**	**0.5400**	**1085**	**2562**
Al + NiO	**2914**	**0.0108**	**1455**	**2913**
Al + Fe_2O_3	**2862**	**0.1404**	**1538**	**2862**
Al + Bi_2O_3	**3046**	**0.4731**	**271.5**	**1564**
Al + WO_3	**2980**	**0.1434**	**3422**	**5555**
Al + MoO_3	**3415**	**0.2425**	**2623**	**4639**

The gas (vapor and oxygen) generation from the Al/NiO thermite is about 2% of the gas produced from the Al/CuO thermite and is much lower than other comparable thermite systems. The production of less gas, in combination with the localized heat generation and adsorption, is desirable for the material joining purpose which requires less component vibration and little flow disturbance [116]. And recently the Al/Ni bimetallic thermite has been developed in performing material bonding and component joining [46,120]. Thus, a throughout investigation on the synthesis

and thermo-chemical characteristics of the Al/NiO nanostructured composites is needed in order to further explore the applications of MICs in manufacturing and other civil industries. The thermite reaction of the Al/NiO system was shown before as Reaction (R3-1).

Although the thermodynamic properties of this reaction are well known for bulk Al/NiO MICs, very few research articles are available on demonstrating the thermo-chemical properties of the nano-structured Al/NiO composites. Recently an interesting Al/NiO geometry was reported for developing an energetic material on the silicon substrate [27]. That process included producing a two-dimensional NiO nano-honeycomb using the thermal oxidation of a Ni thin film and depositing an Al layer onto this honeycomb by thermal evaporation. The energetic material produced from that method showed several advantages such as a low ignition temperature, enhanced interfacial contact area, reduced aluminum oxidation and easier integration into a microsystem. The reported fabrication technology, however, was developed with the presence of a silicon substrate and has not been investigated for these applications including joining and bonding. It is expected that the structure of these honeycombs is not suitable for joining of micro-meter sized components such as electronic wires. A powder type MIC is more desirable for the joining purpose due to its easy delivery to the processing site and flexibility in changing the fuel/oxidizer equivalence ratio and the concentration of the additive by mixing.

In order to achieve high-quality joining, energy production from the thermite reaction and heat management at the bonding location close to the joint are two key parameters and need to be carefully addressed. In this study a copper additive was added into the Al nanoparticle and NiO nanowire composite in order to modify the reaction and thermal properties of the system. This additive plays a few roles. First, the addition of copper into the thermite system provides a heat sink which absorbs sufficient heat from the thermite reaction and prevents the quick heat transfer

from the reaction site. Without the copper powder, heat is easily transferred to the surroundings by means of conduction and convection and energy available for joining will be reduced. Secondly, since the melting point of copper (1085°C) is much lower than the flame temperature of the Al/NiO thermite (2914°C), the added copper powder will melt into liquid which is essential for facilitating the joining process. The presence of the copper in the composite however modifies the concentrations of the Al and NiO in the system and hinders the reaction propagation. In addition, copper may reduce the interfacial contact area between the Al and NiO components. Nevertheless, the addition of copper powder in the Al/NiO MIC provides a method to tune the thermite reaction rate, change the heat transfer path and eventually optimize the MIC for the joining application.

This study focused on the preparation and characterization of well-dispersed Al nanoparticles and NiO nanowires for producing a powder MIC. The fuel rich composites were investigated in order to optimize the effective use of the available surface area of NiO nanowires. The microstructures of Al/NiO reaction products were studied using SEM (scanning electron microscopy), XRD (X-ray diffraction) and SEM-EDX (energy-dispersive X-ray spectroscopy) analysis. DSC (differential scanning calorimetry) and TGA (thermogravimetric analysis) tests were performed to qualify the influences of the equivalence ratio and copper additive on the onset temperature and energy release data.

5.2. Experimental

Al-NiO-Cu and Al-CuO-Cu nanothermite samples were prepared in accordance to the method indicated in chapter 2. The copper micro-powder with a diameter range of 5-8 μm was used as the additive. The selection of the micro-sized copper powder aimed at reducing the effect

of the interfacial contact area between two nano-sized reactants. The compositions indicated in Table 3-1 were employed except sample 1.

The onset temperature of ignition and energy release were investigated using the DSC data. To determine the compositions of reaction products and their microstructures, the Al/NiO/Cu and Al/CuO/Cu pellets with $\Phi = 4$ and the amount of 80% copper additive were heated in argon to 150°C, 450°C and 800°C. These experiments were performed in a glove box and the processed pellets were then examined by SEM, EDAX and XRD.

5.3. Results and discussions

5.3.1. Microstructures of reactants

Figure 5-1 shows two SEM images of an unreacted Al/NiO composite (a) before and (b) after ultrasound mixing with $\Phi = 4$. It is important to maximize the interfacial contact between two reactants when the solid-state reactions are investigated. In Figure 5-1(a) these NiO nanowires were found in bundles and were not mixed well with the agglomerated Al nanoparticles. Figure 5-1(b) shows, after ultrasound mixing, NiO nanowires were decorated with Al nanoparticles and their interfacial contact surface area was expected to increase dramatically. This characteristic is extremely important in improving the ignition performance of nanothermite composites [26]. On the enlarged image in Figure 5-1(b), some NiO nanowires were broken into shorter segments due to ultrasound mixing. This shortening process might slightly enhance the reactivity of these oxidizer nanowires thanks to their increased surface area.

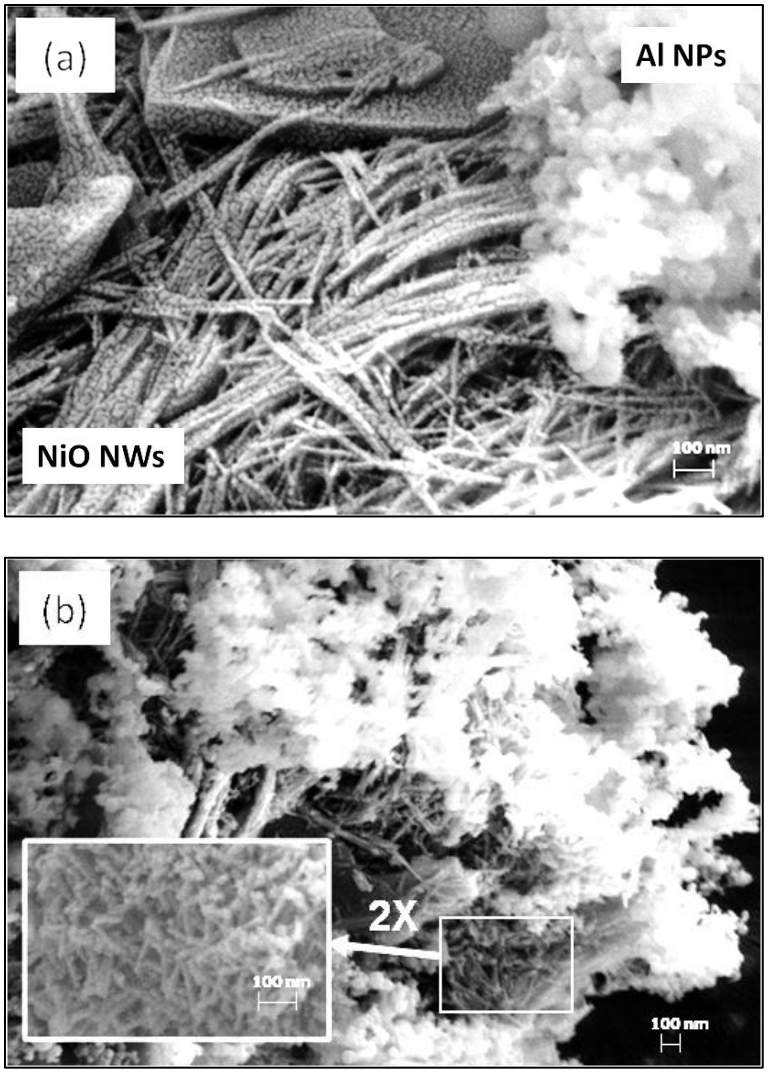

Figure 5-1 SEM images of the Al/NiO composites: (a) before ultrasound mixing; (b) after ultrasound mixing. The insert in (b) shows the shortened nanowires.

5.3.2. Microstructures of products

Figure 5-2 shows three SEM images of the reacted Al/NiO/Cu, shown in 5-2(a) and (b), and Al/CuO/Cu, shown in 5-2(c), composites for $\Phi = 4$ and with the 80% copper additive. Figures 5-2(a) and (b) were images taken from the different locations in the same sample. These composites were heated to 800°C. These two images show that, together with the accompanying EDAX data, the products from the Al/NiO and Al/CuO thermite reactions formed micron-sized

spheres which were embedded in a porous Al_2O_3 matrix. Figures 5-2(a) and (b) reveal two different types of spheres. From the EDAX pattern shown in Figure 5-3(a), which was taken from the sphere (with the size of 30 μm) shown in 5-2(a), the compositions of this sphere were identified as Cu, O, Al and Ni. The atomic ratios of these elements are listed in Table 5-2. These data, supported by the XRD measurement, suggest the sphere is mainly composed of copper with some fraction of Al_2O_3. The signal from Ni is quite small. The 'dotted' sphere in Figure 5-2(b) will be discussed later in this paper. Figure 5-2(c) shows a sphere (with the size of 8 μm) formed from the Al/CuO/Cu composite. Its EDAX pattern, shown in Figure 5-3(b), identifies the elements of Cu, O and Al. Their atomic ratios are listed in Table 5-2 as well. These data indicate the formation of a copper rich sphere. The above analysis based on Figures 5-2 and 5-3 suggests, the average size of metallic spheres produced from the Al/NiO/Cu composite (30 μm) was much bigger than those spheres produced from the Al/CuO/Cu composite (8 μm). The formation of the liquid sphere during the thermite reaction will be discussed later on. The larger size of these spheres produced from the Al/NiO/Cu composite can be attributed to the less gas production and greater energy release from its thermite reaction. The Al/NiO/Cu composites produced the other type of spheres, as discussed later.

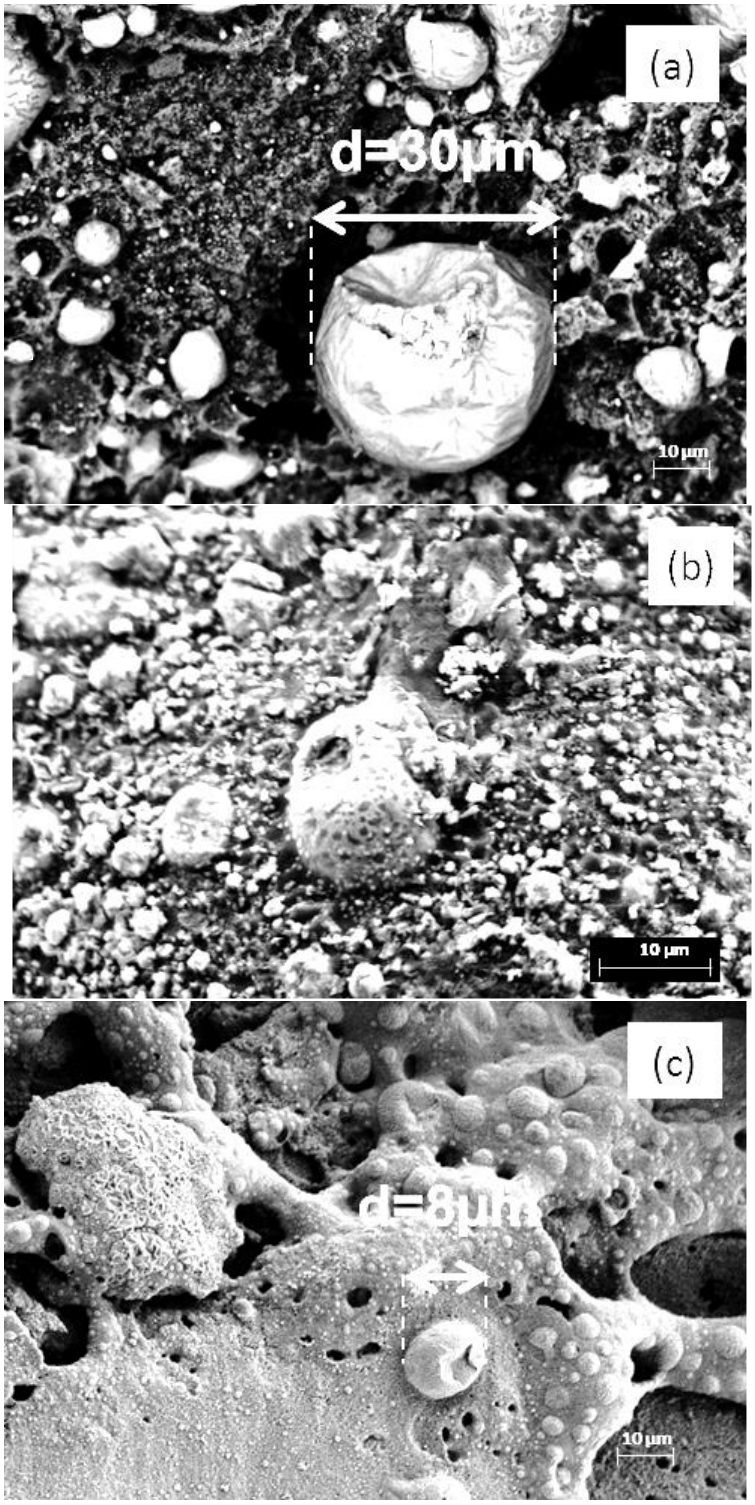

Figure 5-2 SEM images of the metal spheres produced from the thermite reactions of the Al/NiO/Cu composite (a and b) and the Al/CuO/Cu composite (c). (a) and (b) were taken from the same sample. Φ=4 with 80 % copper.

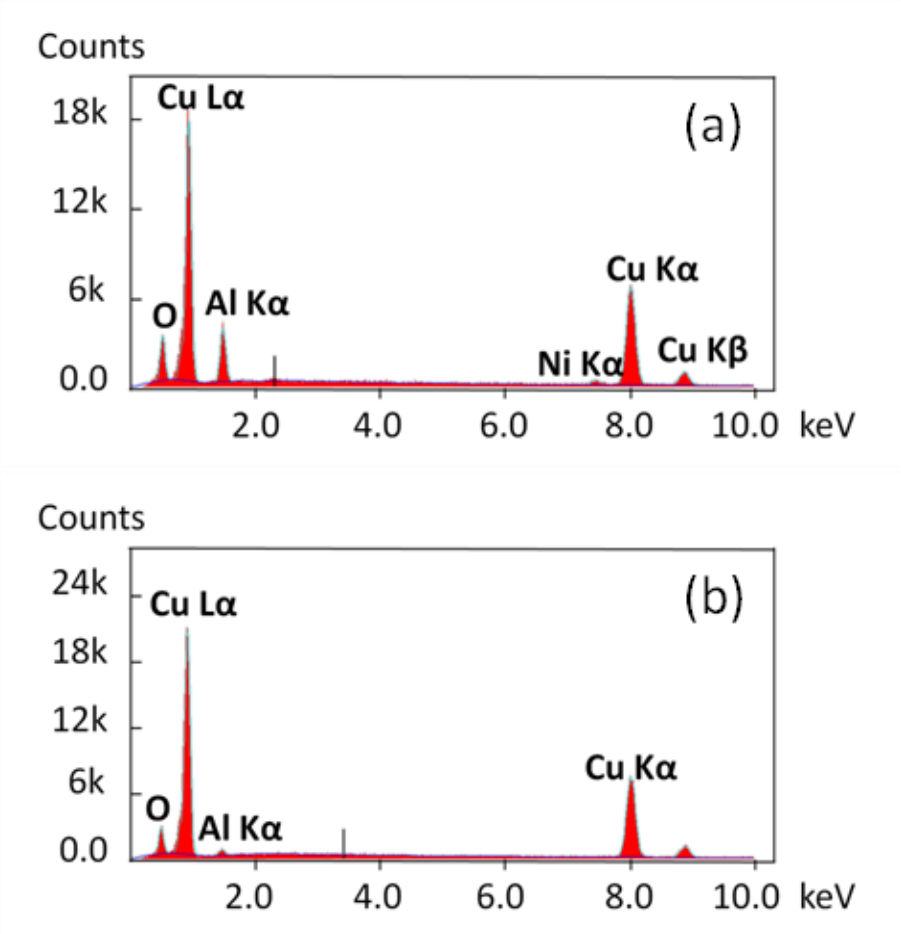

Figure 5-3 EDAX patterns of metallic spheres produced from the thermite reactions: (a) for Figure 5-2-a: Al/NiO/Cu; (b) for Figure 5-2-c: Al/CuO/Cu.

Table 5-2 Elemental compositions of the spheres formed from the Al/NiO/Cu and Al/CuO/Cu composites. Φ=4 with 80 % copper

Element	Al/NiO/Cu (atomic %)	Al/CuO/Cu (atomic %)
Cu	**49.41**	**67.63**
O	**29.29**	**28.19**
Al	**19.33**	**4.19**
Ni	**1.96**	**---**

The XRD patterns were obtained from these two Al/NiO/Cu and Al/CuO/Cu composites for $\Phi = 4$ and with 80% copper additive, after they were processed at different temperatures (150°C, 450°C and 800°C) in Argon. These results are shown in Figure 5-4. Figure 5-4(a) shows that after the pellets of Al/NiO/Cu composites were heated at 150°C and 450°C, the phase of Al_2O_3 was not identified in the processed samples. Instead, Al, NiO and Cu phases were present and confirm no reaction occurred at these two temperatures. When the pellet was heated at 800°C, however, these phase peaks of Al and NiO disappeared and the new phases of Al_2O_3 and AlNi appeared. Note that the identification of Al_2O_3 using XRD is evidential from the previous study [32]. Figure 5-4(a) clearly shows that for the prepared Al/NiO composite, the thermite reaction did not occur when the temperature was lower than 450°C. Figure 5-4(b) shows the XRD patterns from the processed Al/CuO/Cu composites. It is stable at the room temperature. When the Al/CuO/Cu composite was heated up to 800°C, the thermite reaction occurred and the product of Al_2O_3 was detected.

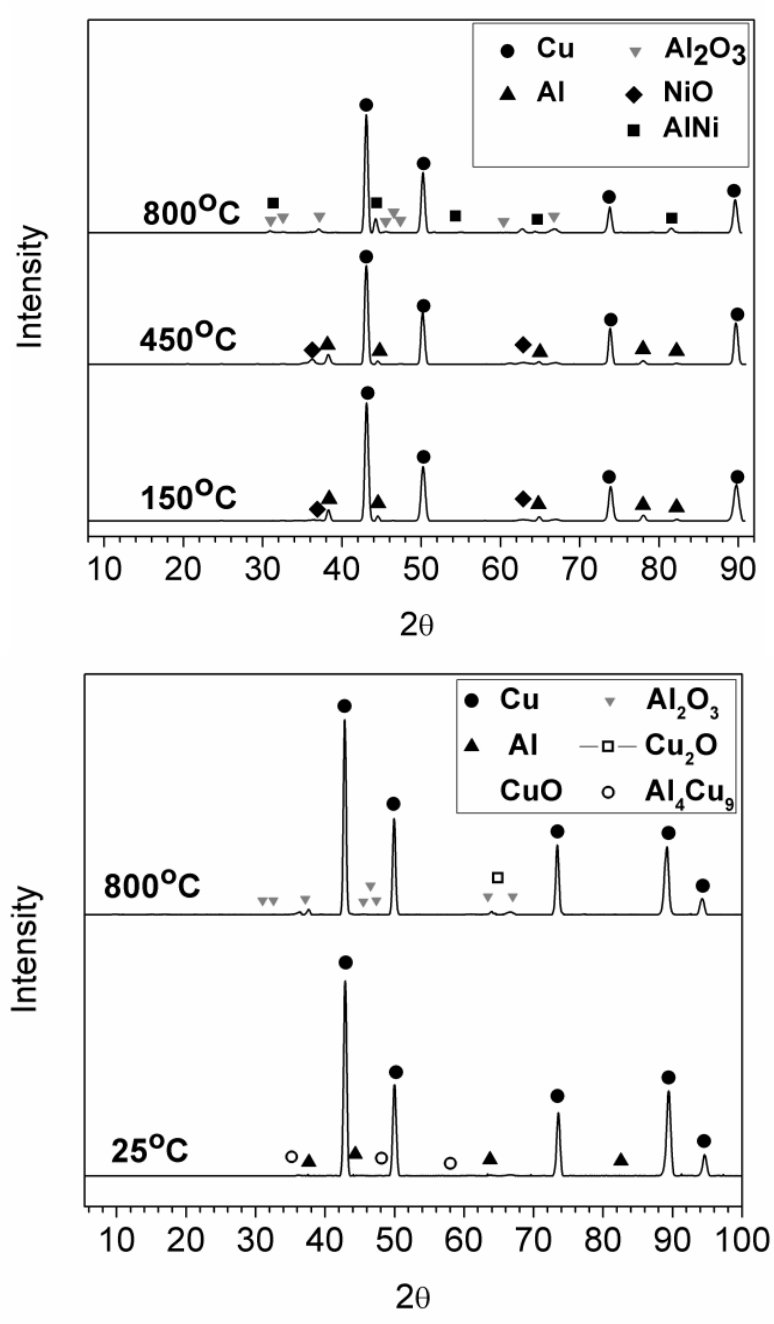

Figure 5-4 The XRD patterns of these composites processed at different temperatures: a) Al/NiO/Cu; b) Al/CuO/Cu. Φ=4 with 80 % copper

It was interesting to find out after the thermite reaction of the Al/NiO/Cu composite occurred, AlNi was produced from the Φ = 4 sample. The formation of the AlNi phase from the thermite reaction of fuel-rich Al/NiO composites was investigated using the following reaction

$$5Al + 3NiO = Al_2O_3 + 3AlNi \qquad \Delta Hr = 3.2\ kJ/g \qquad (R4\text{-}1)$$

which is preferred when the molar ratio of Al/NiO is large. In this study, the Φ = 4 composites shown in Table 3-1 contained abundant Al nanoparticles and thus made the reaction (R4-1) more feasible than (R3-1). Note that the propagation of (R4-1) does not necessarily require the completeness of (R3-1), since the decomposition of NiO may occur first and be followed by the reaction between Al and Ni. A further study on elementary reactions related to (R3-1) and (R4-1) is needed in order to gain more insights on this issue. Since the ΔH value is calculated on mass base, (R4-1) results in a smaller value of J/g than (R3-1). The formation of AlNi was not reported previously from the characterization of Al/NiO nanothermites. A former study tested on a fuel lean Al/NiO (a) (b) composite and therefore the oxidizer NiO was still present in the product, which confirmed the reaction (R3-1) [27]. In comparison, only one thermite peak was observed in this study, as shown later in Figure 5-6, which implies the overlap of Reaction (R4-1) and (R3-1). Indeed these two reactions may occur at the same onset temperature assuming the rate limiting process is the delivery of Al atoms to the oxidizer through either diffusing or cracking the shell. The formation of the AlNi phase from the Al/Ni system was confirmed previously. Zhu et al. observed the formation of the AlNi phase from the micron sized Al-Ni thermite powder when the system temperature reached above 1000°C [100]. They explained the formation of AlNi through a process consisting of several steps in an Al rich environment: $NiAl_3$ is first formed at 750°C form the Al-Ni system, and then Ni_2Al_3 is formed at 900°C, and finally AlNi appears at 1050°C. In this study the formation of these copper spheres, shown in Figure 5-

2, indicated the local temperature was once above the melting point of copper (1085°C). This suggests a possibly similar process to Zhu et al. Figure 5-4(b) compares different compositions of the processed Al/CuO/Cu composites at room temperature and 800°C. It shows that after the pellet was heated at 800°C, the thermite reaction of the Al/CuO/Cu composite produced Al_2O_3, $Cu_2O$and Al_4Cu_9. Note the amount of copper additive and the combustion temperature played roles in forming these products. Figure 5-4 confirms both Al/NiO and Al/CuO composites were ignited when the temperature was heated up to 800°C.

Figure 5-5 shows a high-resolution SEM image of the sphere shown in Figure 5-2(b). This sphere appeared quite differently from the sphere shown in Figure 5-2(a), although they were from the same sample. It has a diameter of about 20 μm, which is close to the other sphere, and both resulted from the higher combustion temperature from the Al/NiO/Cu composite which generates more liquid copper. The EDAX was performed at three locations shown as a, b, and c on this SEM image and the measured atomic spectra are shown in Figure 5-5. Table 5-3 lists the identified elements corresponding to these locations of a, b and the matrix c, respectively. The atomic ratios suggest that the big sphere shown in Figure 5-5 was a composite of AlNi and Al_2O_3. And more specifically, the darker area indicates the Al-rich (Al_2O_3) phase and the brighter area indicates the AlNi phase. This sphere was embedded in the porous Al_2O_3 matrix (location c). The SEM-EDAX analysis further confirms the occurrence of the reaction (R4-1) from the fuel rich composites.

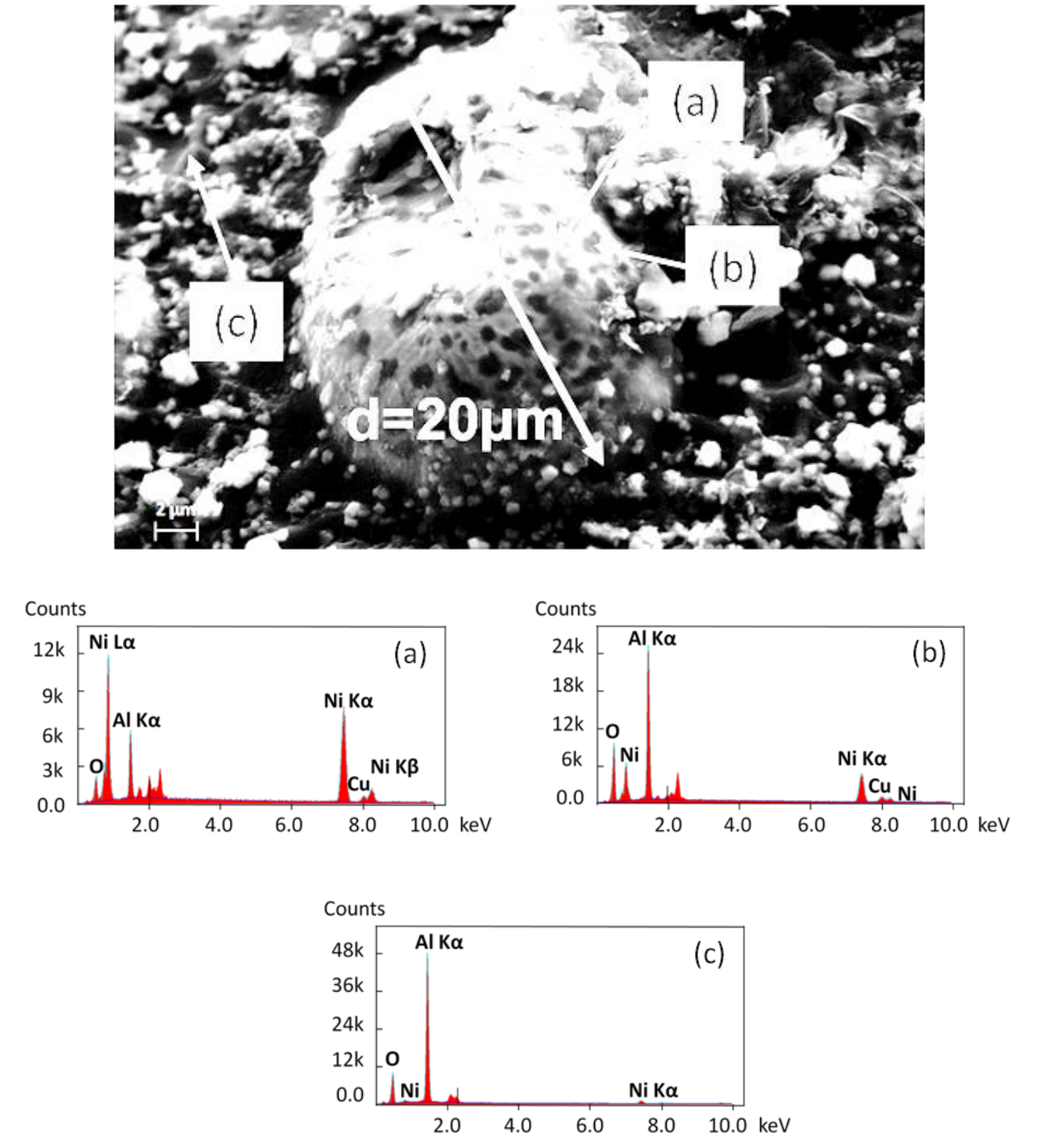

Figure 5-5 High-resolution SEM image of the sphere produce from the Al/NiO/Cu composite and EDX patterns associated to it.

Table 5-3 Compositions of the different phases corresponding to the sphere shown in Figure 4-5 These locations of a, b and c are indicated in Figure 5.

Element	Location a (Atomic %)	Location b (Atomic %)	Location c (Atomic %)
Al	26.36	42.88	55.02
Ni	52.98	16.49	3.54
O	16.66	37.14	40.32
Cu	4	3.49	1.12

5.3.3. Onset temperature and energy release

Figure 5-6 shows the DSC data measured from three Al/NiO/Cu composites with the different equivalence ratios of 0.6, 1.5 and 4, respectively. The mass fraction of copper was 50% in all of these composites. For each curve, there was a clearly observed single exothermic peak corresponding to the thermite reaction. The ignition temperatures were determined from these curves by referring to the onset temperatures of the aforementioned exothermic peaks. Their values for these equivalence ratios of 0.6, 1.5 and 4 were measured as 493.1°C, 490.4°C and 486.5°C respectively. Note that the more fuel (Al nanoparticles) available in the composite caused a slightly decrease in the onset temperature, possibly due to the better contact between the fuel and oxidizer when more nanoparticles were present in the composite. The difference of these ignition temperatures are however quite small and all are below the melting temperature of bulk Al (660°C). The energy release per mass of the composite (E′, in J/g) was calculated using the DSC software by integrating the area under the exothermic peak (as shown in the DSC diagram). Note that this mass for the DSC data included the mass of the fuel, oxidizer and copper

additive. The following equation was used to calculate the energy release per mass of the pure nanothermite (E, in J/g) by taking into account the role of Al_2O_3 shell on Al nanoparticles

$$E = E' \times \frac{Mass_{Al,Al_2O_3,NiO}}{Mass_{Al,NiO}} \quad (5\text{-}1)$$

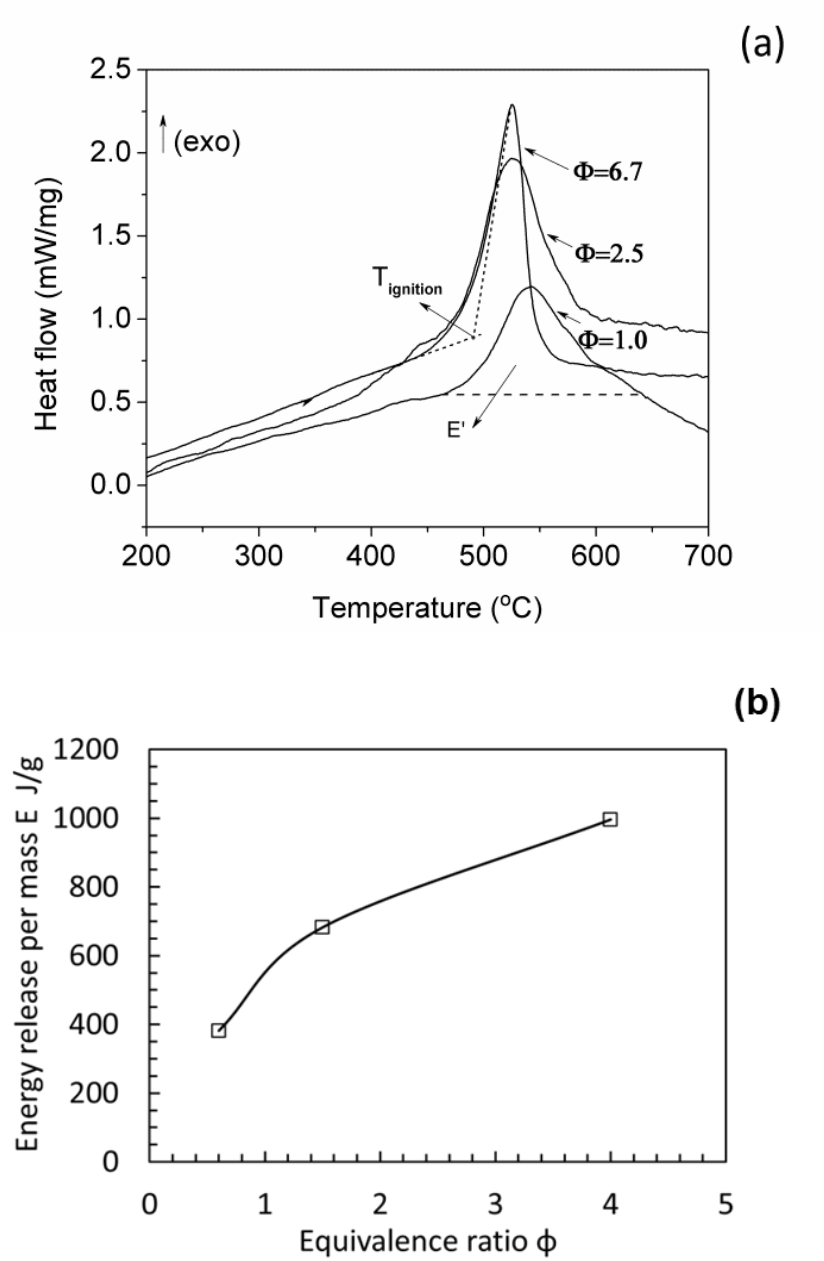

Figure 5-6 (a) The DSC data of these Al/NiO/Cu composites with different equivalence ratios, Tignition was set as the onset temperature of the exothermic peak; (b) The energy release per mass of nanothermite E calculated from the composites with different equivalence ratios

The values of E, shown in Figure 5-6(b), were expected to be smaller than the energy release per mass from the combustion of pure Al/NiO nanothermite (3400 J/g [27]), since the presence of copper provided a heat sink, which absolutely influenced the measured energy release value.

Note that the values of E measured from this study increased with the increasing fuel/oxidizer ratio. This behavior can be explained by the following considerations. First, the DSC measurements were conducted in a non-adiabatic condition therefore the energy release per mass cannot be simply referred to the reaction enthalpy of the thermite reaction. Secondly, the mass used in this study was relatively small (with a few mg) which could cause some discrepancy in both mass and energy measurements. Thirdly, the effect of copper additive cannot be excluded.

Figure 5-7(a) shows the effects of the copper additive on the DSC curves from the Al/NiO/Cu composites with $\Phi = 4$. Generally for these composites, the exothermic peaks appeared at about 450-550°C on the DSC curves and the onset temperatures (i.e., the onset temperatures) of these curves were in the range of 487-496°C. Slightly increasing onset temperatures were observed when the copper amount was changed from 50% to 80%, which may result from the interference of the copper additive with the effective contact between the fuel and oxidizer. The difference was however quite insignificant and indicates the less influence of the micro-sized copper additive on the thermite reaction of nanothermites. The values of energy release per mass of nanothermite E decrease significantly with the increasing copper amount, as shown in Figure 5-7(b). This indeed confirms the heat sink role of the copper additive. More copper in the composite will absorb more heat and the composite system will therefore release less heat to the surroundings (and thus in DSC less heat flow was required).

During the experiments, the heat absorbed by the copper power was utilized in melting the copper powder and caused the formation of large copper rich spheres shown in Figure 5-2. More copper amount in the composite should produce more copper spheres and thus consume more heat.

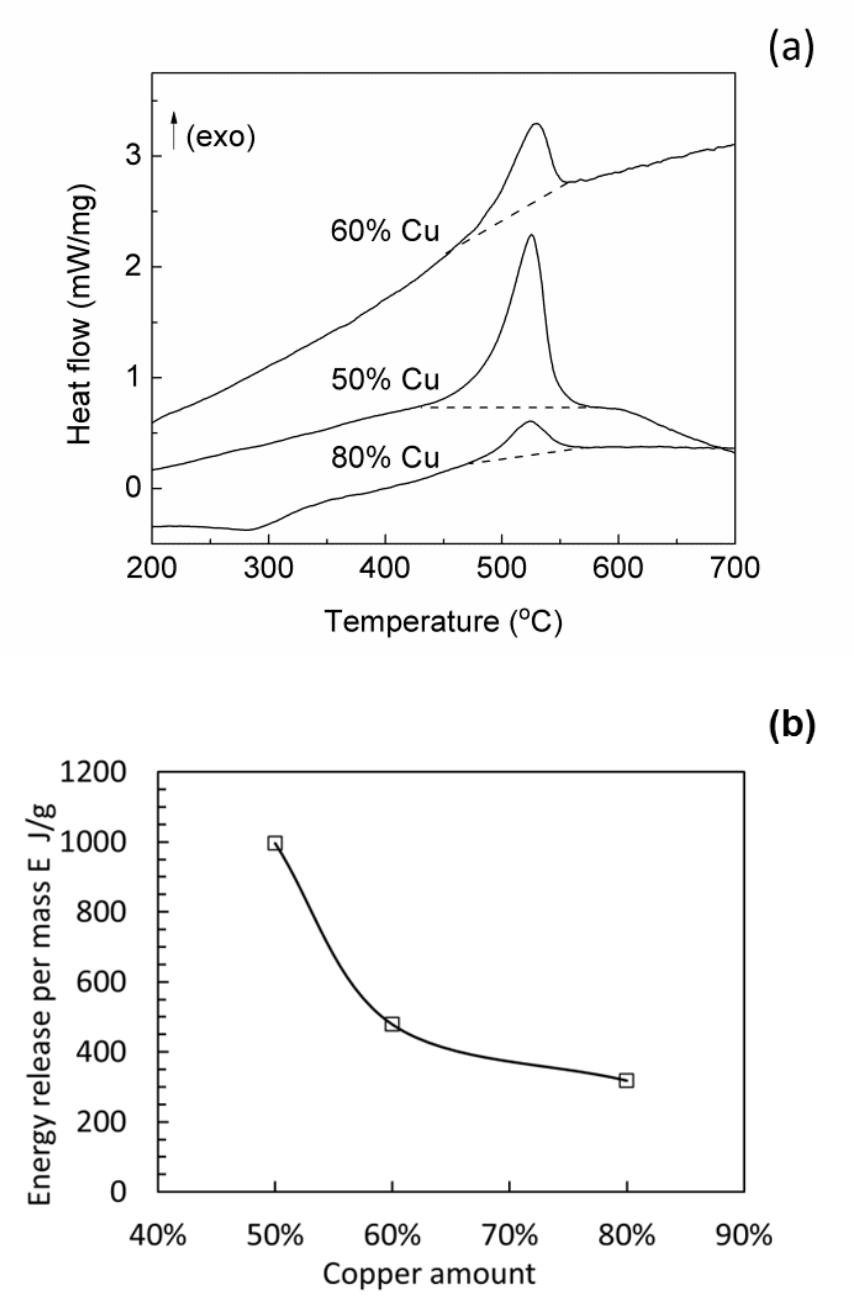

Figure 5-7 a) The DSC diagram of these Al/NiO/Cu composites with different amounts of copper; b) The dependence of the energy release per mass with the copper amount. Φ=4

It is interesting to compare the onset temperatures and energy release per mass values of the Al/NiO/Cu and Al/CuO/Cu composites, because the latter produces the pure copper component from its thermite reaction which may be beneficial to the copper-copper material joining. Figure 5-8 (a) shows the DSC measurements on the Al/CuO/Cu composites for Φ = 4 but with different amounts of the copper additive.

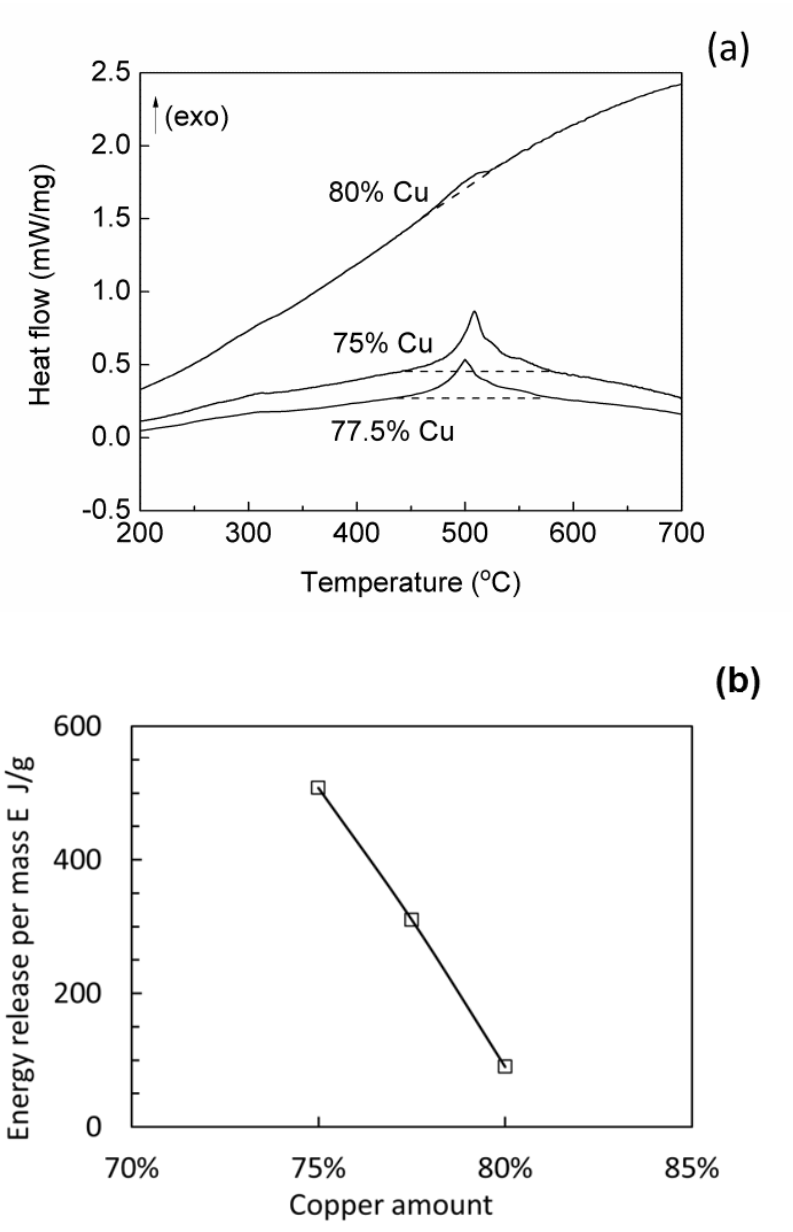

Figure 5-8 a) The DSC diagram of these Al/CuO/Cu composites for Φ=4 with different amounts of copper; b) The dependence of the energy release values with the copper amount.

The DSC curves show a consistent temperature range of these exothermic peaks which correspond to the thermite reactions between Al nanoparticles and CuO nanowires. The measured onset temperatures are 491.2, 484.7 and 488°C for the 75% Cu, 77.5% Cu and 80% Cu amounts, respectively. These values are very consistent and show an independence of the onset temperature of these Al/CuO/Cu composites on the copper additive. In addition, these onset temperatures measured from the Al/CuO/Cu composites are close to the values measured from the Al/NiO/Cu composites, which may suggest the same ignition mechanism of two composites. Figure 5-8(b) shows the measured E values for three Al/CuO/Cu composites. Again the energy release per mass of nanothermite (E) decreased significantly when (b) the copper amount was increased. And for the Al/CuO/Cu composites mixed with a larger amount of copper additive (>70%), the effect of the copper additive on the change in its energy release per mass is more significant due to the additional influence of copper which directly participates in the thermite reaction and subsequently affects the reaction rate. With the same amount of the copper additive in these Al/NiO/Cu and Al/CuO/Cu composites, larger liquid spheres formed from the thermite reaction will feasible a better material joining quality by wetting well the surfaces and forming a brazing layer [100,116]. As shown earlier in Figures 5-2 and 5-5, the Al/NiO/Cu composites produced larger copper spheres than the Al/CuO/Cu composites, due to their greater energy release per mass which was utilized to melt the copper powder. The Al/Ni/CuO composites produced the AlNi spheres as well, as shown in Figure 5-5. Generally speaking, the availability of liquid metals relates to these gas-phase species produced from a thermite reaction, which include vapors of metals (such as Cu and Ni from the Al/CuO and Al/NiO thermites), the elemental oxygen (formed from the decomposition of the oxidizer), and other gaseous reaction

products [27]. A throughout investigation is needed for better understanding the size dependence of the metal spheres on these chemical and physical processes.

5.4. Conclusions

In summary, experimental investigations were performed in order to characterize the produced microstructures of the Al nanoparticle and NiO nanowire composites and understand how the copper additive would affect the onset temperature and the energy release. Two types of metallic spheres were found from the thermite reaction of these composites and were identified as the copper rich spheres and the AlNi composite ones. The formation of AlNi was confirmed by the XRD and EDAX analyses, which suggests that for the fuel rich composites, the thermite reaction directly produced the AlNi phase. It was found as well that the amount of the copper additive did not significantly change the onset temperature but brought about a large influence to the energy release data. In comparison, the Al/CuO/Cu nanothermites produced smaller metal spheres.

CHAPTER 6

Nanothermites for Joining Applications

6.1. Introduction

Nanothermite materials have found special applications in joining specially for joining of dissimilar materials. The attractive factor encouraging the use of these materials for joining is their high energy density and therefore high flame temperature as a self-propagating heat source. As indicated in Appendix A, the adiabatic flame temperature of thermite reactions can reach above 3000K making it capable of melting metals, which is beneficial for joining application. In this chapter, the use of Al-NiO-Cu nanothermite composite for joining was investigated. The Al-NiO was chosen as the primary reaction owing to its low gas generating property since the gas production causes defects in the joining process. A composite of Al-NiO-Cu with Φ=4 and 50% Cu introduced in chapter 5 as a good candidate for joining, was used a joining interlayer. The aim of this chapter is to show the capability of this composite to bond dissimilar materials. Example joints are provided and the microstructure and chemical composition of joint cross sections are tested to ensure the feasibility and quality of the joining process. Glass, ceramic and copper substrates were used. Further mechanical testing is needed to measure the joint strength and related future work is proposed in chapter 7.

6.2. Experimental

6.2.1. Base materials

Water-white microscopic glass slides with dimensions of 1×26×75 mm were used as base material. The slides were washed with acetone and DL water to remove any oil and

contamination on the surface. As another base material, alumina-silica sheets were cut to 50×50 mm squares and were washed with acetone and DL water before joining.

Also, 50 and 250 µm thick copper wires were used to be joined to the glass substrate using the nanothermite composite. The wires were cut to 150 mm long and were washed in nitric acid and DL water to remove any contamination and oxide.

Nanothermite pellets with composition of Al-NiO-Cu (Φ=4 and 50%Cu) were prepared according to chapter 2. The pellets had diameter of 3 mm and thickness of 0.7 mm.

6.2.2. Joining setup

In the first stage, a nanothermite pellet was tested on an alumina-silica substrate. First the substrate was heated to 500°C on hot-plate and then the pellet was placed on it. Then the hot-plate was turned off and the substrate was let cool down to the room temperature.

In the second stage, a Cu wire was placed between the nanothermite pellet and the substrate. The objective was to join the Cu wire to substrate utilizing the heat and molten metal released from the nanothermite reaction. The copper wire was loosely taped to the glass slide with a paper tape and the nanothermite pellet was placed on top of the copper wire. The fixture was then put on a hotplate preheated to 500°C and a small spatula was used to apply pressure on the pellet to keep it in place against the vibration from the reaction and let it touch the surface. Figure 6-1 shows a schematic picture of the joining setup. The hot plate was then turned off and the fixture was cooled down at the room temperature. The paper tapes were then removed (if not fully burnt in the high temperature) and the joint samples of copper wire and glass slide were cross-sectioned and mounted in epoxy. The mounted sample was grinded to 5000 grid and polished by 25µm diamond paste. Optical microscope (OM), SEM, and EDAX were used to further study the cross-sectioned samples.

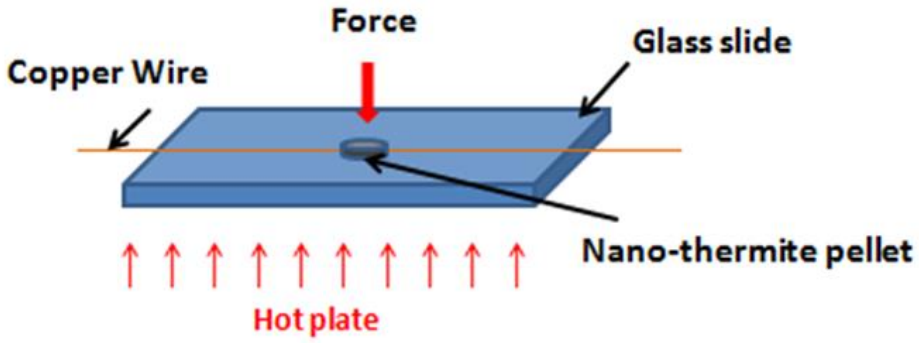

Figure 6-1 Schematic setup for joining copper wire to glass/ceramic substrate

6.3. Results and discussion

Figure 6-2(a) shows the optical microscope image of a glass substrate after igniting nanothermite on it. Products of nanothermite reaction joined to the glass surface and metal spheres were formed on the surface confirming that the metal has liquefied in the high flame temperature of the reaction and has shaped into spheres to minimize its surface energy. These liquid metal spheres wet the glass surface and are beneficial for joining. On the other hand, from chapter 4 we know that the products of nanothermite reaction include Al_2O_3, and liquid AlNi and Cu phases. In addition to molten metal, Al_2O_3 was formed during the reaction and the OM images suggested that this phase made a strong bond to the glass substrate. Figure 6-2(b) is an optical microscope image of a 50 µm copper wire joined to a glass substrate. The sphere shown in the dotted circle is a metal alloy sphere produced by nanothermite reaction. This sphere worked as a soldering/brazing material between copper wire and glass substrate.

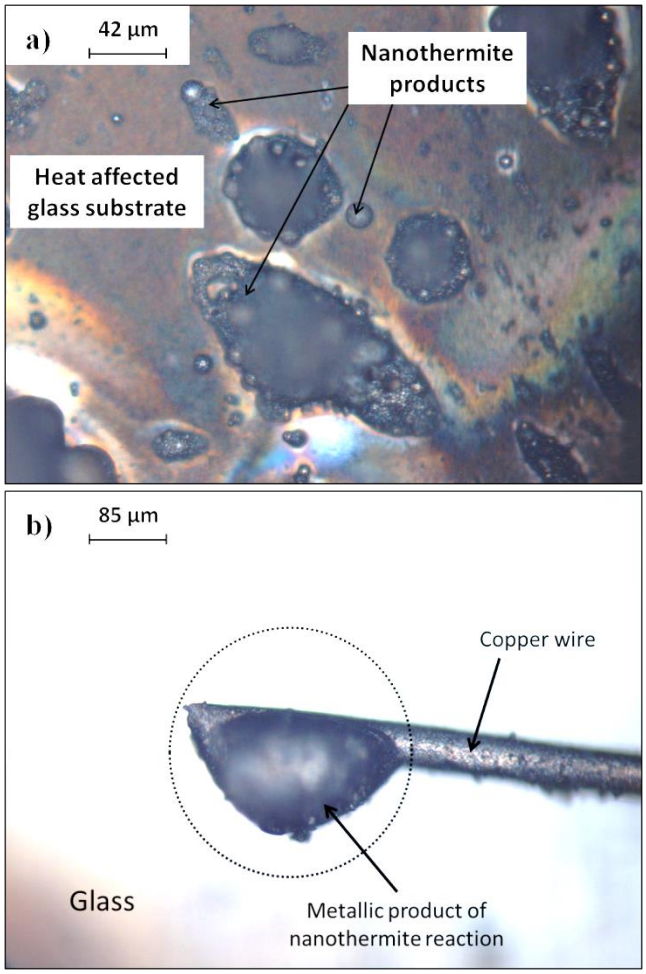

Figure 6-2 Optical microscope image of glass substrate and nanothermite after ignition (a) nanothermite products stuck to glass surface (b) Copper wire joined to glass substrate with metal-alloys soldering/brazing layer produced by nanothermite reaction

More reliable proof of the joint is shown in Figure 6-3(a), (b) and (c) emphasizing that the joint is strong enough to hold the weight of glass substrate while holding the copper wire with tweezers. Figure 6-3 shows the glass-copper joining setup (a) before and (b)-(c) after the reaction.

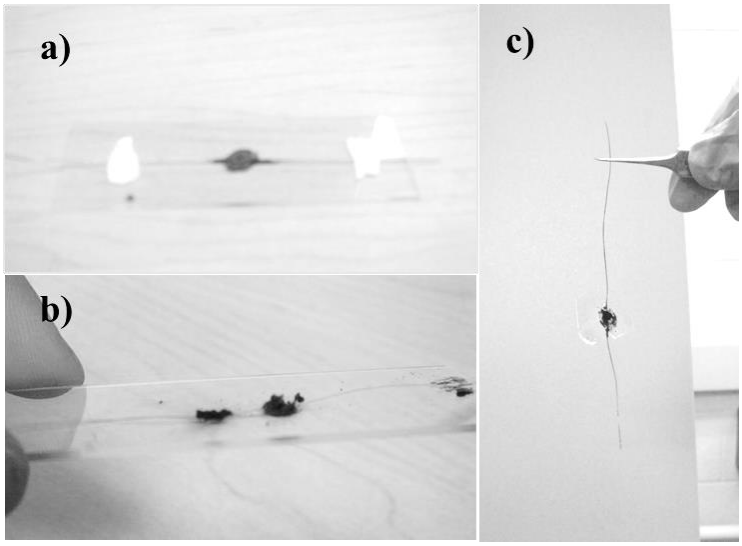

Figure 6-3 Images of glass to copper joint before (a) and after (b)-(c) the ignition- After the reaction, the glass, copper wire, and the reacted nanothermite are bond together.

The joint cross-section of the bonded sample was studied by SEM and is shown in Figure 6-4. AlNi, while the matrix in the left side is Al_2O_3. The joint between the copper wire and nanothermite product seems to have fewer defects compared to the joint between the copper wire and the glass side. However, a strong bond was seen in between the nanothermite product and glass substrate which caused a good mechanical bonding of the copper wire to the glass substrate. It is suggested that if an adequate pressure was applied during the ignition, the quality of the bonds would greatly improve.

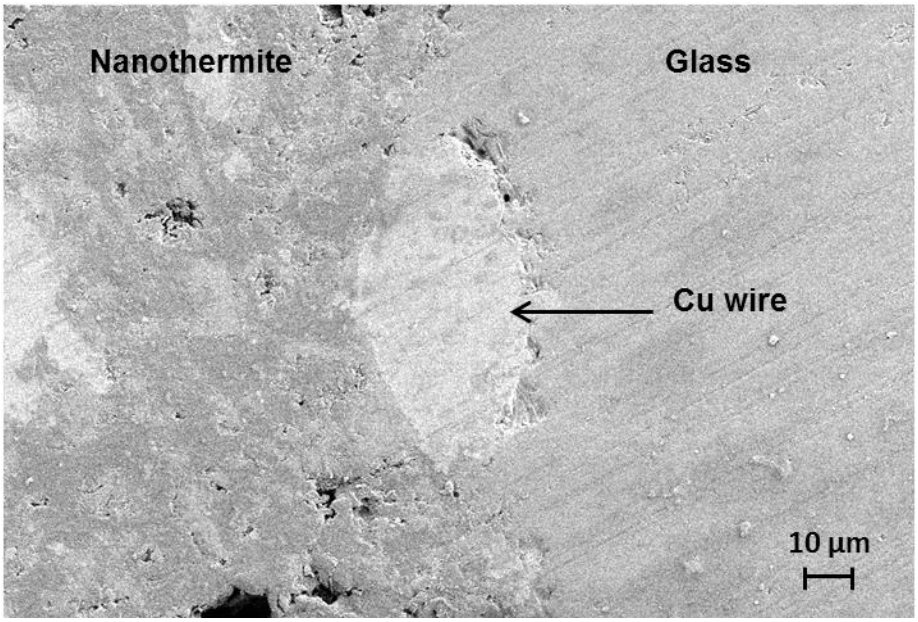

Figure 6-4 SEM image of joint cross-section of glass and copper wire

The nanothermite pellet was also tested on an alumina-silica substrate and a strong joint was achieved between the nanothermite product and the substrate. The joint cross-section was studied by SEM and EDAX which is shown in Figure 6-5. The elemental analysis done by EDAX is listed in Table 6-1 for the points a, b, and c which are shown in Figure 6-5.

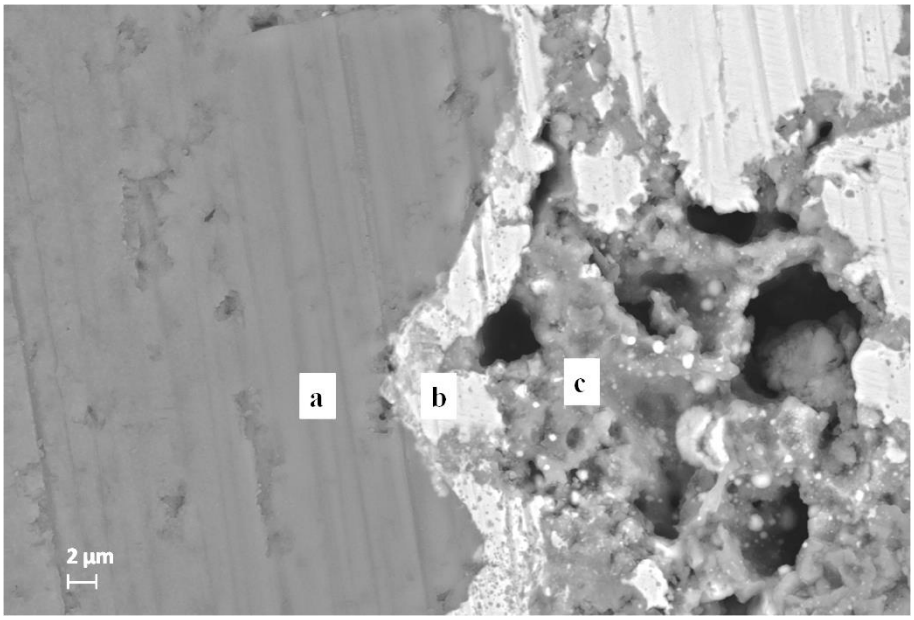

Figure 6-5 SEM image of joint cross-section of nanothermite product and alumina-silica substrate

In Figure 6-5, area (a) shows the alumina-silica with the chemical composition listed in Table 6-1. Phases (b) and (c) are products of thermite reaction which are well joined to the substrate. According to Table 6-1, phase (b) is mostly composed of metals with high concentration of Cu. Phase (c), with the dominant elements of Al and oxygen, is a porous matrix of Al_2O_3.

Table 6-1 EDAX elemental analysis (atomic %) of points a-b-and c shown in Figure 5-7

Point	**O**	**Al**	**Ni**	**Cu**	**Si**	**Na**	**Mg**	**Ti**	**K**	**P**
A	49.55	12.40	0.17	0.30	31.64	2.05	0.69	1.00	0.28	0.88
B	7.32	8.13	18.42	64.78	1.35	—	—	—	—	—
C	45.51	45.04	2.77	3.60	0.13	—	—	—	—	—

It is evident that the nanothermite product is an interpenetrating network of Al_2O_3 and metallic phase. As mentioned before, the metallic phase is molten in the high temperature of the reaction and wets the adjacent surfaces, creating a strong bond. Moreover, the similar nature of Al_2O_3 and alumina silica as ceramics makes them likely to bond together during the nanothermite reaction. Figure 6-6, which is a lower magnification SEM picture of the same joint cross-section in Figure 6-5, shows that the Al_2O_3 phase in the nanothermite product was also joined to the alumina-silica substrate.

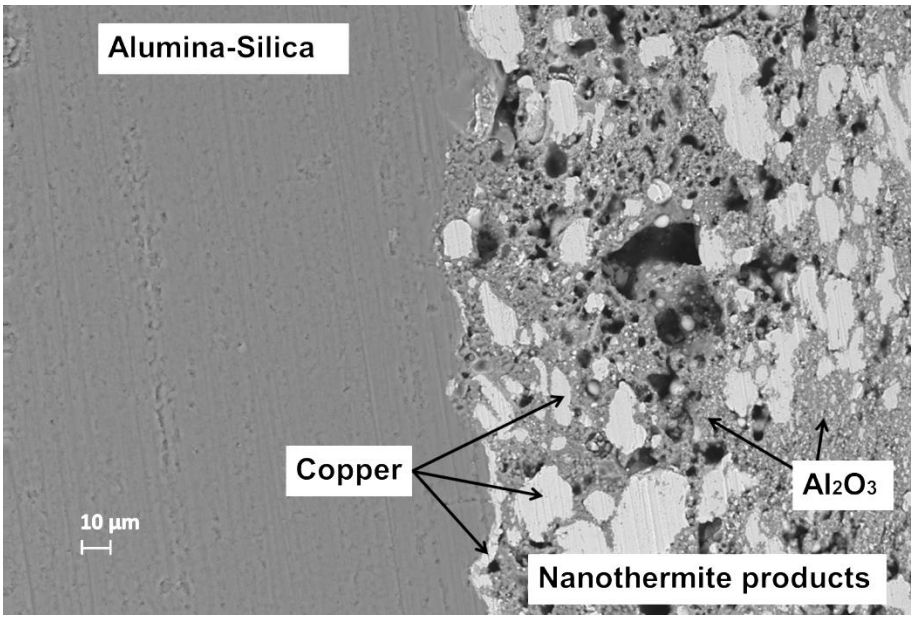

Figure 6-6 SEM image of joint cross-section of nanothermite product and alumina-silica substrate (low magnification)

6.4. Conclusion

The Al-NiO-Cu composite with Φ=4 and 50% copper, was experimentally tested for joining application on glass and alumina silica substrate. Results from optical microscopy, SEM and EDAX showed that this composite while ignited, sticks to the glass and ceramic surfaces and is capable of joining dissimilar surfaces together. The combination of liquid metal phase and Al_2O_3 ceramic phase makes the products of this nanothermite composite to be a very interesting material for advanced joining purposes.

CHAPTER 7

Conclusions and Future Work

In this thesis, I tried to find a good nanothermite composition to be used in joining applications. Al-NiO reaction was chosen due to its lower gas generation amongst other thermite systems. In preliminary studies, Al-NiO nanothermite composites with various equivalence ratios (Φ) of Al nanoparticles and NiO nanowires were synthesized and tested in order to select the equivalence ratio associated with the most functional composition. The factors considered in this selection were the light emission, and controllability. As a result, Al-NiO with Φ=4 was found to be most functional. This composite was then further studied by SEM, EDAX, and XRD to characterize the structure and chemical composition of the reactants and the products of the reaction. SEM results showed that ultrasound mixing of the reactant powders resulted in more homogeneous mixing. The products of Al-NiO composite with Φ=4 were found to be Al_2O_3 and AlNi.

In order to utilize the above composite for joining application, it was needed to limit the heat transfer to the air and keep the generated heat close to the joining area. Therefore, copper micron powder was used as an additive in the mixture to act as a heat sink, increase the burning duration, and decrease the vibration caused by the high thrust from the pure Al-Ni composite. The Al-NiO-Cu composite was compared to an Al-CuO-Cu mixture. SEM results of the reaction products in these two composites revealed that the Al-NiO-Cu produced larger liquid metal phases. This result was further supported by thermal analysis of the Al-NiO-Cu and Al-CuO-Cu composites by differential scanning calorimetry in chapter 5.

Moreover, the SEM observations combined with EDAX and XRD results showed that the fuel-rich Al/NiO/Cu composites produced two types of metallic spheres. Copper spheres were formed from melting and solidification of the copper additive, while AlNi composite spheres were identified by the energy dispersive X-ray spectroscopy and X-ray diffraction analyses. Furthermore, it was found that the amount of the copper additive did not significantly influence the onset temperature of thermite peaks, but caused a dramatic change in energy release. The aforementioned ignition and energetic properties were compared with those from the Al nanoparticle and CuO nanowire composites.

The Al-NiO-Cu composite with Φ=4 and 50% copper, was experimentally tested in joining application. Results from optical microscopy, SEM and EDAX showed that this composite while ignited, sticks to the glass and ceramic surfaces and is capable of joining dissimilar surfaces together. The combination of liquid metal phase and Al_2O_3 ceramic phase makes the products of this nanothermite composite to be a very interesting material for advanced joining purposes. In summary:

Conclusions

- Al/NiO and Al/CuO energetic composites were developed using the NiO/CuO nanowires with an average diameter of about 12 nm and a length of a few microns.
- The sonication process of 2 hours helped produce the well dispersed Al nanoparticles which were decorated on the NiO nanowires.
- Copper filler was added to Al (np)/NiO (nw) and its chemical composition and microstructure were investigated. Two types of metallic spheres were found from the thermite reaction of these composites and were identified as the copper rich spheres and the AlNi composite ones.

- The chemical compositions and microstructures of these composites were examined using XRD, SEM and EDAX, which showed the evidence of the AlNi phase from the fuel rich Al/NiO composites. In comparison, the Al/CuO/Cu nanothermites produced smaller metal spheres.
- Ignition temperature of Al-NiO-50%Cu nanothermites with Φ=0.6, 1.5, and 4 were measured to be 493.1°C, 490.4°C, and 486.5°C respectively, which showed negligible dependence of the ignition temperature on the equivalence ratio (Φ).
- Energy release of the Al-NiO-50%Cu nanothermites was found to be increasing by increasing the equivalence ratio. The energy release for the mixture with Φ=4 was measured to be 1012 J/g.
- The amount of the copper additive did not significantly change the onset temperature but brought about a large influence to the energy release data.
- The ignition temperature for Al-CuO-Cu was measured to be 484-491°C and independent of copper amount. However, the energy release of this composite, decreased by increasing the copper amount.
- The Al-NiO-Cu composite with Φ=4 and 50% copper, was selected for joining application.
- Results from optical microscopy, SEM and EDAX showed that this composite while ignited, joins to the glass and ceramic surfaces and is capable of joining dissimilar surfaces together.
- The combination of liquid metal phase and Al_2O_3 ceramic phase makes the products of this nanothermite composite to be a very interesting material for advanced joining purposes.

Future work

Further investigations are strongly encouraged in future to utilize this unique composite as an interlayer for joining dissimilar materials. The low cost ignition process and self-propagating reaction of this material is its other advantage as an interlayer for joining of dissimilar materials. Although some joining experiments are done in Chapter 6 using this nanothermite composite, further experiments with better conditions seem necessary to prove the promising effect of Al-NiO-Cu nanothermite composite. It is suggested to apply pressure during the joining to achieve more reliable joints. Joint strength testing experiments are also strongly suggested.

Copyright Permission

AMERICAN INSTITUTE OF PHYSICS LICENSE TERMS AND CONDITIONS

Apr 23, 2013

All payments must be made in full to CCC. For payment instructions, please see information listed at the bottom of this form.

License Number	3135041234016
Order Date	Apr 23, 2013
Publisher	American Institute of Physics
Publication	Journal of Applied Physics
Article Title	Size dependence of energetic properties in nanowire-based energetic materials
Author	L. Menon, D. Aurongzeb, S. Patibandla, K. Bhargava Ram, et al.
Online Publication Date	Aug 14, 2006
Volume number	100
Issue number	3
Type of Use	Thesis/Dissertation
Requestor type	Student
Format	Print and electronic
Portion	Figure/Table
Number of figures/tables	1
Title of your thesis / dissertation	Synthesis, characterization and application of nanothermites in joining
Expected completion date	May 2013
Estimated size (number of pages)	120
Total	**0.00 USD**

Terms and Conditions

American Institute of Physics -- Terms and Conditions: Permissions Uses

American Institute of Physics ("AIP") hereby grants to you the non-exclusive right and license to use and/or distribute the Material according to the use specified in your order, on a one-time basis, for the specified term, with a maximum distribution equal to the number that you have ordered. Any links or other content accompanying the Material are not the subject of this license.

1. You agree to include the following copyright and permission notice with the reproduction of the Material: "Reprinted with permission from [FULL CITATION]. Copyright [PUBLICATION YEAR], American Institute of Physics." For an article, the copyright and permission notice must be printed on the first page of the article or book chapter. For photographs, covers, or tables, the copyright and permission notice may appear with the Material, in a footnote, or in the reference list.
2. If you have licensed reuse of a figure, photograph, cover, or table, it is your responsibility to ensure that the material is original to AIP and does not contain the copyright of another entity, and that the copyright notice of the figure, photograph, cover, or table does not indicate that it was reprinted by AIP, with permission, from another source. Under no circumstances does AIP, purport or intend to grant permission to reuse material to which it does not hold copyright.
3. You may not alter or modify the Material in any manner. You may translate the Material into another language only if you have licensed translation rights. You may not use the Material for promotional purposes. AIP reserves all rights not specifically granted herein.
4. The foregoing license shall not take effect unless and until AIP or its agent, Copyright Clearance Center, receives the Payment in accordance with Copyright Clearance Center Billing and Payment Terms and Conditions, which are incorporated herein by reference.

5. AIP or the Copyright Clearance Center may, within two business days of granting this license, revoke the license for any reason whatsoever, with a full refund payable to you. Should you violate the terms of this license at any time, AIP, American Institute of Physics, or Copyright Clearance Center may revoke the license with no refund to you. Notice of such revocation will be made using the contact information provided by you. Failure to receive such notice will not nullify the revocation.
6. AIP makes no representations or warranties with respect to the Material. You agree to indemnify and hold harmless AIP, American Institute of Physics, and their officers, directors, employees or agents from and against any and all claims arising out of your use of the Material other than as specifically authorized herein.
7. The permission granted herein is personal to you and is not transferable or assignable without the prior written permission of AIP. This license may not be amended except in a writing signed by the party to be charged.
8. If purchase orders, acknowledgments or check endorsements are issued on any forms containing terms and conditions which are inconsistent with these provisions, such inconsistent terms and conditions shall be of no force and effect. This document, including the CCC Billing and Payment Terms and Conditions, shall be the entire agreement between the parties relating to the subject matter hereof.

This Agreement shall be governed by and construed in accordance with the laws of the State of New York. Both parties hereby submit to the jurisdiction of the courts of New York County for purposes of resolving any disputes that may arise hereunder.

If you would like to pay for this license now, please remit this license along with your payment made payable to "COPYRIGHT CLEARANCE CENTER" otherwise you will be invoiced within 48 hours of the license date. Payment should be in the form of a check or money order referencing your account number and this invoice number RLNK501006430. Once you receive your invoice for this order, you may pay your invoice by credit card. Please follow instructions provided at that time.

Make Payment To:
Copyright Clearance Center
Dept 001
P.O. Box 843006
Boston, MA 02284-3006

For suggestions or comments regarding this order, contact RightsLink Customer Support:
customercare@copyright.com or +1-877-622-5543 (toll free in the US) or +1-978-646-2777.

Gratis licenses (referencing $0 in the Total field) are free. Please retain this printable license for your reference. No payment is required.

SPRINGER LICENSE
TERMS AND CONDITIONS

Apr 23, 2013

This is a License Agreement between Golnaz Bohlouli-Zanjani ("You") and Springer ("Springer") provided by Copyright Clearance Center ("CCC"). The license consists of your order details, the terms and conditions provided by Springer, and the payment terms and conditions.

All payments must be made in full to CCC. For payment instructions, please see information listed at the bottom of this form.

License Number	3135050352192
License date	Apr 23, 2013
Licensed content publisher	Springer
Licensed content publication	Journal of Thermal Analysis and Calorimetry
Licensed content title	Processing and characterization of aluminum-based nanothermites
Licensed content author	Jan A. Puszynski
Licensed content date	Jan 1, 2009
Volume number	96
Issue number	3
Type of Use	Thesis/Dissertation
Portion	Figures
Author of this Springer article	No
Country of republication	other
Order reference number	
Title of your thesis / dissertation	Synthesis, characterization and application of nanothermites in joining
Expected completion date	May 2013
Estimated size(pages)	120
Total	0.00 USD
Terms and Conditions	

Introduction

The publisher for this copyrighted material is Springer Science + Business Media. By clicking "accept" in connection with completing this licensing transaction, you agree that the following terms and conditions apply to this transaction (along with the Billing and Payment terms and conditions established by Copyright Clearance Center, Inc. ("CCC"), at the time that you opened your Rightslink account and that are available at any time at http://myaccount.copyright.com).

Limited License
With reference to your request to reprint in your thesis material on which Springer Science and Business Media control the copyright, permission is granted, free of charge, for the use indicated in your enquiry.

Licenses are for one-time use only with a maximum distribution equal to the number that you identified in the licensing process.

This License includes use in an electronic form, provided its password protected or on the university's intranet or repository, including UMI (according to the definition at the Sherpa website: http://www.sherpa.ac.uk/romeo/). For any other electronic use, please contact Springer at (permissions.dordrecht@springer.com or permissions.heidelberg@springer.com).

The material can only be used for the purpose of defending your thesis, and with a maximum of 100 extra copies in paper.

Although Springer holds copyright to the material and is entitled to negotiate on rights, this license is only valid, subject to a courtesy information to the author (address is given with the article/chapter) and provided it concerns original material which does not carry references to other sources (if material in question appears with credit to another source, authorization from that source is required as well).

Permission free of charge on this occasion does not prejudice any rights we might have to charge for reproduction of our copyrighted material in the future.

Altering/Modifying Material: Not Permitted
You may not alter or modify the material in any manner. Abbreviations, additions, deletions and/or any other alterations shall be made only with prior written authorization of the author(s) and/or Springer Science + Business Media. (Please contact Springer at (permissions.dordrecht@springer.com or permissions.heidelberg@springer.com)

Reservation of Rights
Springer Science + Business Media reserves all rights not specifically granted in the combination of (i) the license details provided by you and accepted in the course of this licensing transaction, (ii) these terms and conditions and (iii) CCC's Billing and Payment terms and conditions.

Copyright Notice:Disclaimer
You must include the following copyright and permission notice in connection with any reproduction of the licensed material: "Springer and the original publisher /journal title, volume, year of publication, page, chapter/article title, name(s) of author(s), figure number(s), original copyright notice) is given to the publication in which the material was originally published, by adding; with kind permission from Springer Science and Business Media"

Warranties: None

Example 1: Springer Science + Business Media makes no representations or warranties with respect to the licensed material.

Example 2: Springer Science + Business Media makes no representations or warranties with respect to the licensed material and adopts on its own behalf the limitations and disclaimers established by CCC on its behalf in its Billing and Payment terms and conditions for this licensing transaction.

Indemnity
You hereby indemnify and agree to hold harmless Springer Science + Business Media and CCC, and their respective officers, directors, employees and agents, from and against any and all claims arising out of your use of the licensed material other than as specifically authorized pursuant to this license.

No Transfer of License
This license is personal to you and may not be sublicensed, assigned, or transferred by you to any other person without Springer Science + Business Media's written permission.

No Amendment Except in Writing
This license may not be amended except in a writing signed by both parties (or, in the case of Springer Science + Business Media, by CCC on Springer Science + Business Media's behalf).

Objection to Contrary Terms
Springer Science + Business Media hereby objects to any terms contained in any purchase order, acknowledgment, check endorsement or other writing prepared by you, which terms are inconsistent with these terms and conditions or CCC's Billing and Payment terms and conditions. These terms and conditions, together with CCC's Billing and Payment terms and conditions (which are incorporated herein), comprise the entire agreement between you and Springer Science + Business Media (and CCC) concerning this licensing transaction. In the event of any conflict between your obligations established by these terms and conditions and those established by CCC's Billing and Payment terms and conditions, these terms and conditions shall control.

Jurisdiction
All disputes that may arise in connection with this present License, or the breach thereof, shall be settled exclusively by arbitration, to be held in The Netherlands, in accordance with Dutch law, and to be conducted under the Rules of the 'Netherlands Arbitrage Instituut' (Netherlands Institute of Arbitration).***OR:***

All disputes that may arise in connection with this present License, or the breach thereof, shall be settled exclusively by arbitration, to be held in the Federal Republic of Germany, in accordance with German law.

Other terms and conditions:

v1.3

If you would like to pay for this license now, please remit this license along with your payment made payable to "COPYRIGHT CLEARANCE CENTER" otherwise you will be invoiced within 48 hours of the license date. Payment should be in the form of a check or money order referencing your account number and this invoice number RLNK501006433. Once you receive your invoice for this order, you may pay your invoice by credit card.

Please follow instructions provided at that time.

Make Payment To:
Copyright Clearance Center
Dept 001
P.O. Box 843006
Boston, MA 02284-3006

For suggestions or comments regarding this order, contact RightsLink Customer Support: customercare@copyright.com or +1-877-622-5543 (toll free in the US) or +1-978-646-2777.

Gratis licenses (referencing $0 in the Total field) are free. Please retain this printable license for your reference. No payment is required.

REFERENCES

1. Wang, L., Munir, Z. & Maximov, Y. Thermite Reactions - Their Utilization in the Synthesis and Processing. Journal of Materials Science 28, 3693–3708 (1993).
2. Dreizin, E. L. Metal-based reactive nanomaterials. Progress in Energy and Combustion Science 35, 141–167 (2009).
3. Goldschmidt. Verfahren zur Herstellung von Metallen oder Metalloiden oder Legierungen derselben" (Process for the production of metals or metalloids or alloys of the same).
4. Sullivan, K. T. Ignition, Combustion and Tuning of Nanocomposite Thermites. (2010). at <http://drum.lib.umd.edu/handle/1903/11119>
5. Cheng, J. L., Hng, H. H., Lee, Y. W., Du, S. W. & Thadhani, N. N. Kinetic study of thermal-and impact-initiated reactions in Al–Fe_2O_3 nanothermite. Combustion and Flame 157, 2241–2249 (2010).
6. Park, C.-D., Mileham, M., van de Burgt, L. J., Muller, E. A. & Stiegman, A. E. The Effects of Stoichiometry and Sample Density on Combustion Dynamics and Initiation Energy of Al/Fe_2O_3 Metastable Interstitial Composites. The Journal of Physical Chemistry C 114, 2814–2820 (2010).
7. Plantier, K. B., Pantoya, M. L. & Gash, A. E. Combustion wave speeds of nanocomposite Al/Fe_2O_3: the effects of Fe_2O_3 particle synthesis technique. Combustion and Flame 140, 299–309 (2005).
8. Apperson, S. et al. Generation of fast propagating combustion and shock waves with copper oxide/aluminum nanothermite composites. Applied Physics Letters 91, 243109 (2007).
9. Ohkura, Y., Liu, S.-Y., Rao, P. M. & Zheng, X. Synthesis and ignition of energetic CuO/Al core/shell nanowires. Proceedings of the Combustion Institute 33, 1909–1915 (2011).
10. Shende, R. et al. Nanoenergetic Composites of CuO Nanorods, Nanowires, and Al-Nanoparticles. Propellants, Explosives, Pyrotechnics 33, 122–130 (2008).
11. Jian, G., Piekiel, N. W. & Zachariah, M. R. Time-Resolved Mass Spectrometry of Nano-Al and Nano-Al/CuO Thermite under Rapid Heating: A Mechanistic Study. The Journal of Physical Chemistry C 116, 26881–26887 (2012).
12. Sanders, V. E. et al. Reaction Propagation of Four Nanoscale Energetic Composites (Al/MoO_3, Al/WO_3, Al/CuO, and $B_{12}O_3$). Journal of Propulsion and Power 23, 707–714 (2007).
13. Séverac, F., Alphonse, P., Estève, A., Bancaud, A. & Rossi, C. High-Energy Al/CuO Nanocomposites Obtained by DNA-Directed Assembly. Advanced Functional Materials 22, 323–329 (2012).
14. Sullivan, K. T., Kuntz, J. D. & Gash, A. E. Electrophoretic deposition and mechanistic studies of nano-Al/CuO thermites. Journal of Applied Physics 112, 024316 (2012).
15. Umbrajkar, S. M., Schoenitz, M. & Dreizin, E. L. Exothermic reactions in Al–CuO nanocomposites. Thermochimica Acta 451, 34–43 (2006).
16. Wang, J., Hu, A., Persic, J., Wen, J. Z. & Norman Zhou, Y. Thermal stability and reaction properties of passivated Al/CuO nano-thermite. Journal of Physics and Chemistry of Solids 72, 620–625 (2011).
17. Weismiller, M. R., Malchi, J. Y., Yetter, R. A. & Foley, T. J. Dependence of flame propagation on pressure and pressurizing gas for an Al/CuO nanoscale thermite. Proceedings of the Combustion Institute 32, 1895–1903 (2009).

18. Kaili Zhang, Rossi, C., Petrantoni, M. & Mauran, N. A Nano Initiator Realized by Integrating Al/CuO-Based Nanoenergetic Materials With a Au/Pt/Cr Microheater. Journal of Microelectromechanical Systems 17, 832–836 (2008).
19. Zhou, X. et al. Influence of Al/CuO reactive multilayer films additives on exploding foil initiator. Journal of Applied Physics 110, 094505 (2011).
20. Son, S. F. et al. Combustion of Nanoscale Al/MoO_3 Thermite in Microchannels. Journal of Propulsion and Power 23, 715–721 (2007).
21. Sun, J., Pantoya, M. L. & Simon, S. L. Dependence of size and size distribution on reactivity of aluminum nanoparticles in reactions with oxygen and MoO_3. Thermochimica Acta 444, 117–127 (2006).
22. Gibot, P. et al. Synthesis of WO_3 nanoparticles for superthermites by the template method from silica spheres. Solid State Sciences 13, 908–914 (2011).
23. Sullivan, K. T., Chiou, W.-A., Fiore, R. & Zachariah, M. R. In situ microscopy of rapidly heated nano-Al and nano-Al/WO_3 thermites. Applied Physics Letters 97, 133104 (2010).
24. Puszynski, J. A., Bulian, C. J. & Swiatkiewicz, J. J. Processing and Ignition Characteristics of Aluminum-Bismuth Trioxide Nanothermite System. Journal of Propulsion and Power 23, 698–706 (2007).
25. Wang, L., Luss, D. & Martirosyan, K. S. The behavior of nanothermite reaction based on Bi_2O_3/Al. Journal of Applied Physics 110, 074311 (2011).
26. Rossi, C. et al. Nanoenergetic Materials for MEMS: A Review. Journal of Microelectromechanical Systems 16, 919–931 (2007).
27. Zhang, K. et al. Integrating Al with NiO nano honeycomb to realize an energetic material on silicon substrate. Applied Physics A 94, 957–962 (2008).
28. Valliappan, S., Swiatkiewicz, J. & Puszynski, J. A. Reactivity of aluminum nanopowders with metal oxides. Powder Technology 156, 164–169 (2005).
29. S. H. Fischer & M. C. Grubelich. A Survey of Combustible Metals, Thermites, and Intermetallics for Pyrotechnic Applications. in (Sandia National Laboratories, 1996).
30. Meric, C., Atik, E. & Sahin, S. Mechanical and metallurgical properties of welding zone in rail welded via thermite process. Science and Technology of Welding & Joining 7, 172–176 (2002).
31. derlin, k. u. a. Oberbau-Schweissen. 8, (Mainz, Eisenbahn-Fachverlag).
32. Drake, T. NS Engineering Department's Role in Thoroughbred Transportation. at <http://www.sec.gov/Archives/edgar/data/702165/000070216507000154/drake1.htm>
33. Fischer, S. H. & Grubelich, M. C. in (1996).
34. Aumann, C., Skofronick, G. & Martin, J. Oxidation Behavior of Aluminum Nanopowders. Journal of Vacuum Science & Technology B 13, 1178–1183 (1995).
35. Pantoya, M. L. & Granier, J. J. Combustion behavior of highly energetic thermites: Nano versus micron composites. Propellants, Explosives, Pyrotechnics 30, 53–62 (2005).
36. Wei, D., Dave, R. & Pfeffer, R. Mixing and characterization of nanosized powders: An assessment of different techniques. Journal of Nanoparticle Research 4, 21–41 (2002).
37. Tillotson, T. et al. Nanostructured energetic materials using sol–gel methodologies. Journal of Non-Crystalline Solids 285, 338–345 (2001).
38. Gash, A. E. et al. Use of epoxides in the sol-gel synthesis of porous iron(III) oxide monoliths from Fe(III) salts. Chemistry of Materials 13, 999–1007 (2001).

39. Gash, A. E., Tillotson, T. M., Satcher Jr, J. H., Hrubesh, L. W. & Simpson, R. L. New sol–gel synthetic route to transition and main-group metal oxide aerogels using inorganic salt precursors. Journal of Non-Crystalline Solids 285, 22–28 (2001).
40. Gash, A. E., Satcher Jr., J. H., Simpson, R. L. & Clapsaddle, B. J. Nanostructured energetic materials with sol-gel methods. in Materials Research Society Symposium - Proceedings 800, 55–66 (2003).
41. Clapsaddle, B. J. et al. Synthesis and characterization of mixed metal oxide nanocomposite energetic materials. in Materials Research Society Symposium - Proceedings 800, 91–96 (2003).
42. Mehendale, B. et al. Nanoenergetic Composite of Mesoporous Iron Oxide and Aluminum Nanoparticles. Journal of Energetic Materials 24, 341–360 (2006).
43. Ma, E., Thompson, C. V., Clevenger, L. A. & Tu, K. N. Self-propagating explosive reactions in Al/Ni multilayer thin films. Applied Physics Letters 57, 1262–1264 (1990).
44. Barbee TW & Weihs T. Ignitable heterogeneous stratified structure for the propagation of an internal exothermic chemical reaction along an expanding wavefront and method of making the same.
45. Wang, J. et al. Room-temperature soldering with nanostructured foils. Appl Phys Lett 83, 3987–3989 (2003).
46. Wang, J. et al. Joining of stainless-steel specimens with nanostructured Al/Ni foils. J Appl Phys 95, 248–256 (2004).
47. Duckham, A. et al. Reactive nanostructured foil used as a heat source for joining titanium. J Appl Phys 96, 2336–2342 (2004).
48. Gavens, A. J., Van Heerden, D., Mann, A. B., Reiss, M. E. & Weihs, T. P. Effect of intermixing on self-propagating exothermic reactions in Al/Ni nanolaminate foils. Journal of Applied Physics 87, 1255–1263 (2000).
49. Blobaum, K. J., Reiss, M. E., Plitzko, J. M. & Weihs, T. P. Deposition and characterization of a self-propagating CuO_x/Al thermite reaction in a multilayer foil geometry. Journal of Applied Physics 94, 2915 (2003).
50. Blobaum, K. J. et al. Investigating the reaction path and growth kinetics in CuOx/Al multilayer foils. Journal of Applied Physics 94, 2923–2929 (2003).
51. Dreizin EL & Schoenitz M. Nano-composite energetic powders prepared by arrested reactive milling. (2006).
52. Schoenitz, M., Ward, T. S. & Dreizin, E. L. Fully dense nano-composite energetic powders prepared by arrested reactive milling. Proceedings of the Combustion Institute 30, 2071–2078 (2005).
53. Umbrajkar, S., Trunov, M. A., Schoenitz, M., Dreizin, E. L. & Broad, R. Arrested reactive milling synthesis and characterization of sodium-nitrate based reactive composites. Propellants, Explosives, Pyrotechnics 32, 32–41 (2007).
54. Umbrajkar, S. M., Schoenitz, M. & Dreizin, E. L. Control of structural refinement and composition in Al-MoO_3 nanocomposites prepared by arrested reactive milling. Propellants, Explosives, Pyrotechnics 31, 382–389 (2006).
55. Umbrajkar, S. M., Seshadri, S., Schoenitz, M., Hoffmann, V. K. & Dreizin, E. L. Aluminum-Rich Al-MoO3 Nanocomposite Powders Prepared by Arrested Reactive Milling. Journal of Propulsion and Power 24, 192–189 (2008).

56. Ward, T. S., Chen, W., Schoenitz, M., Dave, R. N. & Dreizin, E. L. A study of mechanical alloying processes using reactive milling and discrete element modeling. Acta Materialia 53, 2909–2918 (2005).
57. Chowdhury, S., Sullivan, K., Piekiel, N., Zhou, L. & Zachariah, M. R. Diffusive vs Explosive Reaction at the Nanoscale. The Journal of Physical Chemistry C 114, 9191–9195 (2010).
58. Menon, L. et al. Size dependence of energetic properties in nanowire-based energetic materials. Journal of Applied Physics 100, 034317 (2006).
59. Shimojo, F., Nakano, A., Kalia, R. K. & Vashishta, P. Enhanced reactivity of nanoenergetic materials: A first-principles molecular dynamics study based on divide-and-conquer density functional theory. Applied Physics Letters 95, 043114 (2009).
60. Sullivan, K. T. et al. Ignition and Combustion Characteristics of Nanoscale Al/$AgIO_3$: A Potential Energetic Biocidal System. Combustion Science and Technology 183, 285–302 (2010).
61. Son, S. F. PROPAGATION STUDIES OF METASTABLE INTERMOLECULAR COMPOSITES (ME). (2002).
62. Kim, J. S. et al. Direct characterization of phase transformations and morphologies in moving reaction zones in Al/Ni nanolaminates using dynamic transmission electron microscopy. Acta Materialia 59, 3571–3580 (2011).
63. Cherukara, M. J., Vishnu, K. G. & Strachan, A. Role of nanostructure on reaction and transport in Ni/Al intermolecular reactive composites. Physical Review B - Condensed Matter and Materials Physics 86, (2012).
64. Swiston, A. J., Hufnagel, T. C. & Weihs, T. P. Joining bulk metallic glass using reactive multilayer foils. Scripta Materialia 48, 1575–1580 (2003).
65. GIBSON N, LLOYD FC & PERRY GR. FIRE HAZARDS IN CHEMICAL PLANT FROM FRICTION SPARKS INVOLVING THE THERMITE REACTION. 26–35 (1967).
66. Strunina, A. G., Martem'yanova, T. M., Barzykin, V. V. & Ermakov, V. I. Ignition of gasless systems by a combustion wave. Combust Explos Shock Waves 10, 449–455 (1974).
67. Ermakov, V. I., Strunina, A. G. & Barzykin, V. V. An experimental study of ignition of gasless systems by a combustion wave. Combust Explos Shock Waves 12, 185–190 (1977).
68. Strunina, A. G., Ermakov, V. I. & Averson, E. A. Limiting conditions of ignition of gasless systems by a combustion wave. Combust Explos Shock Waves 15, 484–489 (1980).
69. Kostin, S. V., Strunina, A. G. & Barzykin, V. V. Experimental investigation of the transient combustion regimes of low-gas heterogeneous systems. Combust Explos Shock Waves 18, 524–529 (1983).
70. Chernenko, E. V., Afanas'eva, L. F., Lebedeva, V. A. & Rozenband, V. I. Inflammability of mixtures of metal oxides with aluminum. Combust Explos Shock Waves 24, 639–646 (1989).
71. Levitas, V. I., Asay, B. W., Son, S. F. & Pantoya, M. Melt dispersion mechanism for fast reaction of nanothermites. Applied Physics Letters 89, 071909 (2006).
72. Levitas, V. I., Asay, B. W., Son, S. F. & Pantoya, M. Mechanochemical mechanism for fast reaction of metastable intermolecular composites based on dispersion of liquid metal. Journal of Applied Physics 101, 083524 (2007).
73. Levitas, V. I., Pantoya, M. L. & Dikici, B. Melt dispersion versus diffusive oxidation mechanism for aluminum nanoparticles: Critical experiments and controlling parameters. Applied Physics Letters 92, 011921 (2008).

74. Levitas, V. I. Burn time of aluminum nanoparticles: Strong effect of the heating rate and melt-dispersion mechanism. Combustion and Flame 156, 543–546 (2009).
75. Trunov, M. A., Schoenitz, M., Zhu, X. & Dreizin, E. L. Effect of polymorphic phase transformations in Al_2O_3 film on oxidation kinetics of aluminum powders. Combustion and Flame 140, 310–318 (2005).
76. Rai, A., Park, K., Zhou, L. & Zachariah, M. R. Understanding the mechanism of aluminium nanoparticle oxidation. Combustion Theory and Modelling 10, 843–859 (2006).
77. Henz, B. J., Hawa, T. & Zachariah, M. R. On the role of built-in electric fields on the ignition of oxide coated nanoaluminum: Ion mobility versus Fickian diffusion. Journal of Applied Physics 107, 024901 (2010).
78. Firmansyah, D. A. et al. Microstructural Behavior of the Alumina Shell and Aluminum Core Before and After Melting of Aluminum Nanoparticles. The Journal of Physical Chemistry C 116, 404–411 (2012).
79. Zhou, L., Piekiel, N., Chowdhury, S. & Zachariah, M. R. Time-resolved mass spectrometry of the exothermic reaction between nanoaluminum and metal oxides: The role of oxygen release. Journal of Physical Chemistry C 114, 14269–14275 (2010).
80. Rai, A., Lee, D., Park, K. & Zachariah, M. R. Importance of Phase Change of Aluminum in Oxidation of Aluminum Nanoparticles. The Journal of Physical Chemistry B 108, 14793–14795 (2004).
81. Dubrovin, A. S., Slepova, L. V. & Kuznetsov, V. L. Effect of density on the combustion of aluminothermic compositions. Combust Explos Shock Waves 6, 60–67 (1972).
82. Balakir, E. A. et al. Rate of combustion of exothermal mixtures. Combust Explos Shock Waves 11, 36–38 (1976).
83. Serkov, B. B., Maksimov, E. I. & Merzhanov, A. G. Combustion of condensed systems in a mass-force field. Combust Explos Shock Waves 4, 349–352 (1971).
84. Karataskov, S. A., Yukhvid, V. I. & Merzhanov, A. G. Regularities and mechanism of combustion of melting heterogeneous systems in a mass force field. Combust Explos Shock Waves 21, 687–689 (1986).
85. Ivanov, G. V., Surkov, V. G., Viktorenko, A. M., Reshetov, A. A. & Ivanov, V. G. Anomalous dependence of the combustion rate of thermite mixtures on the pressure. Combust Explos Shock Waves 15, 266–268 (1979).
86. Yukhvid, V. I., Borovinskaya, I. P. & Merzhanov, A. G. Influence of pressure on the laws governing the combustion of molten heterogeneous systems. Combust Explos Shock Waves 19, 277–279 (1983).
87. Puszynski, J. A., Bulian, C. J. & Swiatkiewicz, J. J. The effect of nanopowder attributes on reaction mechanism and ignition sensitivity of nanothermites. in Materials Research Society Symposium Proceedings 896, 147–158 (2006).
88. Moore, K., Pantoya, M. L. & Son, S. F. Combustion behaviors resulting from bimodal aluminum size distributions in thermites. J Propul Power 23, 181–185 (2007).
89. Prentice, D., Pantoya, M. L. & Clapsaddle, B. J. Effect of nanocomposite synthesis on the combustion performance of a ternary thermite. Journal of Physical Chemistry B 109, 20180–20185 (2005).
90. Yetter, R. A., Risha, G. A. & Son, S. F. Metal particle combustion and nanotechnology. Proceedings of the Combustion Institute 32, 1819–1838 (2009).
91. Beckstead M.W. A Summary of Aluminum Combustion. in published in RTO-EN-023. (2003).

92. Puszynski, J. A. Processing and characterization of aluminum-based nanothermites. Journal of Thermal Analysis and Calorimetry 96, 677–685 (2009).
93. Park, K., Lee, D., Rai, A., Mukherjee, D. & Zachariah, M. R. Size-Resolved Kinetic Measurements of Aluminum Nanoparticle Oxidation with Single Particle Mass Spectrometry. The Journal of Physical Chemistry B 109, 7290–7299 (2005).
94. Huang, Y., Risha, G. A., Yang, V. & Yetter, R. A. Combustion of bimodal nano/micron-sized aluminum particle dust in air. in 31 II, 2001–2009 (2007).
95. Maksimov E. I., Merzhanov A. G. & Shkior V. M. Combust. Explos. Shock Waves (Engl. Transl.) 2[4] 15 (1965).
96. Kstylev V. M. & Nabatov V. G. J. Eng. Phys. 9 259 (1965).
97. Wang L. L. (1991).
98. Netzsch STA 409 Manual. (2011).
99. Schoenitz, M., Umbrajkar, S. M. & Dreizin, E. L. Kinetic Analysis of Thermite Reactions in Al-MoO3 Nanocomposites. Journal of Propulsion and Power 23, 683–687 (2007).
100. Zhu, H. X. & Abbaschian, R. In-situ processing of NiAl–alumina composites by thermite reaction. Materials Science and Engineering: A 282, 1–7 (2000).
101. Mehra, O. K., Bose, D. K. & Gupta, C. K. MOLYBDENUM METAL BY THE ALUMINOTHERMIC REDUCTION OF CALCIUM MOLYBDATE. Metall Trans 4, 691–694 (1973).
102. BELITSKUS D. Aluminothermic production of metals and alloys. J Met 24, 30–34 (1972).
103. Carlson, O. N. REDUCTION OF OXIDES BY METALS. Prog in Extr Metall 1, 187–206 (1973).
104. Munir, Z. A. & Anselmi-Tamburini, U. Self-propagating exothermic reactions: The synthesis of high-temperature materials by combustion. Materials Science Reports 3, 277–365 (1989).
105. Odawara, O. & Ikeuchi, J. STUDY ON COMPOSITE MATERIALS WITH CENTRIFUGAL-THERMIT PROCESS. Nippon Kinzoku Gakkaishi 45, 316–321 (1981).
106. Merzhanov, A. G. Combustion processes that synthesize materials. J Mater Process Technol 56, 222–241 (1996).
107. Key, A. J. THERMIT PROCESS FOR RAILWELDING. Met Constr 16, 419–422 (1984).
108. Zarechenskii, A. V., Leshchinskii, L. K. & Chigarev, V. V. SPECIAL FEATURES OF MELTING FLUX-CORED STRIPS WITH THERMITE MIXTURES. Weld Prod 32, 51–53 (1985).
109. Lindsay, W., Teasdale, D., Milanovic, V., Pister, K. & Fernandez-Pello, C. Thrust and electrical power from solid propellant microrockets. 2. Actuators. in Micro Electro Mechanical Systems, 2001. MEMS 2001. The 14th IEEE International Conference on 606–610 (2001).
110. Tanaka, S. et al. MEMS-Based Solid Propellant Rocket Array Thruster with Electrical Feedthroughs. TRANSACTIONS OF THE JAPAN SOCIETY FOR AERONAUTICAL AND SPACE SCIENCES 46, 47–51 (2003).
111. Zhang, K. L., Chou, S. K., Ang, S. S. & Tang, X. S. A MEMS-based solid propellant microthruster with Au/Ti igniter. Sensors and Actuators A: Physical 122, 113–123 (2005).
112. Larangot, B. et al. Solid propellant micro-rockets–towards a new type of power MEMS. Proceedings of the AIAA Nanotech 2, 9–11 (2002).
113. Lewis, D. H., Janson, S. W., Cohen, R. B. & Antonsson, E. K. Digital micropropulsion. Sensors and Actuators A: Physical 80, 143–154 (2000).

114. Teasdale, D., Milanovic, V., Chang, P. & Pister, K. S. J. Microrockets for Smart Dust. Smart Materials and Structures 10, 1145–1155 (2001).
115. Apperson, S. et al. Nanothermite-Based Microsystem for Drug Delivery and Cell Transfection. (DTIC Document, 2008). Retrieved from http://oai.dtic.mil/oai/oai?verb=getRecord&metadataPrefix=html&identifier=ADA505079
116. Zhou, Y. & Institute of Materials, M. Microjoining and nanojoining. (Woodhead Publishing and Maney Publishing, on behalf of the Institute of Materials, Minerals & Mining ; CRC Press, 2008).
117. Miyamoto, Y., Nakamoto, T., Koizumi, M. & Yamada, O. Ceramic-to-metal welding by a pressurized combustion reaction. Journal of Materials Research 1, 7–9 (1986).
118. Pascal, C., Marin-Ayral, R. M. & Tedenac, J. C. Joining of nickel monoaluminide to a superalloy substrate by high pressure self-propagating high-temperature synthesis. Journal of alloys and compounds 337, 221–225 (2002).
119. Bahrami Motlagh, E., Vahdati Khaki, J. & Haddad Sabzevar, M. Welding of aluminum alloys through thermite like reactions in Al-CuO-Ni system. Materials Chemistry and Physics 133, 757–763 (2012).
120. Cao, J., Song, X. G., Wu, L. Z., Qi, J. L. & Feng, J. C. Characterization of Al/Ni multilayers and their application in diffusion bonding of TiAl to TiC cermet. Thin Solid Films 520, 3528–3531 (2012).
121. Blobaum, K. J., Van Heerden, D., Gavens, A. J. & Weihs, T. P. Al/Ni formation reactions: Characterization of the metastable Al 9Ni 2 phase and analysis of its formation. Acta Materialia 51, 3871–3884 (2003).
122. Lu, C. et al. Simple Template-Free Solution Route for the Controlled Synthesis of $Cu(OH)_2$ and CuO Nanostructures. The Journal of Physical Chemistry B 108, 17825–17831 (2004).
123. Wang, J. Personal Communication. (2010).
124. Hu, A. Personal Communication. (2010).
125. Kleinke, H. Thermal analysis, Netzsch STA 409. Retrieved from http://kleinke.uwaterloo.ca/equip.html
126. CAMJ equipment. at <http://mme.uwaterloo.ca/~camj/equipment/diffraction.html>
127. Wen, J. Z. et al. Characterization of thermochemical properties of Al nanoparticle and NiO nanowire composites. Nanoscale Research Letters 8, 184 (2013).
128. Apperson, S. J. et al. Characterization of Nanothermite Material for Solid-Fuel Microthruster Applications. Journal of Propulsion and Power 25, 1086–1091 (2009).
129. Howell, J. A., Mohney, S. E. & Muhlstein, C. L. Developing Ni–Al and Ru–Al intermetallic films for use in microelectromechanical systems. Journal of Vacuum Science & Technology B: Microelectronics and Nanometer Structures 29, 042002 (2011).
130. Martirosyan, K. S. Nanoenergetic Gas-Generators: principles and applications. Journal of Materials Chemistry 21, 9400 (2011).
131. Sullivan, K. et al. Simultaneous Pressure and Optical Measurements of Nanoaluminum Thermites: Investigating the Reaction Mechanism. Journal of Propulsion and Power 26, 467–472 (2010).
132. Fischer, S. H. & Grubelich, M. C. Theoretical Energy Release of Thermites, Intermetallics and Combustion Metals. (1998).
133. Zhang, J., Liu, J., Peng, Q., Wang, X. & Li, Y. Nearly Monodisperse Cu 2 O and CuO Nanospheres: Preparation and Applications for Sensitive Gas Sensors. Chemistry of Materials 18, 867–871 (2006).

134. Ahn, J. Y., Kim, W. D., Cho, K., Lee, D. & Kim, S. H. Effect of metal oxide nanostructures on the explosive property of metastable intermolecular composite particles. Powder Technology 211, 65–71 (2011).
135. Siegert, B., Comet, M., Muller, O., Pourroy, G. & Spitzer, D. Reduced-Sensitivity Nanothermites Containing Manganese Oxide Filled Carbon Nanofibers. The Journal of Physical Chemistry C 114, 19562–19568 (2010).
136. Thiruvengadathan, R. et al. Combustion characteristics of novel hybrid nanoenergetic formulations. Combustion and Flame 158, 964–978 (2011).
137. Pantoya, M. L. et al. in Defense Applications of Nanomaterials 891, 227–240 (American Chemical Society, 2005).
138. Evteev, A. V., Levchenko, E. V., Riley, D. P., Belova, I. V. & Murch, G. E. Reaction of a Ni-coated Al nanoparticle to form B_2-NiAl: A molecular dynamics study. Philosophical Magazine Letters 89, 815–830 (2009).
139. Levchenko, E. V., Evteev, A. V., Riley, D. P., Belova, I. V. & Murch, G. E. Molecular dynamics simulation of the alloying reaction in Al-coated Ni nanoparticle. Computational Materials Science 47, 712–720 (2010).
140. Prakash, A., McCormick, A. V. & Zachariah, M. R. Tuning the Reactivity of Energetic Nanoparticles by Creation of a Core−Shell Nanostructure. Nano Letters 5, 1357–1360 (2005).
141. Ramos, A. S. & Vieira, M. T. Intermetallic compound formation in Pd/Al multilayer thin films. Intermetallics 25, 70–74 (2012).
142. Lee, S.-G. & Chung, Y.-C. Molecular dynamics investigation of interfacial mixing behavior in transition metals (Fe, Co, Ni)-Al multilayer system. Journal of Applied Physics 105, 034902 (2009).
143. Noro, J., Ramos, A. S. & Vieira, M. T. Intermetallic phase formation in nanometric Ni/Al multilayer thin films. Intermetallics 16, 1061–1065 (2008).
144. Cava, S. et al. Structural characterization of phase transition of Al_2O_3 nanopowders obtained by polymeric precursor method. Materials Chemistry and Physics 103, 394–399 (2007).
145. Dean, S. W., Pantoya, M. L., Gash, A. E., Stacy, S. C. & Hope-Weeks, L. J. Enhanced Convective Heat Transfer in Nongas Generating Nanoparticle Thermites. Journal of Heat Transfer 132, 111201 (2010).

APPENDICES

Appendix A

Table 1- reproduced from Fischer and Grubelich et al.[29]

reactants		Adiabatic reaction temperature (K)			Gas production		Heat of reaction	
Constituent	g/cm^3	w/o phase changes	W phase changes	State Intermetallic product	Moles gas per 100 g	G gas per g	-Q, cal/g	-Q cal/cm^3
2Al+3AgO	6.085	7503	3253	l-g	gas	0.7519	0.8083	896.7
2Al+3Ag_2O	6.386	4941	2436	liquid	l-g	0.4298	0.4636	504.8
2A1+B_2O_3	2.524	2621	2327	s-l	solid	0	0	780.7
2Al+Bi_20_3	7.188	3995	3253	l-g	gas	0.4731	0.8941	506.1
2Al+3CoO	5.077	3392	3201	liquid	l-g	0.043	0.0254	824.7
8Al+3Co_3O_4	4,716	3938	3201	liquid	l-g	0.2196	0.1294	1012
2A1+Cr_2O_3	4.19	2789	2327	s-l	liquid	0	0	622
2Al+3CuO	5.109	5718	2843	liquid	l-g	0.54	0.3431	974.1
2Al+3Cu_2O	5.28	4132	2843	liquid	l-g	0.1221	0.0776	575.5
2Al+Fe_2O_3	4.175	4382	3135	liquid	l-g	0.1404	0.0784	945.4
8Al+3Fe_3O_4	4.264	4057	3135	liquid	l-g	0.0549	0.0307	878.8
2Al+3HgO	8.986	7169	3253	l-g	gas	0.5598	0.9913	476.6
10Al+3I_2O_5	4.119	8680	>3253*	gas	gas	0.6293	1	1486
4Al+3MnO_2	4.014	4829	2918	liquid	gas	0.8136	0.447	1159
2Al+MoO_3	3.808	5574	3253	l-g	liquid	0.2425	0J2473	1124
10Al+3Nb_2O_5	4.089	3240	2705	liquid	Solid	0	0	600.2
2Al+3NiO	5.214	3968	3187	liquid	l-g	0.0108	0.0063	822.3
2Al+Ni_2O_3	4.045	5031	3187	liquid	I-g	0.465	0.2729	1292
2Al+3PbO	8.018	3968	2327	s-l	gas	0.4146	0.8591	337.4
4Al+3PbO_2	7.085	6937	3253	l-g	gas	0.5366	0.9296	731.9
8Al+3Pb_3O_4	7.428	5427	3253	l-g	gas	0.4215	0.8466	478.1
2Al+3PdO	7.281	5022	3237	liquid	l-g	0.6577	0.6998	754.3
4Al+3SiO_2	2.668	2010	1889	solid	liquid	0	0	513.3
2Al+3SnO	5.54	3558	2876	liquid	l-g	0.107	0.127	427
4Al+3SnO_2	5.356	5019	2876	liquid	l-g	0.2928	0.3476	686.8
lOAl+3Ta_20_5	6.339	3055	2452	liquid	solid	0	0	335.6
4Al+3TiO_2	3.59	1955	1752	solid	liquid	0	0	365.1
I6AI+3U_3O_8	4.957	1406	1406	solid	solid	0	0	487.6
10Al+3V_2O_5	3.107	3953	3273	l-g	liquid	0.0699	0.0356	1092
4Al+3WO_2	8.085	4176	3253	l-g	solid	0.0662	0.0675	500.6
2Al+WO_3	5.458	5544	3253	l-g	liquid	0.1434	0.1463	696.4

Appendix B

DSC graph for Al-NiO (Φ=4) in Argon

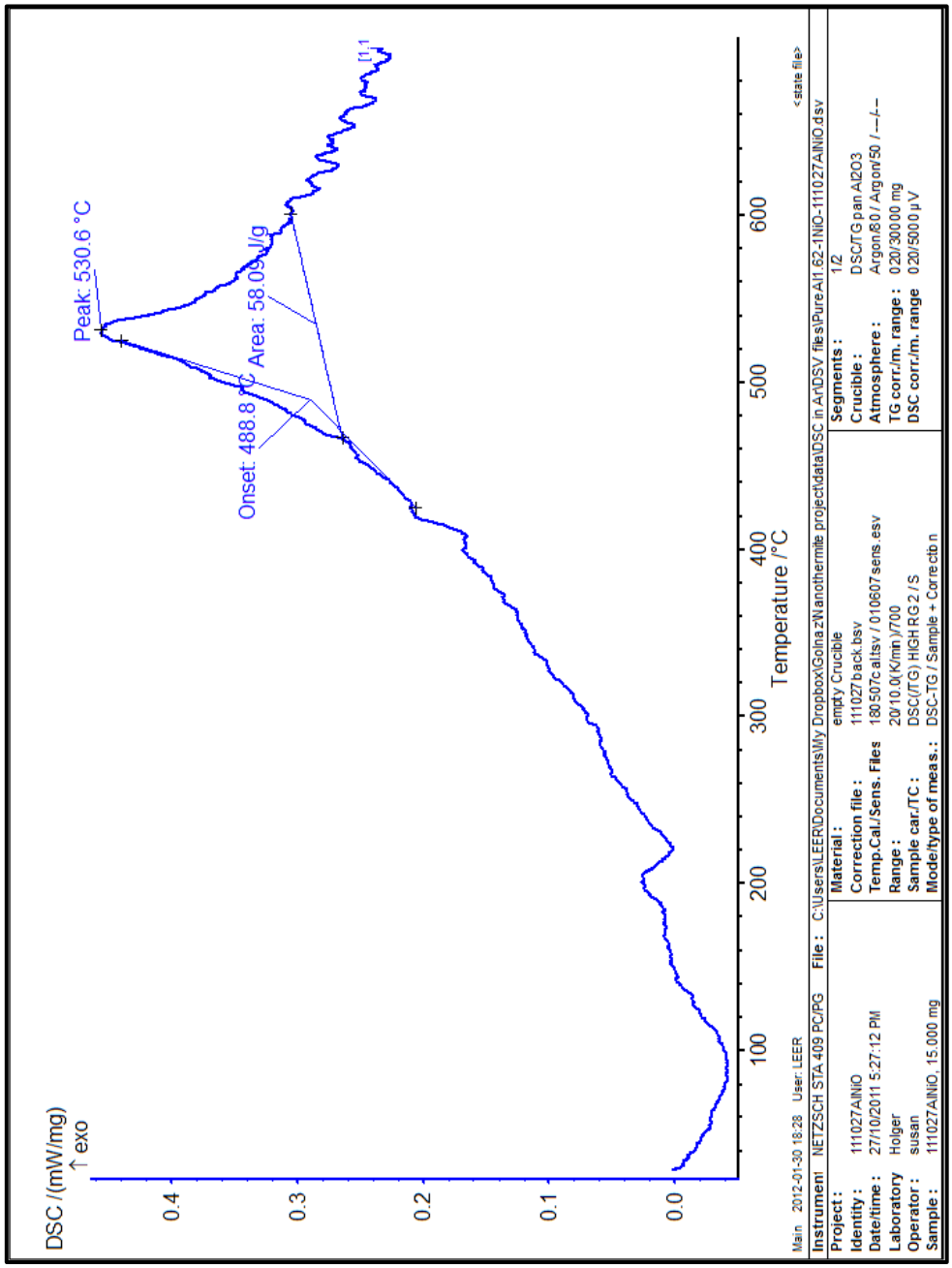

Appendix C

Additional SEM images of nanothermite composites

SEM pictures of various nanothermite composites in different conditions are presented here.

Following table explains the specific condition for each set of figures presented in this appendix.

Image set #	Composition	Equivalence ratio	Cu mass	Heat source	Preparation method	Sample form
1	Al-NiO	4	0	___*	Manual mixing/dry	Loose powder
2	Al-NiO	4	0	___	Ultrasound	Loose powder
3	Al-NiO-Cu	4	50	___	Ultrasound	Loose powder
4	Al-NiO-Cu	4	50	___	Ultrasound	Pellet
5	Al-NiO-Cu	4	50	DSC	Ultrasound	pellet
6	Al-NiO-Cu	4	80	DSC	Ultrasound	Pellet
7	Al-NiO-Cu	4	33	Flame	Ultrasound	Loose powder
8	Al-NiO-Cu	4	33	Flame	Ultrasound	Loose powder
9	Al-CuO-Cu	4	50	___	Ultrasound 20 min	Loose powder
10	Al-CuO-Cu	4	77.5	Hot plate	ultrasound	pellet
11	Al-CuO-Cu	4	80	DSC	Ultrasound	Pellet
12	Al-NiO-Sn	4	80% Sn	DSC	Ultrasound	pellet
13	Al-Fe2O3-Sn	4	80%Sn	DSC	Ultrasound	pellet

*These samples were not heated and images show the composites before reaction.

Additional SEM images of nanothermite composites

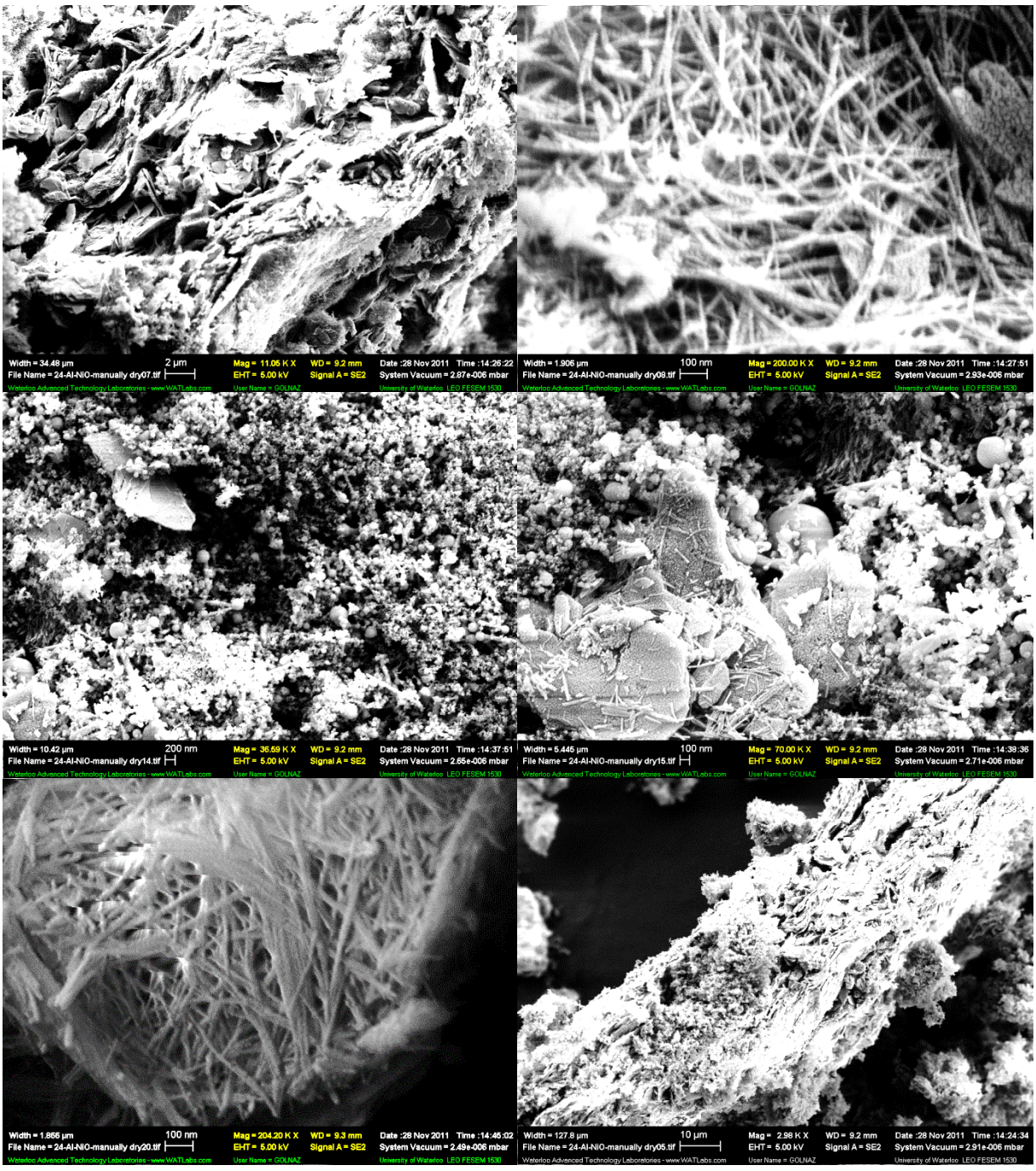

Image set 1

Additional SEM images of nanothermite composites

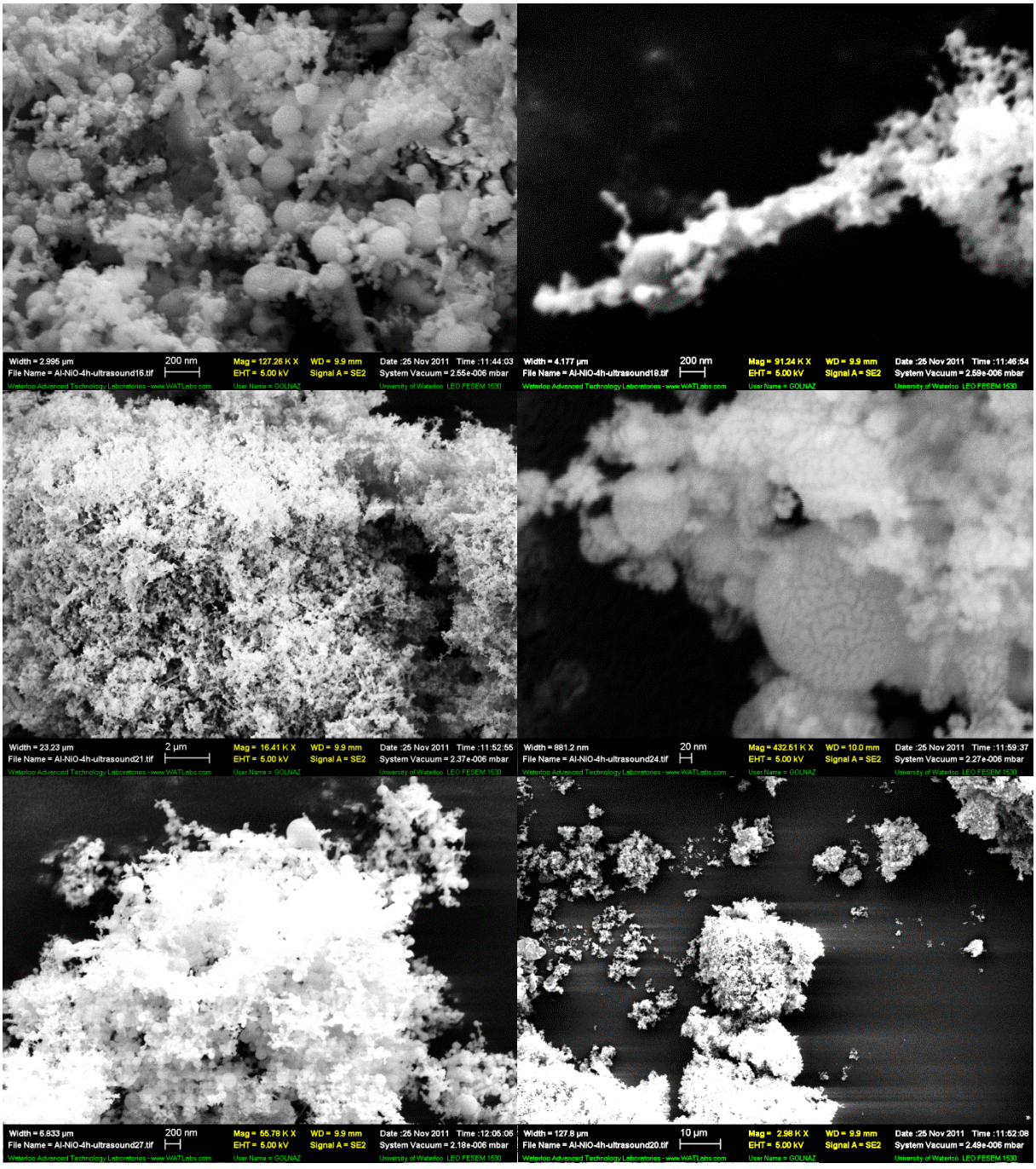

Image set 2

Additional SEM images of nanothermite composites

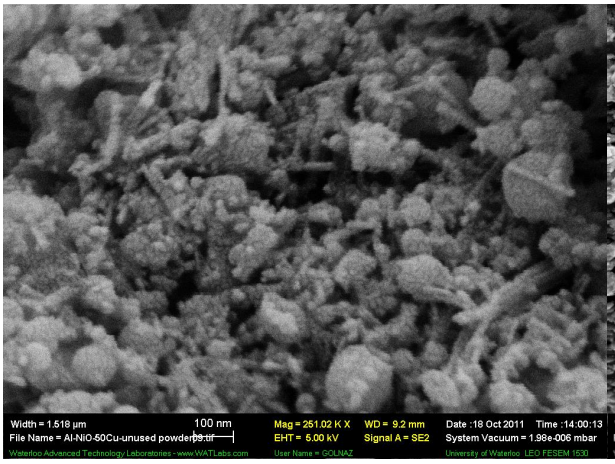

Image 3

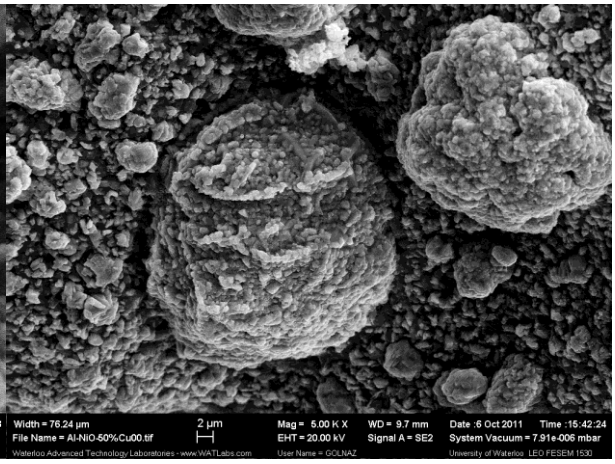

Image 4

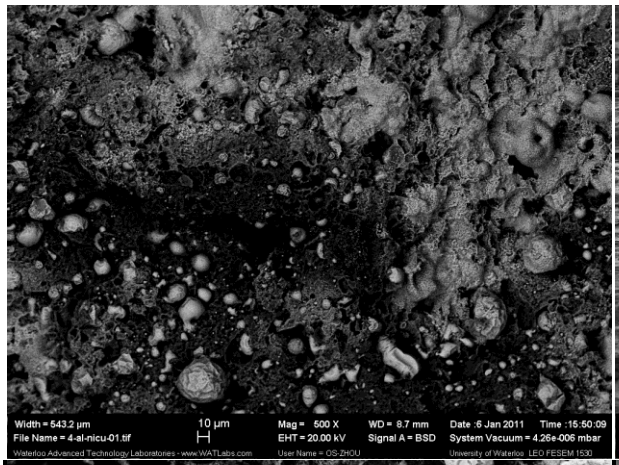

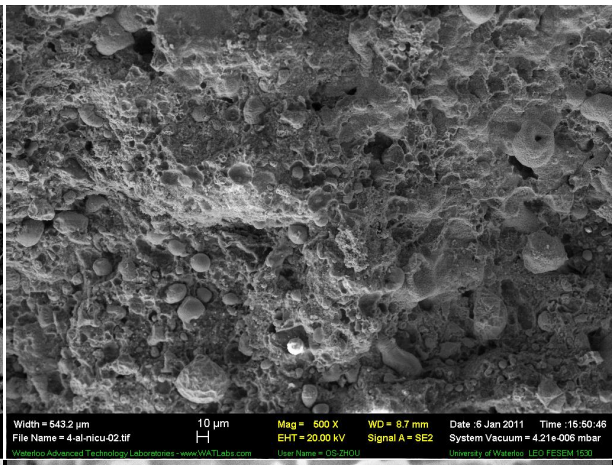

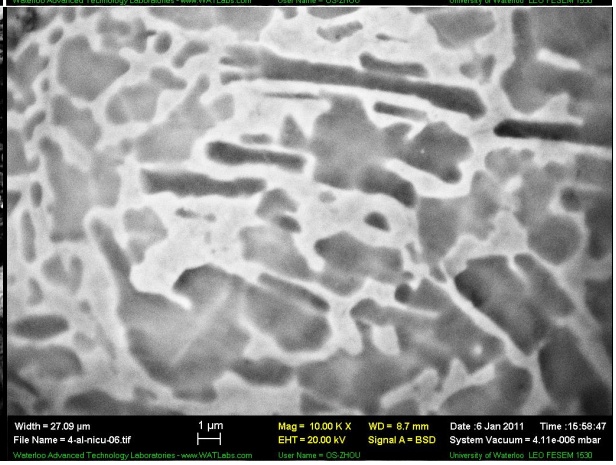

Image set 5

Additional SEM images of nanothermite composites

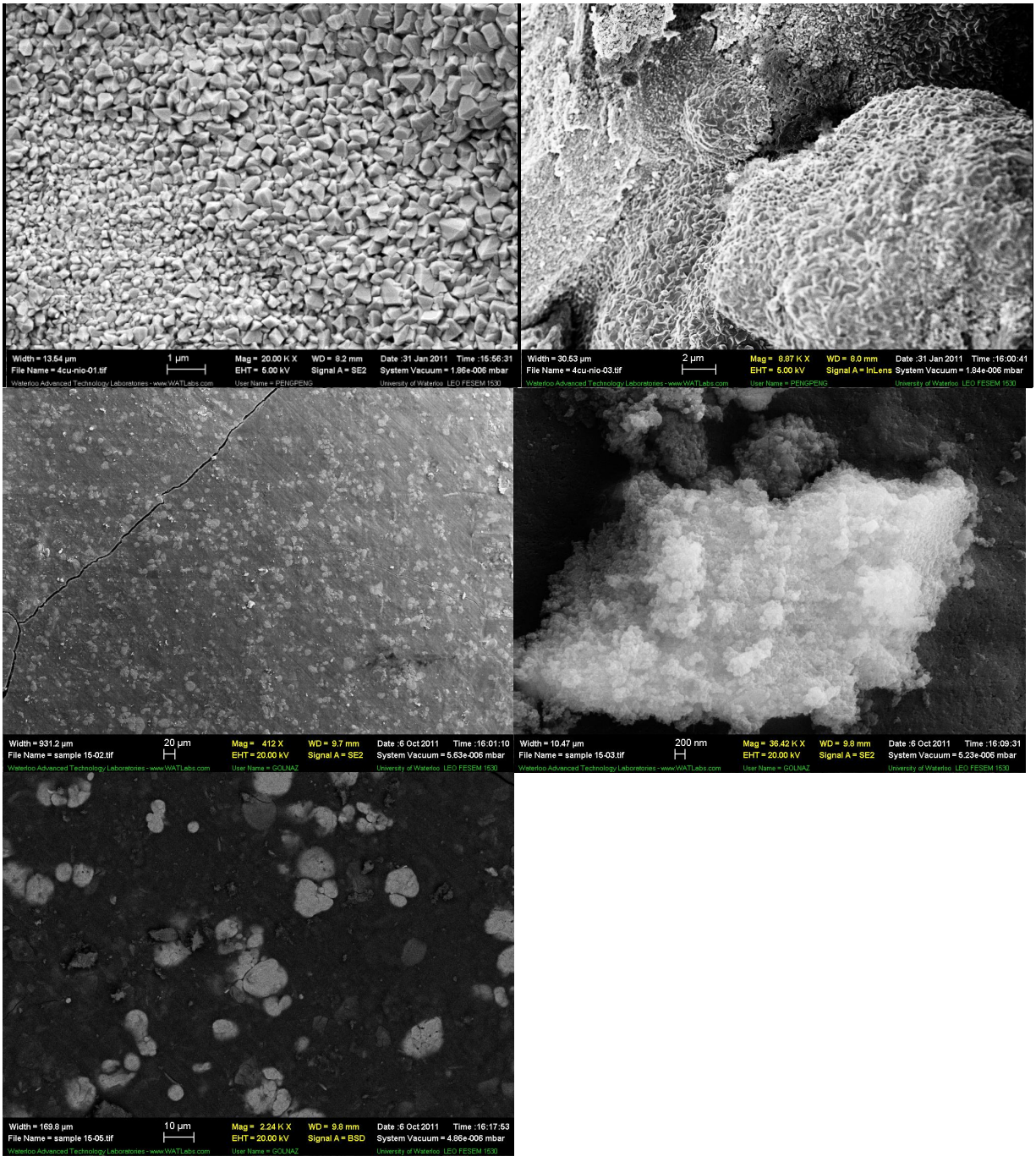

Image set 6

Additional SEM images of nanothermite composites

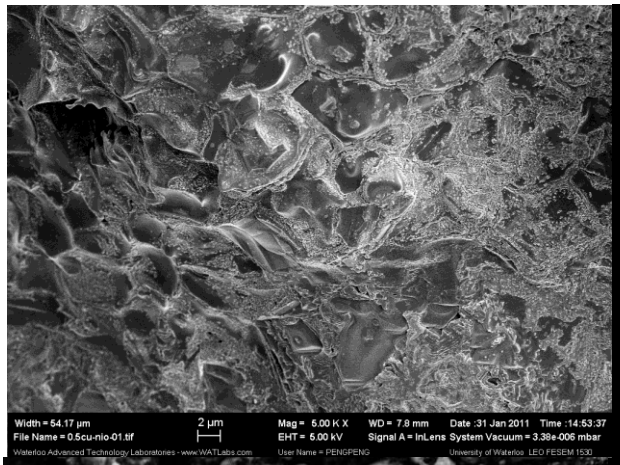

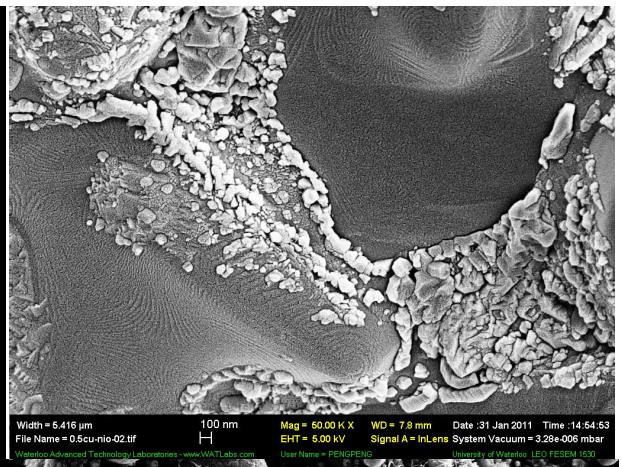

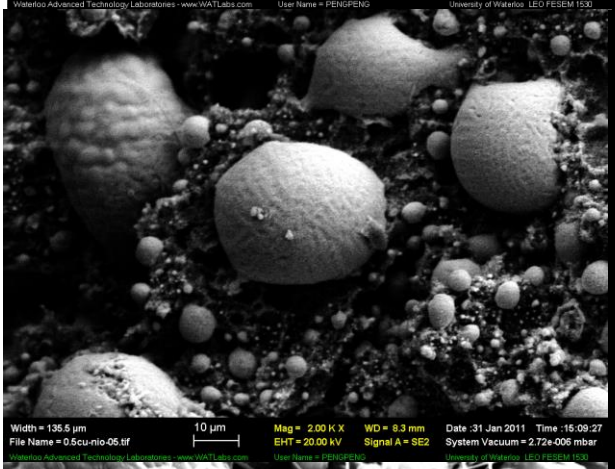

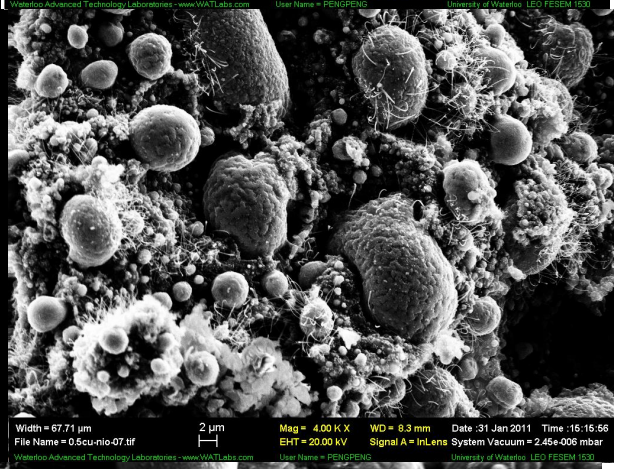

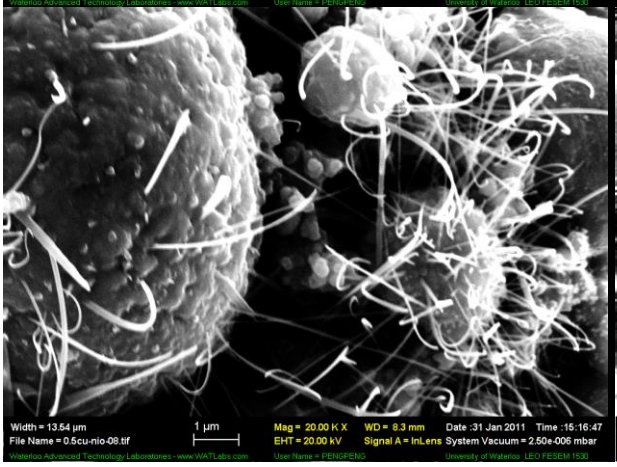

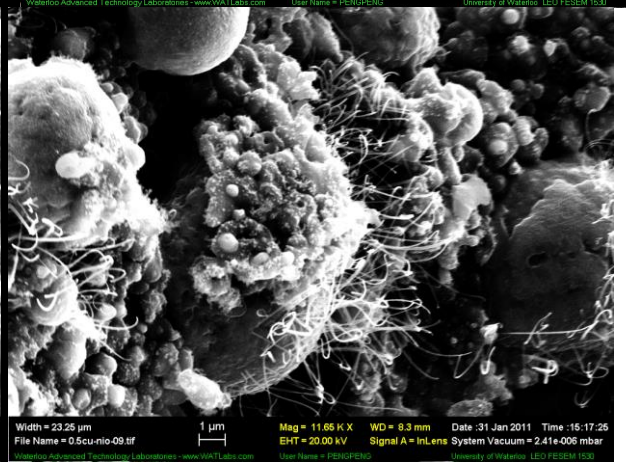

Additional SEM images of nanothermite composites

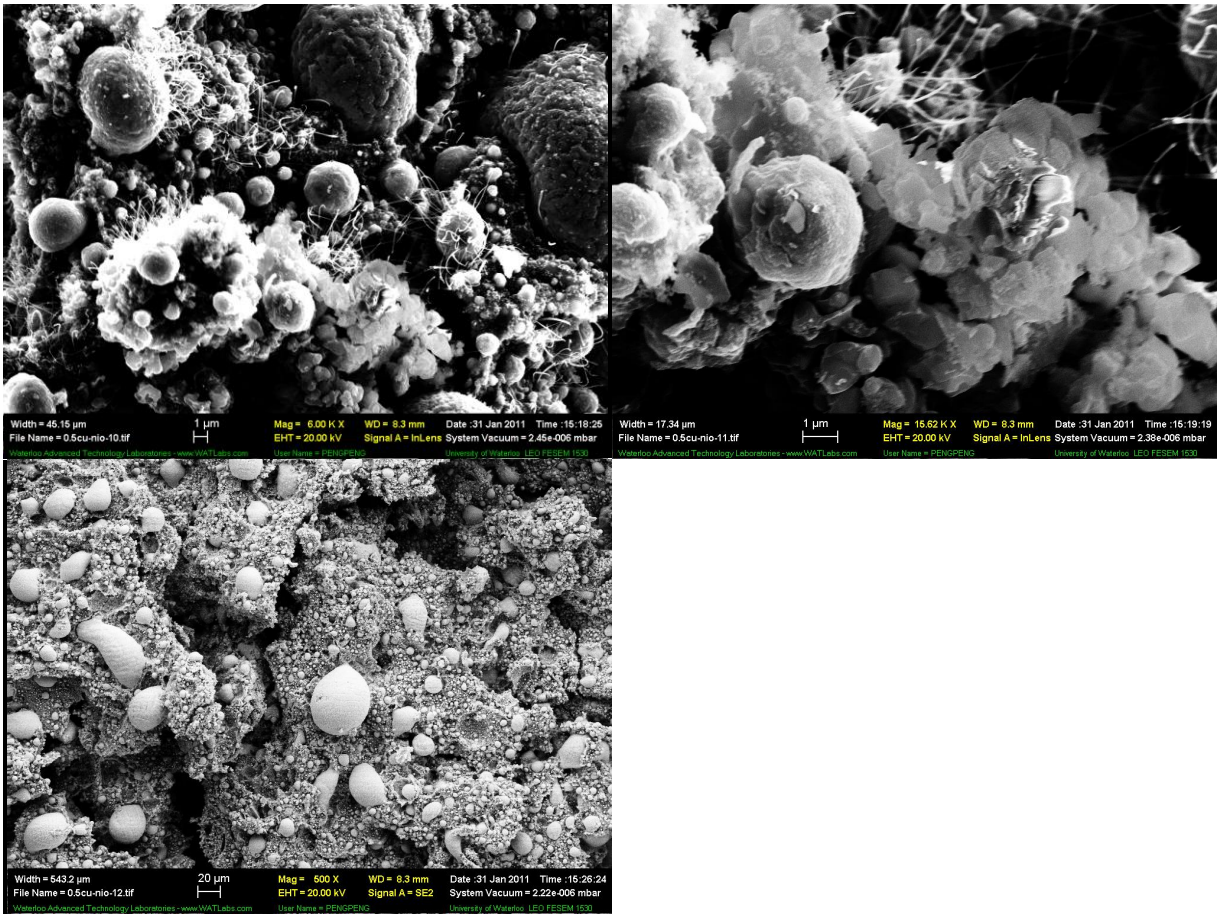

Image set 7

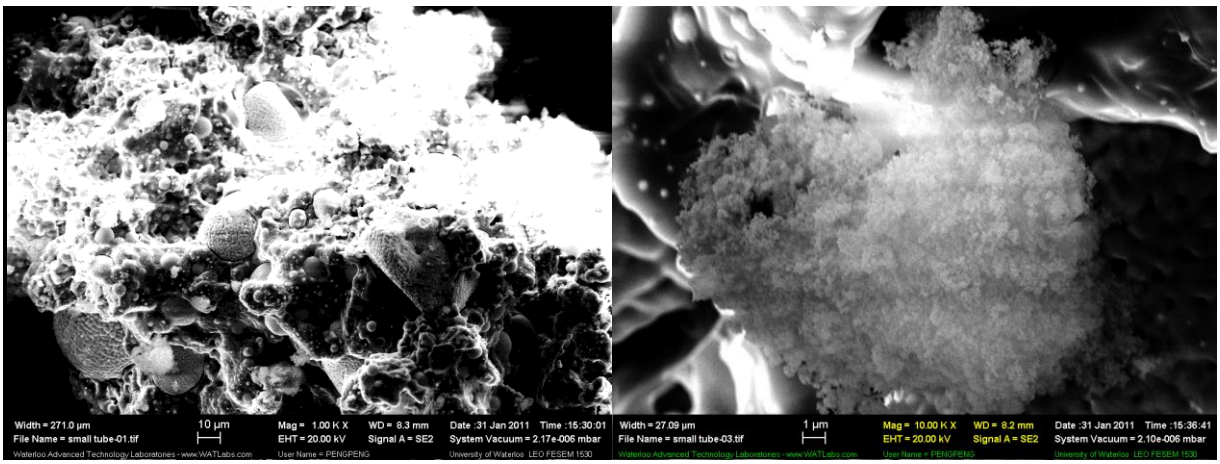

Image set 8

Additional SEM images of nanothermite composites

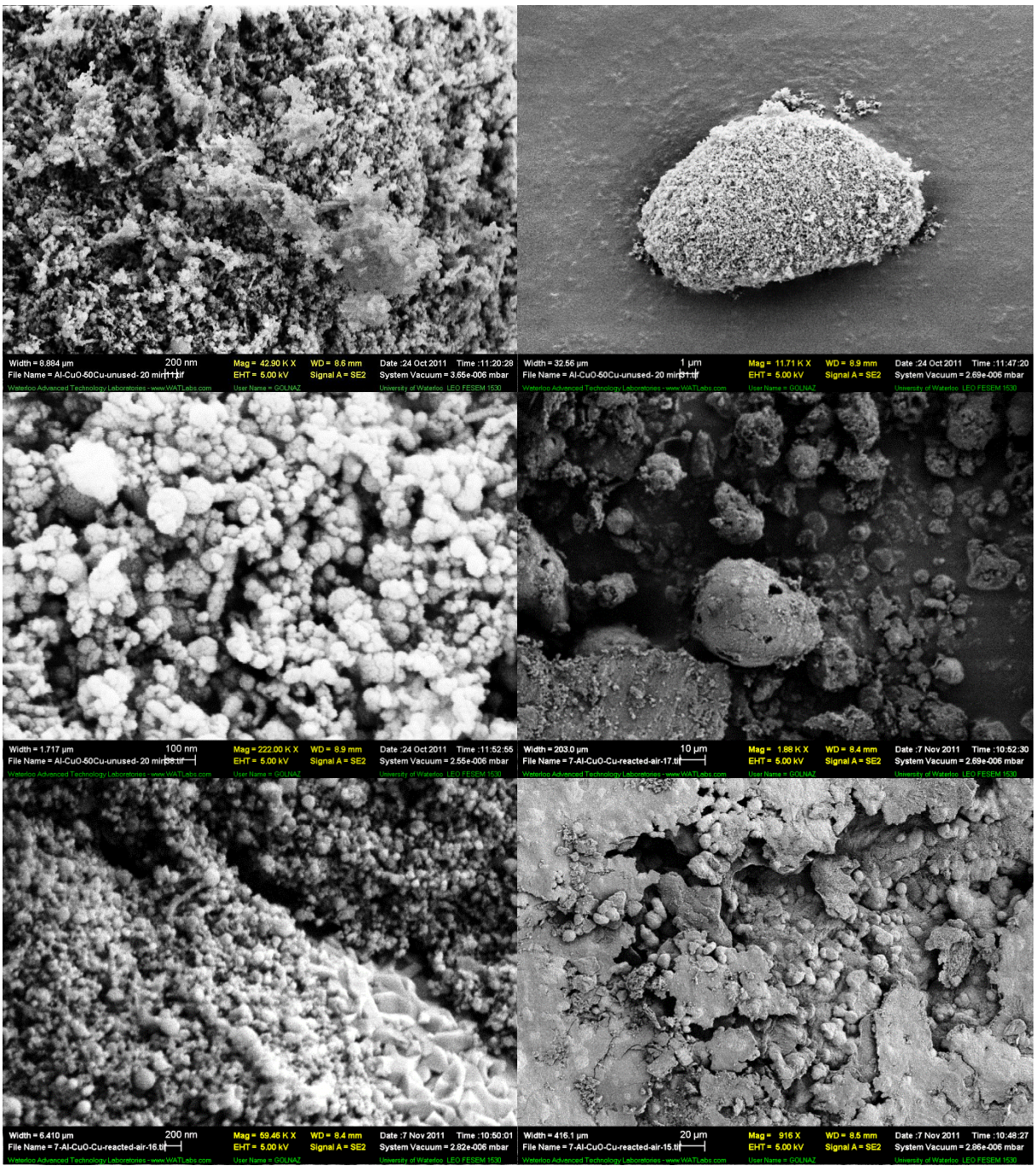

Image set 9

Additional SEM images of nanothermite composites

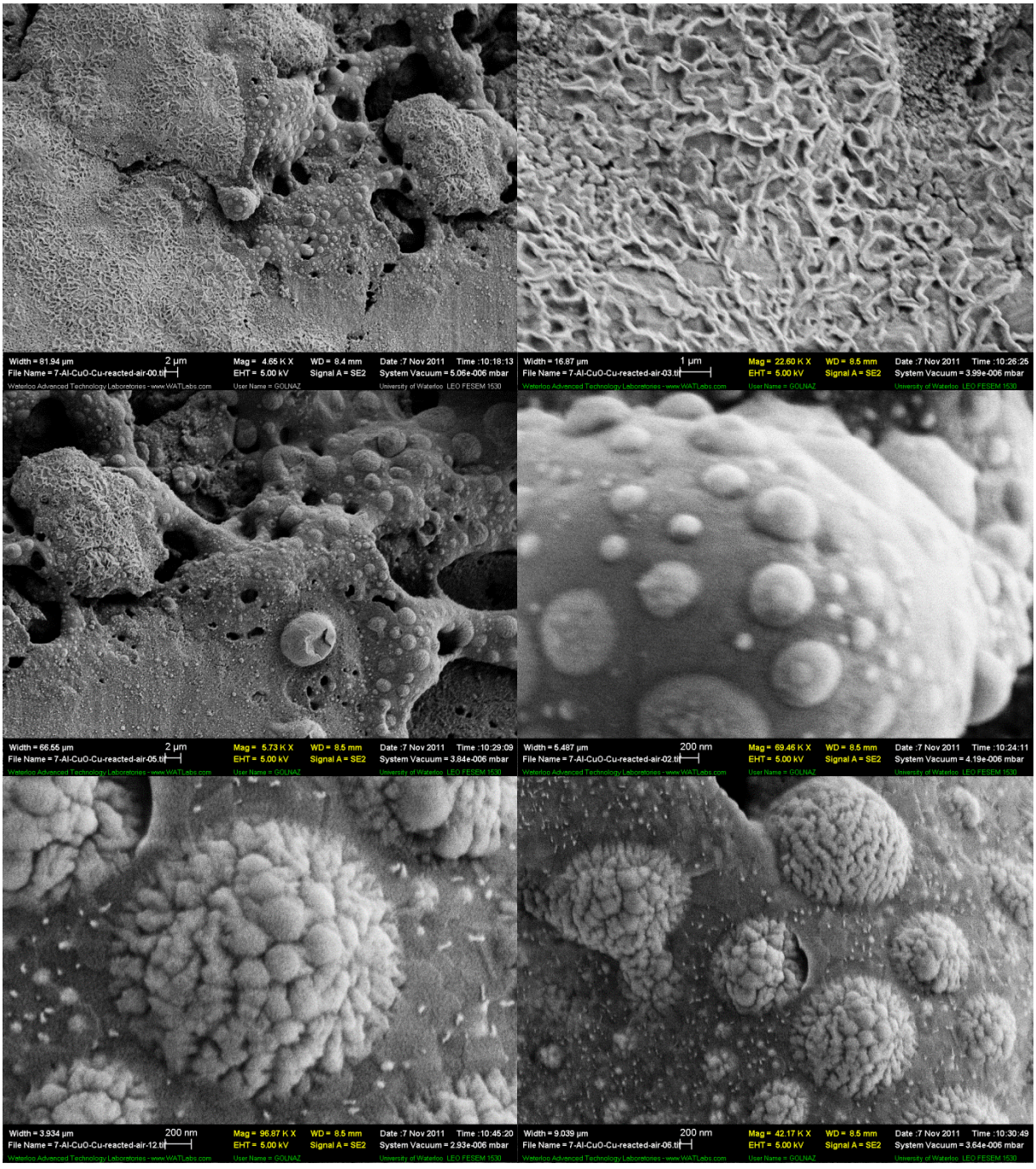

Image set 10

Additional SEM images of nanothermite composites

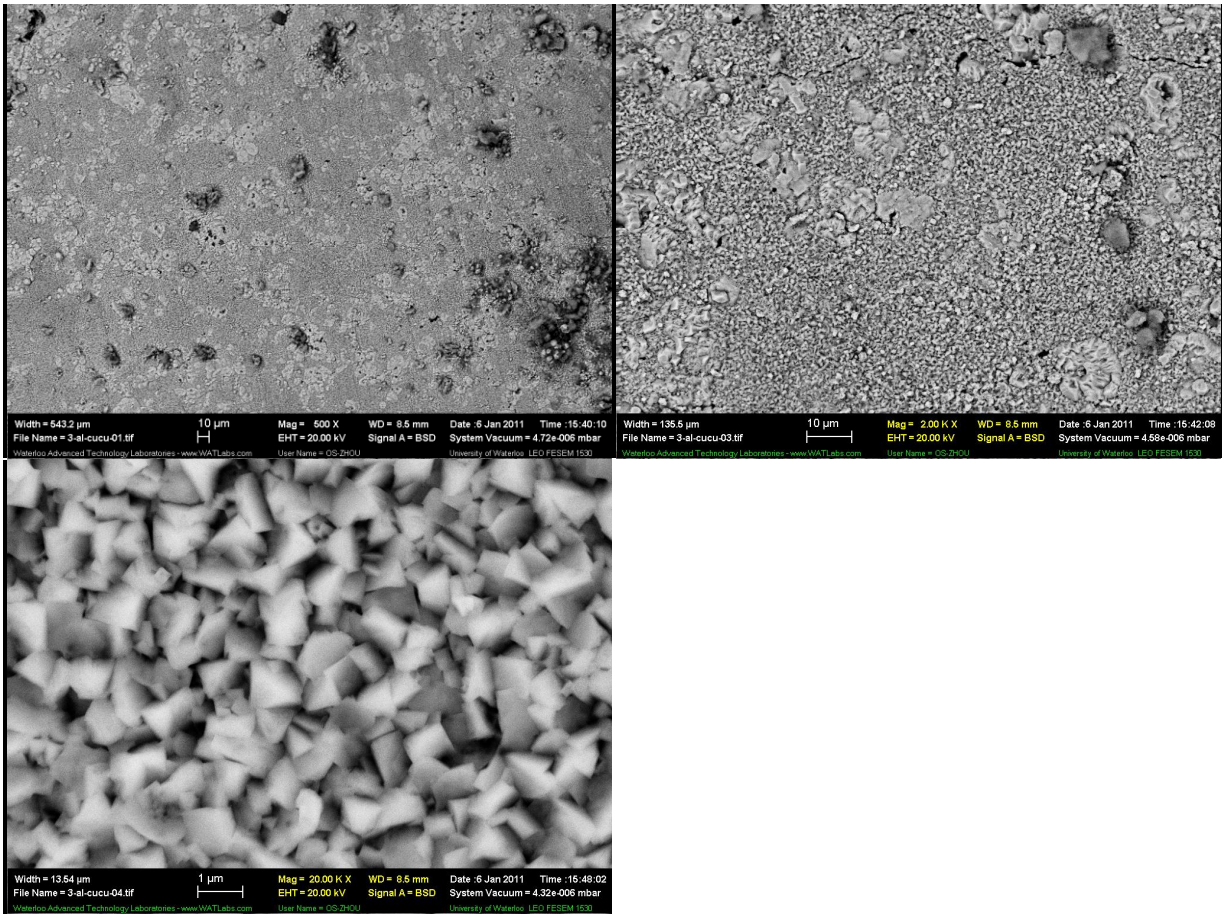

Image set 11

Additional SEM images of nanothermite composites

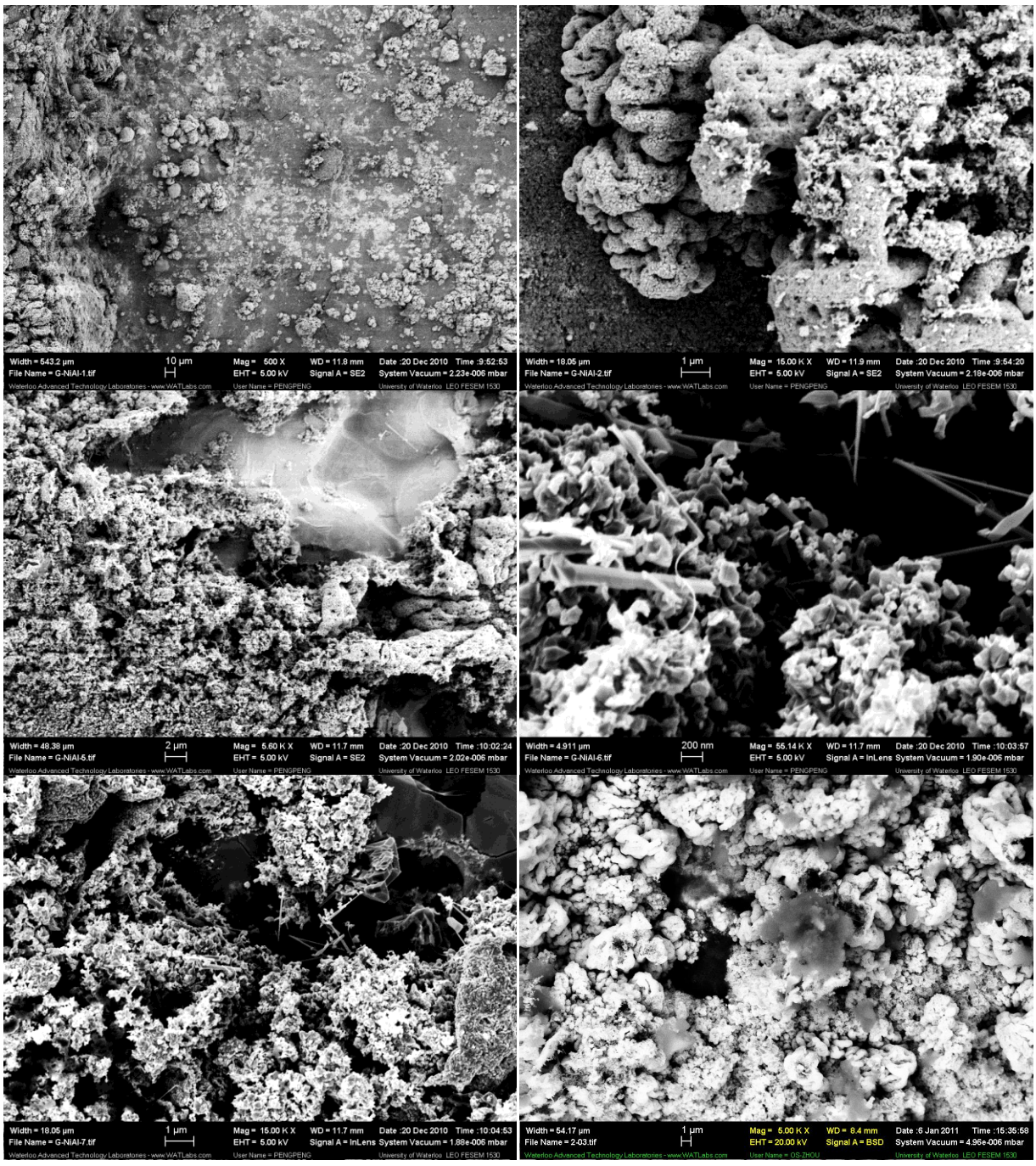

Image set 12

Additional SEM images of nanothermite composites

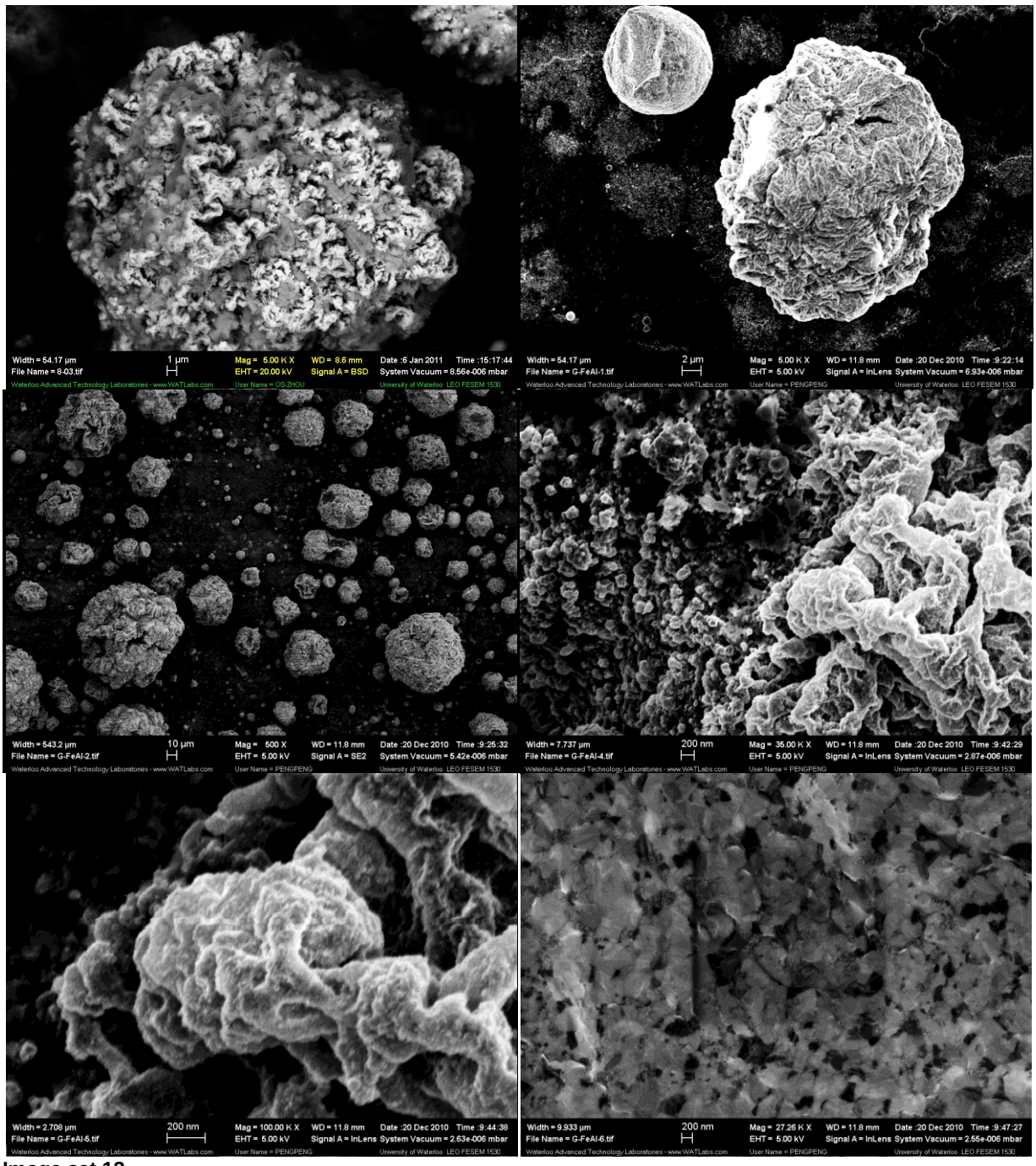

Image set 13

Appendix D

DSC and TGA graphs of Al-NiO-Sn

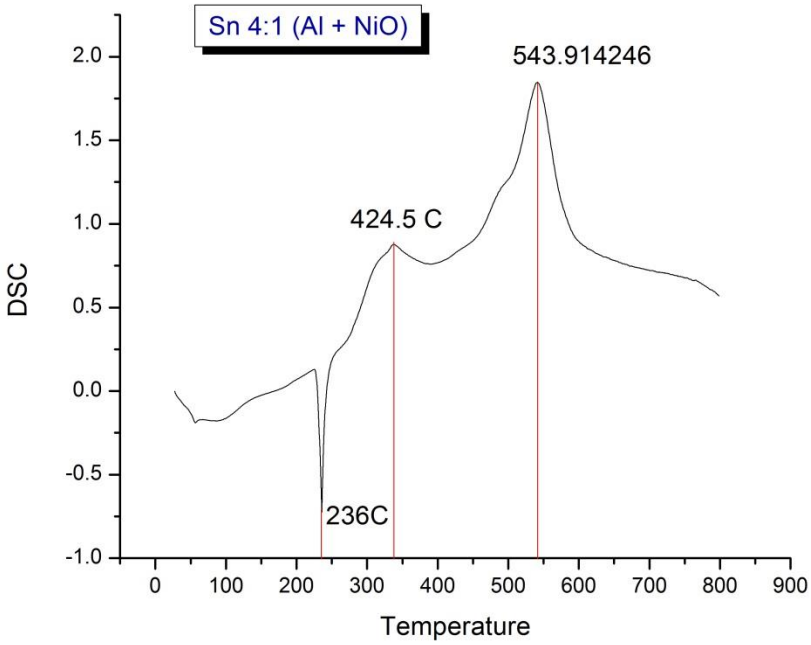

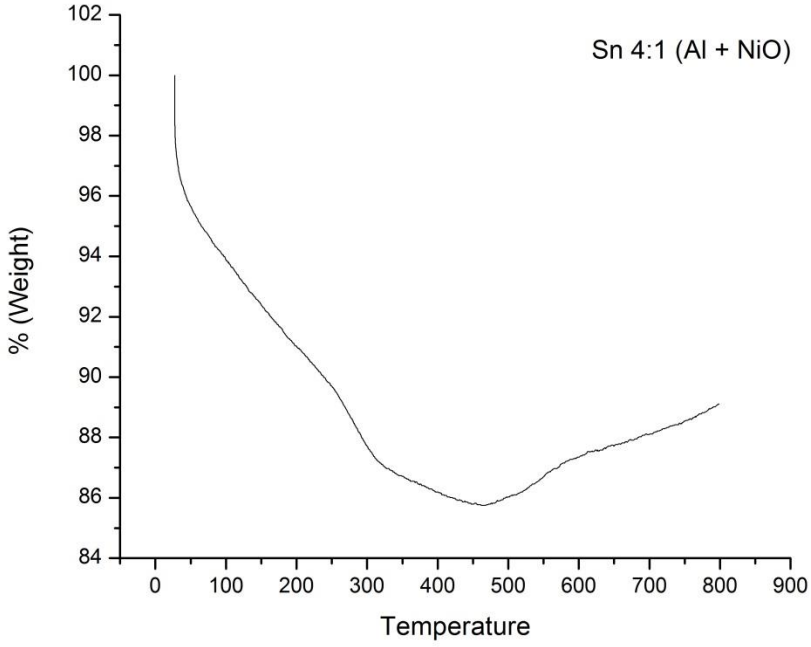

Appendix E

Additional SEM images of joint cross-sections

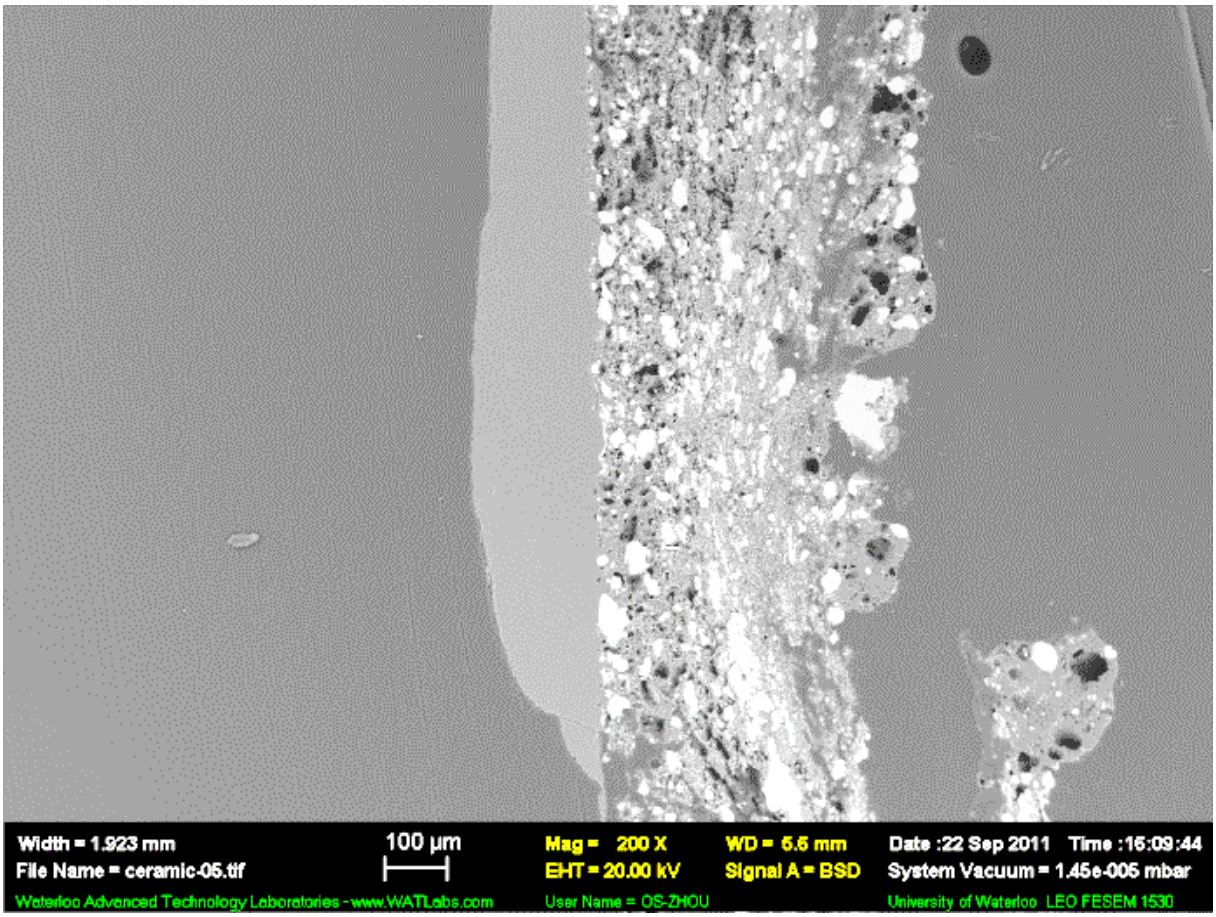

Image 14 SEM image of nanothermite/alumina-silica ceramic joint cross-section; Nanothermite reaction products are at the right side and the alumina-silica ceramic is at the left side

Additional SEM images of joint cross-sections

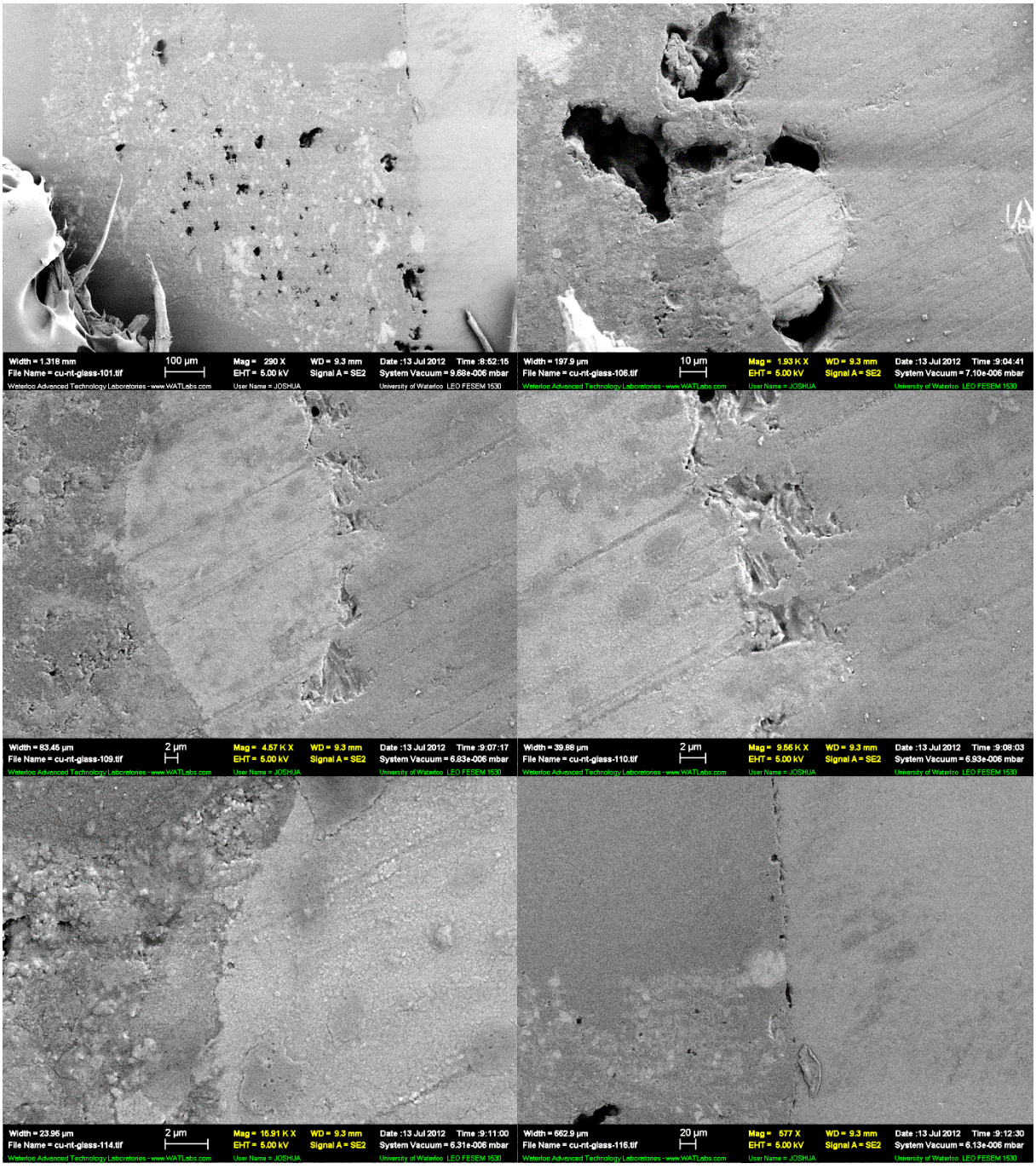

Image set 15 SEM images of nanothermite/Cu wire/glass joint cross section